Annual Report 2025

Leibniz-Institut für Kristallzüchtung im Forschungsverbund Berlin e.V.

IKZ aims to strengthen Europe's supply of critical crystalline materials for key technologies through two strategic priorities: attracting & training the next generation of crystal growth experts and enabling the provision of large-diameter crystals (4" - 8") for electronics, photonics, and future large-scale research infrastructures.

PROF. DR. THOMAS SCHRÖDER

Preface

Photo: Tina Merkau

Dear Readers,

The German Joint Science Conference, composed of federal & state authorities, is responsible for the funding of all non-university research organizations in Germany. For the Leibniz association, the German Science conference requests to evaluate each of the 96 Leibniz institute every seven years. The Leibniz evaluation procedure checks to which degree the institute´s strategy in science & technology complies on the one hand with its founding mission and to which degree the institute management follows on the other hand Leibniz quality standards.

IKZ welcomed the Leibniz evaluation commission on 3rd & 4th December 2025 and the official statement of the Senat of the Leibniz association is expected to be published in Summer 2026. Nevertheless, it is safe to state today that IKZ will be funded for the new evaluation period from 2026 to 2032. Despite harsh circumstances like Corona pandemics, energy crisis and inflation, IKZ could demonstrate substantial growth in the evaluation period 2018 to 2025. From an average value of about 110 persons in 2018, IKZ staff increased by about 30 % to a number of around 150 people. The IKZ budget increased correspondingly by about 40 % to a value of close to 20 Million € in 2025. This success is only possible by our team work among scientific, technical & administrative staff; explicitly, I wish to include all colleagues in the FVB Joint Administration.

The year 2025 was also characterized by major activities to upgrade IKZ´s science & technology infrastructure. Only if technology cycles and infrastructure invest cycles do not diverge, IKZ will be able in future to pursue state-of-the-art research & development programs for academic & industrial partners. It must be pointed out that the IKZ institute budget alone, despite above mentioned funding successes, does not allow anymore to fund major investments due to high inflation (in particular salary & consumable costs). It is only by successful applications to Berlin European Regional Development Funds (ERDF) that IKZ could realize major investments in the last years. Although in Berlin ERDF funding requests an institute co-payment of at least 60 % to the total project budget, IKZ took the opportunity to successfully apply for three major ERDF projects: Firstly, we upgrade the IKZ electron microscopy infrastructure (2024-2026; total budget: ~ 6 Million €), secondly, we upgrade the Gallium oxide prototyping program by a 2" MOCVD reactor (2025-2027; total budget: ~6 Million €) and thirdly, we invest in Czochralski growth stations for oxide & fluoride crystal prototyping (2026-2028: total budget ~4 Mio €). These invests will be of high value in future to attract not only further modern research projects but also talented young scientists to pursue their career perspectives at IKZ.

The European crystal growth community is receiving increasing political & industrial awareness in recent years due to the erosion of free trade in the world by geopolitical turmoil. IKZ as the leading EU flagship institute on the science & technology of crystals identified two major action points to support EU on the supply of critical crystals for key technologies. Firstly, IKZ wishes to intensify its education & training activities to attract more young talents to the field of crystal science & technology. Skilled staff is urgently needed by academic & commercial partners to push ahead ambitious scientific & technological projects. Secondly, IKZ plans to upscale and adopt its crystal growth infrastructure to crystal dimensions of 4" to 8". Technological imperatives by key technologies in electronics & photonics as well as by unprecedented demands on high quality crystals for future large-scale research facilities (e.g. Einstein Telescope (ET), Large enriched Germanium experiment for Neutrinoless Double Beta Decay (Legend) 1000, Petra IV- ultimate 4D X-ray Microscope) require a central EU crystal innovation hub. To the best of my knowledge, IKZ is the only place in EU which hosts in-house all scientific / technological / administrative expertise to successfully build up & run such an ambitious future crystal research & development program. To demonstrate our international leading position, we assembled scientific & technological highlights in the IKZ Annual Report 2025.

Enjoy the lecture of IKZ Annual Report 2025 and you are welcome to visit us at IKZ in Berlin-Adlershof.

With best regards

THOMAS SCHRÖDER

IKZ Annual Report 2025

Content

The Institute

The Leibniz-Institut für Kristallzüchtung (IKZ)

is an international competence center for science & technology as well as service & transfer for crystalline materials. The R&D activities cover basic and applied research up to pre-industrial development.

Crystalline materials are the key to the realization of electronic and photonic solutions to social challenges. This includes artificial intelligence (communication, sensor technology, etc.), energy (renewable energies, energy conversion etc.) and health (medical diagnostics, modern surgical instruments etc.). The IKZ develops innovations in crystalline materials by combining inhouse expertise in equipment engineering, numerical simulation and crystal growth to provide highest quality crystalline materials with tailored properties.

In the future, the institute will also intensify its efforts to promote innovation by crystalline materials in cooperation with partners from technology platforms as well as industrial companies. This includes the reliable evaluation and benchmarking of innovative crystalline prototype materials for disruptive technology approaches.

The research and service tasks of the institute include:

- Development of technologies for growth, processing and characterization of bulk crystals and of crystalline structures with dimensions in the micro- and nanometer range and of comprehensive growth technologies
- Supply of crystals with non-standard specifications for research and development purposes
- Modelling and investigation of crystal growth processes
- Experimental and theoretical investigations of the influence of process parameters on crystal growth processes and crystal quality
- Development of technologies for the chemo-mechanical processing of crystalline samples and scientific investiga tion of related processes
- Physico-chemical characterisation of crystalline solids and development of suitable methods; investigation of the correlation between crystalline structures and properties
- Development and construction of components for growth, processing and characterization of crystals

The further materials research towards applications will drive innovations by crystalline materials:

- Crystal prototypes development for the reliable benchmarking of innovative crystals with tailored properties for key technologies in electronics and photonics
- Prototype supply of innovative crystals up to small-scale batches – with tailored properties and specifications – for reliable technology research, including preparations for market introduction
- Development of wafering processes for new materials, fine processing of special optical crystals.

Materials presently in development (examples):

- Wide band gap semiconductors (aluminium nitride, oxides) for high temperature, power- and optoelectronics
- Oxide and fluoride crystals for acousto-electronics, laser-, opto- and sensor-technology
- Silicon for power electronics
- Isotopically pure semiconductors (silicon and germanium) for quantum technology
- Gallium arsenide for wireless communication and in high-frequency technology
- Silicon/germanium-crystals for radiation detectors and diffraction gratings, crystalline Si/Ge layers for thermoelectric devices
- Ferroelectric and semiconducting oxide layers for micro- and power electronics, sensor applications or data storage

Photo: Berit Kraushaar

IKZ as family-friendly employer

The institute intends to create a co-operative and open working environment for all employees.

It places special emphasis on the reconcilability of job and family, offering flexible working time models as well as full or part-time employments. In 2015, the institute has been awarded the audit berufundfamilie certificate for its family-friendly human resources policy. During the following three years, we have been implementing the objectives defined in this process. The certification has been renewed in 2018, 2021 and in 2024.

The certificate is issued under the auspices of the German Federal Minister for Families and the German Federal Economics Minister.

More information is available under **beruf-und-familie.de**

Zertifikat seit 2015
audit beruf**und**familie

Organisation chart

as of 30 June 2025

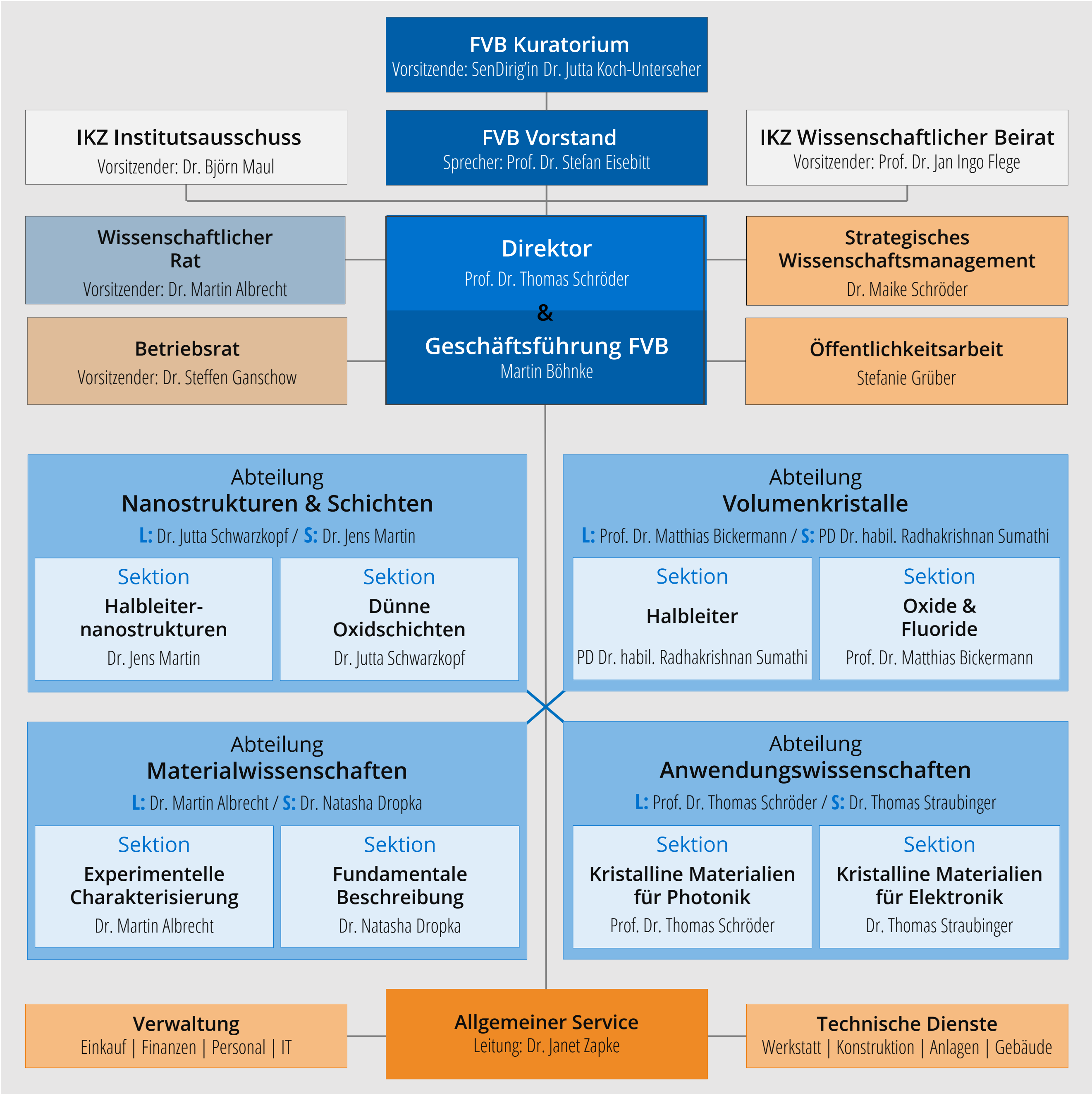

Scientific advisory board

as of 30 June 2025

Chairman

Prof. Dr. Jan Ingo Flege
Brandenburgische Technische Universität Cottbus-Senftenberg (BTU),
Germany

Deputy Chairman

Dr. Roger H.M.S. Loo
IMEC,
Belgium

Members

Prof. Dr. Claudia Draxl
Humboldt-Universität zu Berlin,
Germany

Prof. Dr. Marc Eichhorn
Fraunhofer IOSB,
Germany

Dr. Martin M. Frank
IBM, Thomas J. Watson Research Center,
USA

Dr. Kolja Haberland
LayTec AG,
Germany

Dr. Benedikt Kramm
PVA TePla AG,
Germany

Dipl.-Ing. Michael Rosch
Freiberger Compound Materials GmbH,
Germany

Prof. Dr. Clara Saraceno
Ruhr Universität Bochum,
Germany

Dr. Georg Schwalb
Siltronic AG,
Germany

Prof. Dr. Siddha Pimputkar
Lehigh University, Department of Materials Science and Engineering,
USA

Prof. Dr. Thomas Südmeyer
University of Neuchâtel, Physics Institute,
Switzerland

Representative of the state of Berlin

Dr. Björn Maul
Senate Department for Higher Education and Research, Health and Long-Term Care,
Berlin, Germany

Representative of the Federal Republic of Germany

Dr. Dirk Ziemann
Federal Ministry of Research, Technology and Space (BMFTR),
Unit 513, Communication and security of digital systems
Berlin, Germany

2025 in figures

18.2 Mio
Budget total

12.7 Mio €
Institutional funding

5.5 Mio €
Third-party funding

- **11.7 %** EU
- **18.9 %** Federal
- **6.9%** Leibniz Association
- **3.4 %** Crystal sales / service
- **11.9 %** Industry
- **18.5 %** German Research Foundation (DFG)
- **2.7 %** other
- **26.0 %** State Berlin (incl. ERDF)

Graduates

3 Doctoral theses

9 Bachelor's and Master's theses

Publications

118
Articles in peer-reviewed journals and book chapters

Inter-nationalization

Staff members from
23
countries

Staff

149 total

45% Infrastructure

55% Research

Women

30%	24%	26%
Total Staff	Scientific employees	PhD students

Presentations

55
At national and international conferences, workshops, seminars

IKZ Annual Report 2025

IKZ 2025

|Events

International workshops and scientific exchange

Workshops, conferences and dialogue with partners from science and public policy brought together researchers from Germany and abroad and provided a platform for scientific discussion within the crystal growth community and connected research with application.

// 5.-7. Mai 2025
Workshop „Artificial Intelligence and Transmission Electron Microscopy (TEM)“
Prof. Dr. Sergei Kalinin received the IKZ International Fellowship Award 2025 for his pioneering contributions to AI-driven electron microscopy.
Photo: IKZ

// 30. April 2025
Visit by Berlin State Secretary Dr. Henry Marx
Photo: Anne Riemann

// 6. - 7. October 2025
Materials for Advanced Detectors Workshop 2025 (MAD25)
Photo: IKZ

// 15. - 16. September 2025
3rd DGKK Workshop on “Growth Kinetics, Layer Transfer of Ultrathin Layers and 2D Materials”
Photo: IKZ

Supporting early-career researchers and an inclusive working environment

IKZ supported young talent through outreach and internship programs in 2025, while continuing its work on equal opportunities and family-friendly employment conditions.

// 1. October 2025
Jugend forscht award winner completes research internship at IKZ
Photo: Stiftung Jugend forscht e.V.

// 9. April 2025
Girls' Day 2025: Exciting insights into the world of work at IKZ
Photo: IKZ

// 5. February 2025
Promoting diversity and inclusion in science: IKZ embraces equal opportunity and an innovative work environment by signing the Diversity Charter
Photo: Stefanie Grüber

// 17. June 2025
Science meets work-life balance: IKZ receives berufundfamilie audit certificate for the fourth time
Photo: © berufundfamilie Service GmbH

Strengthening research infrastructure and technology platforms

With two new laboratories, research facilities and strategic investments, IKZ expanded its capabilities in crystal growth, materials research and technology transfer.

// 29. January 2025
Opening ceremony of the Joint Laboratory JAMA
Photo: Stefanie Grüber

// September 2024
Technology development for semiconductor material gallium oxide launched
Photo: Stefanie Grüber

// 8. October 2025
IKZ strengthens its hardware basis for crystal prototyping R & D for future power electronics markets
Photo: IKZ

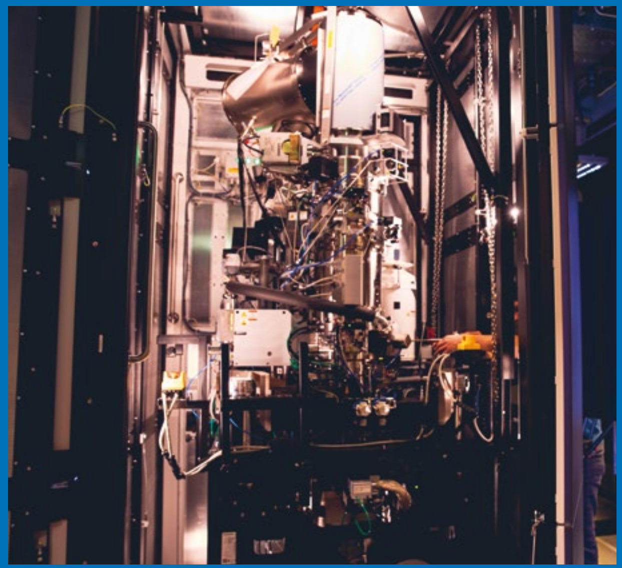

// 8. October 2025
ALISE: New application lab for in situ electron microscopy strengthens research and SMEs in Berlin-Adlershof
Photo: Dan Zhou

Our doctoral students
Photo: Stefanie Grüber

| People

Report of the doctoral students

2025 was again marked by a plethora of communal activities, novelties, new arrivals and a strong community.

Throughout the year, a variety of PhD events brought our doctoral community together, including our regular monthly seminars and the annual summer barbecues. These gatherings offered valuable opportunities for academic exchange and inter-disciplinary discussion while also fostering informal connections in a relaxed atmosphere. By bringing doctoral students together beyond their day-to-day research, these events played an important role in strengthening our sense of community and encouraging lasting professional and personal relationships.

The end of the last year was again celebrated with visits to various Christmas markets and a Christmas party to end the year on a high note, looking back at achievements and challenges ahead.

Another important development was the appointment of a second doctoral representative, Gaetano Bonetti. As a result, the representation of the doctoral community is now carried out by a dedicated duo. The two-person representation fosters close collaboration, allowing ideas to be developed collectively, responsibilities to be shared efficiently, and new initiatives to emerge through the combined strengths of both representatives. Together, a number of plans to increase the visibility of the doctoral students and improve their work life at the institute. The latter in particular encompasses the initiation of the program "Discover IKZ", to organize guided tours through the labs of IKZ, displaying the spectrum of analytical methods at the institute's disposal. Furthermore, an overhaul of the PhD-guidelines was initiated. Both representatives therefore undertook a concerted effort together with the doctoral communities in devising new and updating a number of the existing paragraphs of the guidelines. As of this point, the new draft has been discussed with the management with deliberations still ongoing.

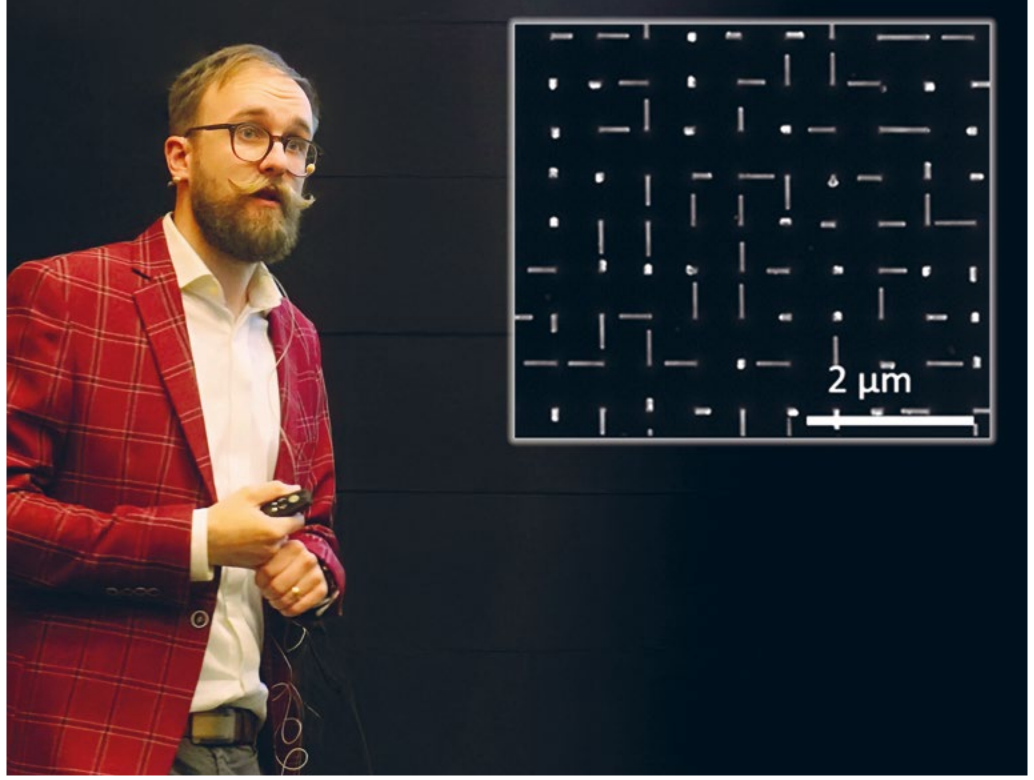

Dr. Owen C. Ernst | Goethe University Frankfurt am Main; Right: SEM image of silicon nanostructures.
Photo: Kirstin Kliemt

| Awards

Owen C. Ernst receives the DGKK Young Talent Award 2025

The Deutsche Gesellschaft für Kristallzüchtung und Kristallwachstum e.V. (DGKK) awarded IKZ graduate Dr. Owen C. Ernst the Young Scientist Award, endowed with 2500 €, for his outstanding scientific achievements in the field of nucleation and growth of complex structures of thin metal films on crystalline surfaces.

Classical nucleation theory forms the basis for describing the thermodynamics of material growth. It explains a wide range of growth processes, from the formation of nanoscopic droplets to the development of microcrystallites and bulk crystals. However, under certain conditions, alternative approaches provide a more realistic description of material formation and morphology. These alternatives include the theory of dewetting and the theory of dissipative structures.

At the IKZ, Dr. Owen C. Ernst investigated the influence of system parameters on structure formation and how the resulting metal structures can be used for the epitaxy of semiconductor structures. As a result of his work, the formation of material structures can not only be described but even predicted with the help of dewetting theory. By extending the theory with concepts from non-equilibrium thermodynamics, he enabled its application to previously inaccessible material systems, including materials for energy conversion.

Owen C. Ernst completed his doctoral research on "Consideration and extension of dewetting theory for the sophisticated synthesis of energy conversion materials" at the IKZ, graduating summa cum laude. In 2022, he became head of the Junior Scientist Group "Structure Formation and Local Growth of Semiconductor Materials". Since 2024, he has been a group leader at the Brandenburg University of Technology Cottbus–Senftenberg (BTU), where his research focuses on the chemistry and physics of isotopically engineered semiconductor crystals for quantum technologies. He is also co-founder of the IKZ spin-off quantum grade materials (qgm), which aims to make these materials available to the European market.

Next level semiconductors: The silicon materials science behind the quantum age

As a materials scientist and junior research group leader at the IKZ, Dr. Kevin-Peter Gradwohl focuses on the cutting edge of semiconductor materials. His team specializes in designing and growing ultra-pure, silicon-germanium (SiGe)-based quantum materials and complex heterostructures. In this interview, the Austrian physicist shares his serendipitous journey to Berlin, how a lifelong fascination with minerals shaped his academic career, and why upgrading these sophisticated semiconductor structures to the laws of quantum mechanics is paving the way for a new computing era.

| Interview

You are from Austria. What brought you to the IKZ in Berlin?

KEVIN-PETER GRADWOHL Haha, yes, that's a great question. Looking back, I've been at the IKZ for eight years now, but coming to Berlin was pure coincidence!

In early 2018, I was a materials science student at Montanuniversität Leoben, working as a research assistant under Prof. Christian Teichert. I was investigating the crystal facets of tellurium inclusions in cadmium zinc telluride, a material used in X-ray detectors like airport security scanners. It was a side project between my Bachelor's and Master's theses, part of an academic exchange with partners in China.

Prof. Teichert sent me to present these results at the first German-Austrian Conference on Crystal Growth in Vienna, which was co-organized by Dr. Wolfram Miller from the IKZ. There, I connected with Dr. Frank Kießling and Dr. Christiane Frank-Rotsch from the IKZ semiconductor department. I really liked their work on gallium arsenide, and it seemed they enjoyed my talk as well; either way, they spontaneously invited me to Berlin. It turned out there was an open PhD position on the Czochralski growth of isotope-enriched germanium crystals for deep-underground neutrino experiments. I applied, and the visit quickly turned into a job interview.

From there, everything accelerated at lightning speed: the conference was in February, I visited the IKZ in March, got the job in April, rushed to finish my Master's thesis, passed my final board exams on Friday, October 19th (I still remember the exact date), and moved to Berlin with just a single suitcase on Sunday to start my first workday on Monday. What began as a whirlwind transition for a PhD turned into a long-term scientific home, first as a doctoral student and now as a junior research group leader.

Most people have no idea what "crystal growth" actually means. How do you develop a passion for such a niche field?

KEVIN-PETER GRADWOHL For me, it started with a fascination for the discrete, geometric beauty of nature. I have been an avid mineral collector since childhood, captivated by how perfectly ordered structures with sharp, flat facets can form out of geological chaos. But I never expected this private passion to launch my academic career.

During my Master's studies, I noticed that a specific mineral from my collection possessed a layered atomic structure that looked like it could be easily cleaved, while also showing magnetic properties. At the time, a brilliant Postdoc in our lab, Aleksandar Matković, was researching two-dimensional materials. We decided to test a theory: I mechanically exfoliated the mineral down to atomic layers, and we discovered that these isolated 2D flakes maintained a strong magnetic signal at room temperature. What started on my mineral shelf turned into a high-impact publication in npj 2D Materials and Applications.

However, I wanted to do more than just collect what nature provided; I wanted to grow my own crystals and control exactly where the atoms sit in the lattice. That drive brought me to the IKZ. Meanwhile, Aleksandar built a highly successful research track around these 2D magnets, securing an ERC Starting Grant. In a beautiful twist of scientific fate, our paths have crossed again: he will be a professor and department head right here at the IKZ. Following the atoms from my shelf straight into the lab completely hooked me on this field.

| Vita

Kevin-Peter Gradwohl

Since 2022: Junior Research Group Leader for SiGe-based Quantum Materials, Leibniz-Institut für Kristallzüchtung (IKZ), Berlin, Germany
2018–2021: Scientific Employee & Doctoral Program, Humboldt-Universität zu Berlin / IKZ
Degree: Dr. rer. nat. (Experimental Physics), Summa cum laude
2017–2018: OeAD Exchange Program, NWPU, Xi'an, China
2017–2018: Masters Program in Materials Science, Montanuniversität Leoben, Austria
Degree: Dipl.-Ing. (Pass with Honors)
2016–2018: Industrial Internship at Infineon, Villach &. Dresden, Austria and Germany, respecively
2014–2017: Bachelors Program in Materials Science, Montanuniversität Leoben, Austria
Degree: BSc. (Pass with Honors)
2013–2014: Civil Service (Zivildienst) at Lebenshilfe Weiz, Austria, day care for adults with complex, severe disabilities
2008–2013: Higher Technical Education Institute (HTL), Mechanical engineering, Weiz, Austria
Degree: Higher School Certificate in Engineering, Pass with Distinction (grade 1.0)
Diploma Thesis: Sustainable automotive fueling via wood gas systems

What is your research group working on right now, and how could your results change our future?

KEVIN-PETER GRADWOHL We are living in a new Golden Age of Semiconductors. Driven by the explosive demand for technologies like Artificial Intelligence, microchips have become the most critical high-tech commodity on Earth. Today's chips are absolute marvels: trillions of integrated transistors are packed onto a single silicon crystal with near-atomic precision.

But as global data demands scale exponentially, classical computing boundaries are looming. My junior research group wants to push this highly advanced semiconductor platform into the next frontier: semiconductor-based quantum computing.

To do that, standard industrial semiconductors are not enough. We need a new class of "quantum-grade" materials, which we design and grow at the IKZ. We engineer silicon and germanium crystals down to the isotopic level, completely purifying them of natural nuclear spins that would otherwise destroy fragile quantum information. Backed by our DFG projects, we build complex, ultra-clean material structures. Essentially, we are taking the world's most sophisticated manufacturing platform and upgrading it to harness the laws of quantum mechanics.

If we succeed, we provide the material basis for a new computing era, redefining everything from medicalmolecularsimultions,newbatterytechnologies,to secure data encryption, and the future of AI. The progress in our field is truly stunning.

An institute thrives on more than just lab work. Where are you engaged outside of the growth chambers?

KEVIN-PETERGRADWOHL The painful reality of being a group leader is that I cannot spend as much time hands-on in the lab anymore, the honest answer is a lot of office paperwork!

But what sparks true joy is sharing knowledge, because science moves forward through collaboration. A massive motivation is passing on this "nerdy" fascination to the next generation. I have an excellent team of PhD students, and I teach the master-level crystal growth lecture at Humboldt-Universität zu Berlin under the leadership of the IKZ director, Prof. Thomas Schröder. Beyond teaching, I am heavily involved in international science organization, serving on the committee for the ICSI/ISTDM conference series and working within the DGK and DGKK. Within the DGKK, we are currently gearing up to organize the European School on Crystal Growth (ESCG 2027) right here at the IKZ Berlin. For me, a group leader has a responsibility to foster international networks, mentor early-career researchers, and keep our community vibrant.





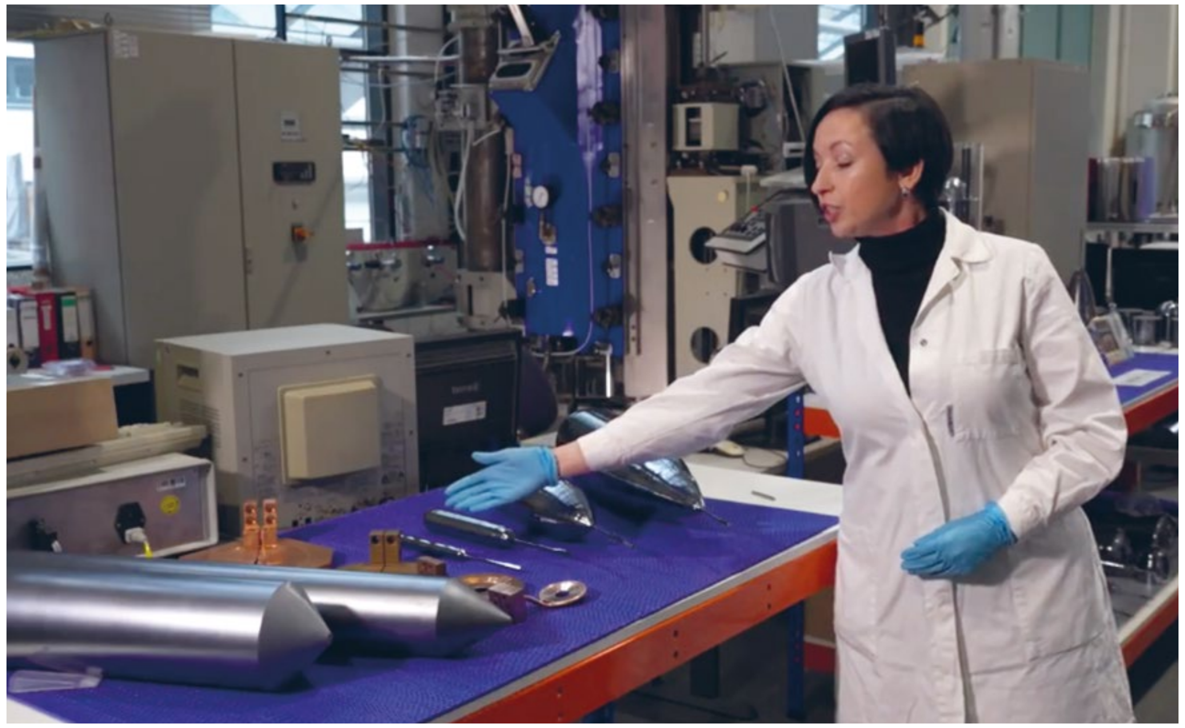
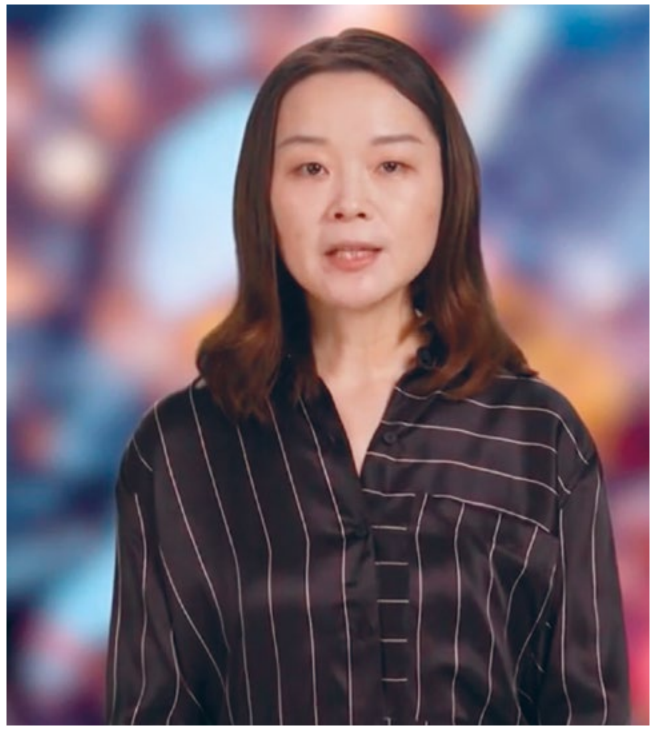

|IKZ Online Lectures

From crystal growth fundamentals to advanced materials

The IKZ Online Lectures introduce key topics in crystal growth and materials research. Covering areas such as bulk crystals, thin films, photonics, electronics, characterization, simulation, and AI-supported methods, the format offers students, early-career researchers, and external audiences an accessible overview of IKZ expertise. The lectures combine basic knowledge with current research results, supporting education and training in crystal growth and materials science. All lectures are freely available on the IKZ website, with new topics and contributions from IKZ researchers added continuously.

View of an AlN crystal growth experiment in progress (T ~ 2300°C)
Photo: IKZ

AlN – from crystal to technology: How IKZ is building Europe’s native aluminum nitride platform

Every technological revolution begins long before the first product reaches the market. The performance of tomorrow’s semiconductor devices will increasingly depend not only on sophisticated device architectures but also on the availability of large, high-quality substrate materials. For aluminum nitride (AlN), this challenge has become one of the defining research activities at the Leibniz-Institut für Kristallzüchtung (IKZ). Over the past decade, we have systematically developed the scientific understanding, technological expertise and processing capabilities required to transform native AlN from a promising research material into a future semiconductor platform. Over the past year, important progress has been made, combining scientific advances with a strategic industrial partnership aimed at scaling the technology towards industrially relevant wafer diameters.

Native AlN has emerged as one of the most promising substrate materials for next-generation power electronics and deep-ultraviolet photonics. Its outstanding material properties provide the basis for high-performance AlGaN-based devices with improved efficiency, reliability and thermal management. Yet these advantages can only be fully exploited when large, structurally perfect bulk crystals and epi-ready substrates become available. At IKZ, crystal growth, defect control, wafer preparation, and structural characterization are developed in close combination to address this challenge. We have established a comprehensive technology platform that spans virtually the complete value chain. Expertise in physical vapor transport (PVT) crystal growth has been complemented by process modelling, crystal characterization, precision wafering, chemical-mechanical polishing and advanced metrology. Together, these capabilities enable continuous optimization from the first crystal nucleus to the finished epi-ready substrate.

Today, we routinely achieve threading dislocation densities below 104 cm^{-2}, while selected regions and seed crystals are virtually dislocation-free. Crystal quality is verified by high-resolution X-ray diffraction, X-ray topography and three-dimensional X-ray diffraction laminography. Rocking curves with exceptionally low full widths at half maximum underline the excellent crystalline perfection. One particularly important milestone was the development of a growth concept enabling lateral crystal expansion angles exceeding 45°. This achievement is not presented as a replacement for established approaches, but as a particularly efficient route towards faster diameter enlargement while maintaining the crystal quality required for electronic-grade substrates. By reducing the number of intermediate crystal generations required during scaling, the concept shortens the pathway towards larger wafer diameters and supports future industrial manufacturing.

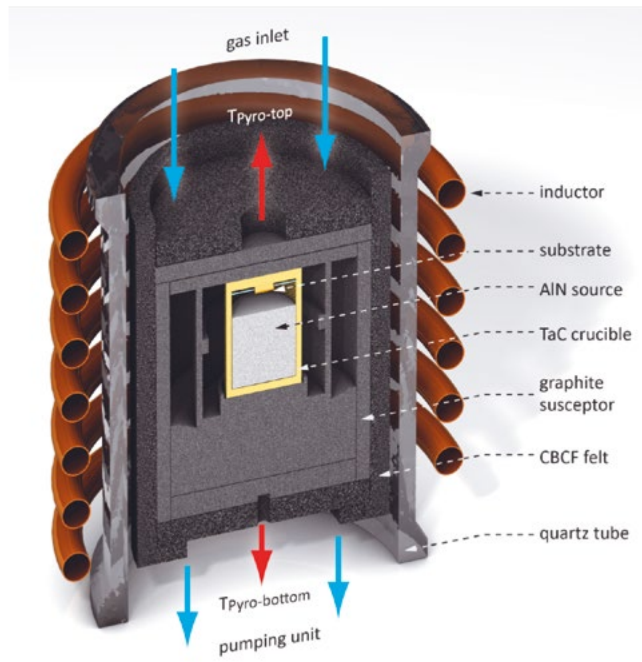

3D sketch of the reactor and the growth setup
Photo: IKZ

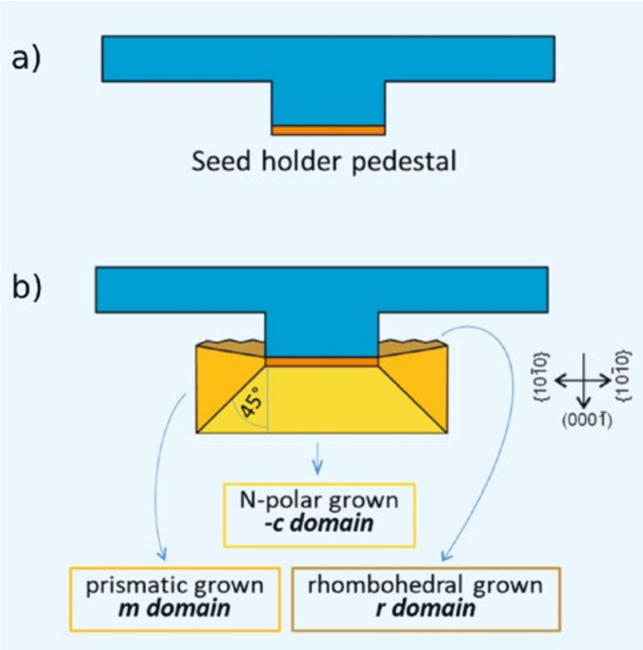

Fig. 1
Simplified sketch of the seed holder design;
(a) TaC pedestal with mounted N-polar seed;
(b) full faceted grown crystal with an expansion angle of ~45°.
Image: IKZ

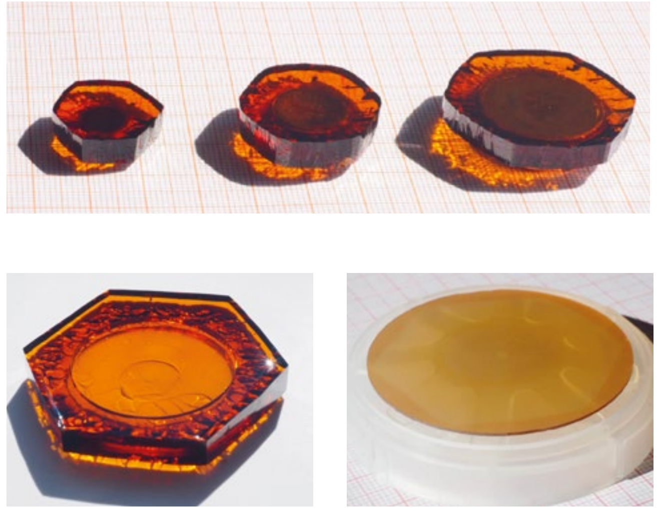

Fig. 2
Top: Three AlN crystals of subsequent crystal generations with 45° expanison angle (¾ inch, 1 inch, and 1½ inch in diameter)
Left: AlN crystal with 2 inch in diameter
Right: Al-polar epi-ready 2 inch AlN prototype substrate
Photo: IKZ

IKZ's expertise extends far beyond crystal growth. Precision sawing, lapping, polishing and chemical-mechanical polishing (CMP) have been optimized to produce epi-ready substrates with atomically smooth surfaces. Atomic force microscopy confirms sub-nanometer surface roughness, while precise off-cut control fulfils the demanding requirements of homoepitaxial growth. IKZ therefore combines bulk crystal growth with precision wafer processing and state-of-the-art characterization techniques. The close interaction between crystal growth, processing and analysis enables continuous feedback, allowing defects to be identified, growth conditions to be refined and substrate quality to be steadily improved. The result is a complete process chain capable of delivering epi-ready native AlN substrates for research and future industrial applications. IKZ is the first institute in the EU to offer AlN wafers for purchase to research partners through its IKZ Crystal Service.

Scaling to 4 inches – a strategic partnership with PVA TePla and Siltronic

A defining highlight of the last year is the launch of a joint initiative with PVA TePla and Siltronic to establish the technological basis for 4-inch native AlN substrates. This partnership represents a logical next step in transferring scientific excellence into industrial implementation. Each partner contributes complementary expertise. IKZ provides internationally recognized expertise in AlN crystal growth, including an established 2-inch AlN baseline process, as well as in substrate preparation and materials science. PVA TePla contributes its extensive experience in industrial crystal-growth equipment and process engineering and provides IKZ with a PVT growth system designed to accommodate AlN crystals with diameters of 100 mm and beyond. Siltronic brings decades of expertise in wafer manufacturing, process integration, and industrial-scale production, while providing industrial funding to support and advance AlN growth experiments at IKZ during this phase of the project. Together, the partners are addressing one of the key challenges for future AlN technology: transferring laboratory-scale achievements into scalable manufacturing concepts. Beyond its technical objectives, the collaboration demonstrates how research institutes and industrial partners can jointly strengthen Europe's semiconductor ecosystem. Establishing a reliable European supply chain for native AlN substrates is expected to benefit future applications in power electronics, deep-UV photonics and other emerging semiconductor technologies.

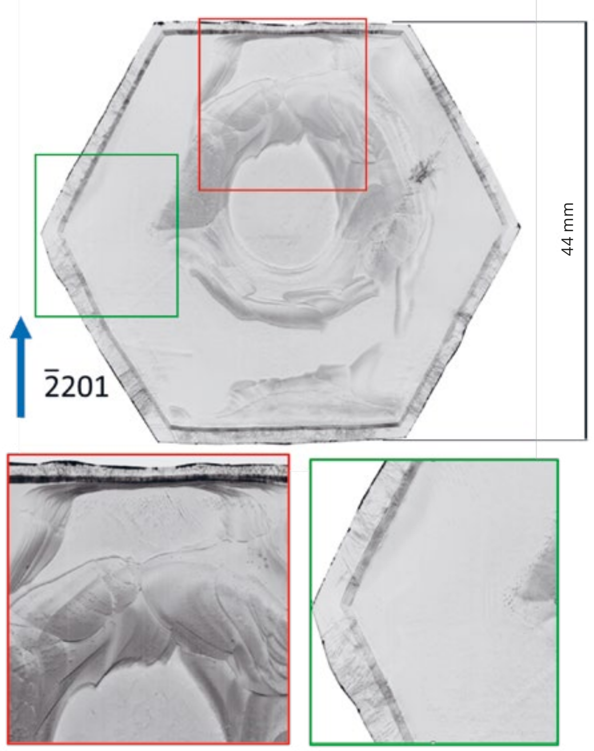

Fig. 3
XRT transmission image (recorded by Lutz Kirst from IAF Freiburg with an Rigaku XRTmicron). Large areas along the <11$\bar{2}$0> directions which are virtually dislocation-free areas (within the green box). Areas with dislocation densities ~1-2x10^3/cm^2 along the <1$\bar{1}$00> directions (red box) *Images: Lutz Kirst*

Fig. 4
AlN growth reactor from PVA Tepla for AlN crystals with diameters of 100mm and beyond (installed in crystal growth hall in IKZ)
Photo: IKZ

IKZ, the PVA TePla AG, and the Siltronic AG – are combining their expertise in a pioneering project to scale up aluminum nitride (AlN) crystal growth.
The project focuses on the fabrication of 4-inch AlN substrates to enable advanced applications in high-power electronics and ultraviolet photonics.

Volume Crystals

Section Semiconductors
Section Oxides & Fluorides

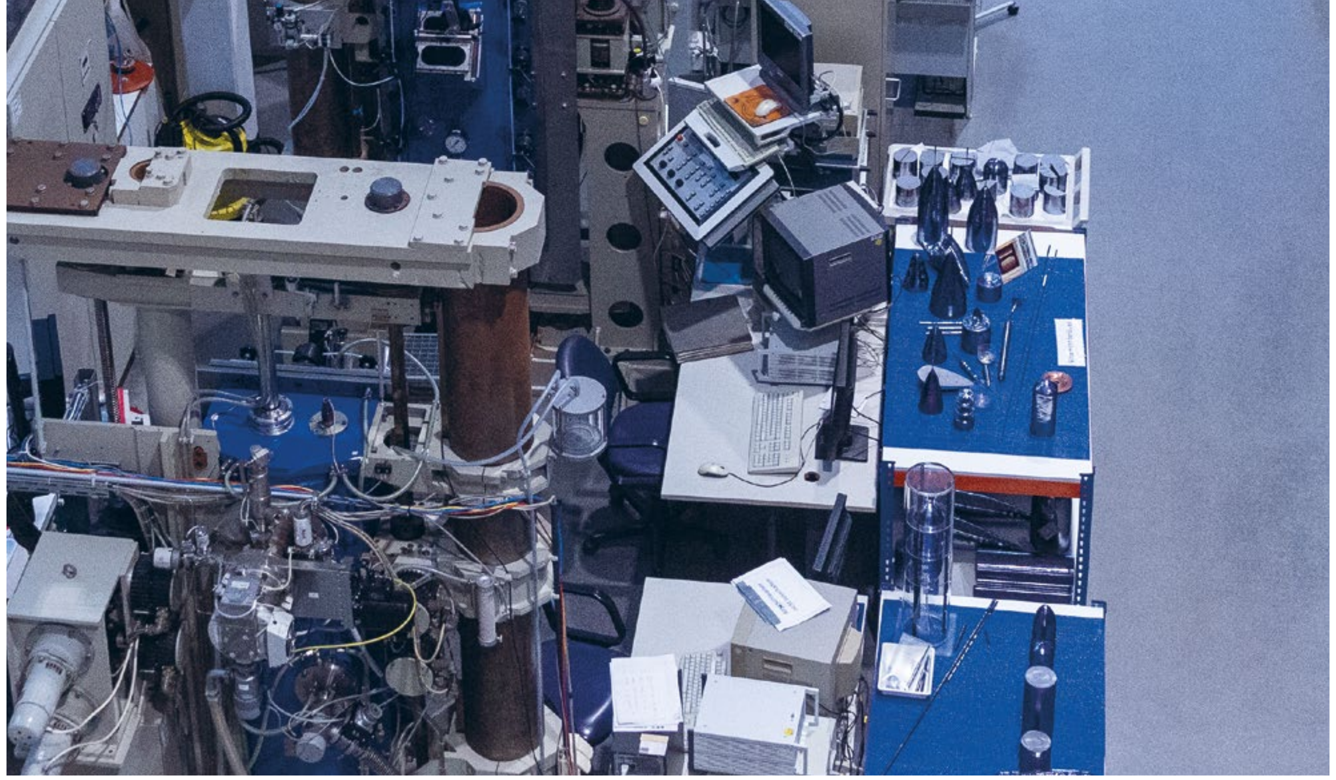

Czochralski growth system *Photo: Berit Kraushaar*

A. N. SUBRAMANIAN, C. RICHTER, A. GYBIN, M. P. KABUKCUOGLU, E. HAMANN, M. ZUBER, M. OEZKENT, C. GUGUSCHEV, U. JUDA, T. SCHROEDER, N. V. ABROSIMOV, R. RADHAKRISHNAN SUMATHI, K.-P. GRADWOHL.

Leibniz-Institut für Kristallzüchtung (IKZ), Berlin, Germany

On the Czochralski growth of Si_xGe_{1-x} crystals as substrates for strained Ge quantum well heterostructures

Czochralski-grown Ge-rich SiGe bulk crystals could become a better substrate platform for strained Ge quantum-well heterostructures than the strain-relaxed SiGe buffer layers used today. Ge/SiGe heterostructures are a leading platform for hole-spin qubits because strained Ge offers low effective mass, strong electrostatic tunability, and operation above 1 K [1]. Conventional graded epitaxial SiGe buffers inherently develop threading dislocations and cross-hatch compositional undulations, introducing strain fluctuations, charge noise, and nonuniformity that limit qubit performance. This motivates the exploration of Ge-rich SiGe grown as a bulk single crystal, with wafers used directly as substrates.

Our publication [2] presents proof-of-concept growth of Si_xGe_{1-x} bulk crystals as a potential replacement for CVD-grown virtual substrates. Using the Czochralski method with continuous Si feeding into a Ge melt, wafers up to about 15 mm in diameter were obtained with Si concentrations of roughly 16–18 at.%. These wafers exhibit improved compositional homogeneity compared to conventional epitaxial Ge-rich SiGe buffers. In particular, $Si_{0.16}Ge_{0.84}$ wafers show compositional fluctuations < 0.4 at.% and dislocation densities < 3×10⁶ cm⁻², while the central wafer region shows no measurable composition fluctuation and fewer than 10^5 dislocations per cm^2. Taken together, these results suggest that the concept is technologically feasible.

The growth of Ge-rich SiGe bulk single crystals with high Si content remains challenging due to the Si–Ge phase diagram. Near the Ge-rich crystallization regime, Si dissolves only slowly into the melt but segregates strongly into the crystal, leading to abrupt composition changes and melt inhomogeneities during growth. These effects promote constitutional supercooling and polycrystalline growth, limiting previous single-crystal growth to approximately x=0.15. Therefore, achieving Si concentrations of about 18 at.% while maintaining single crystallinity (Fig. 1 a) represents an important step toward stable bulk growth at higher Si concentrations in Ge-rich SiGe bulk crystals.

For crystal growth, 750 g of high-purity Ge were melted and seeded with a [100]-oriented Ge crystal. After neck formation, six Si rods were gradually immersed into the melt to provide continuous Si feeding. A Si rod immersion rate of 0.5 mm/h and a pulling rate of 1.5 mm/h yielded a net growth rate of about 1.0 mm/h. The continuous-feed approach minimized abrupt composition changes.

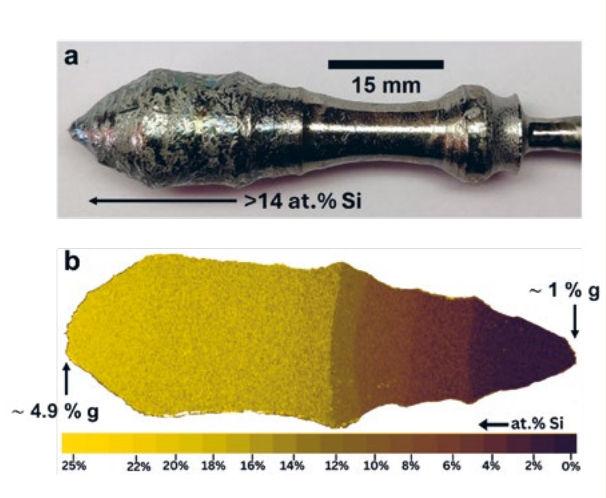

Fig. 1 a) Grown Si_xGe_{1-x} crystal with the marked region containing more than 14 at.% Si (b) XRF map of the crystal depicting the measured Si distribution

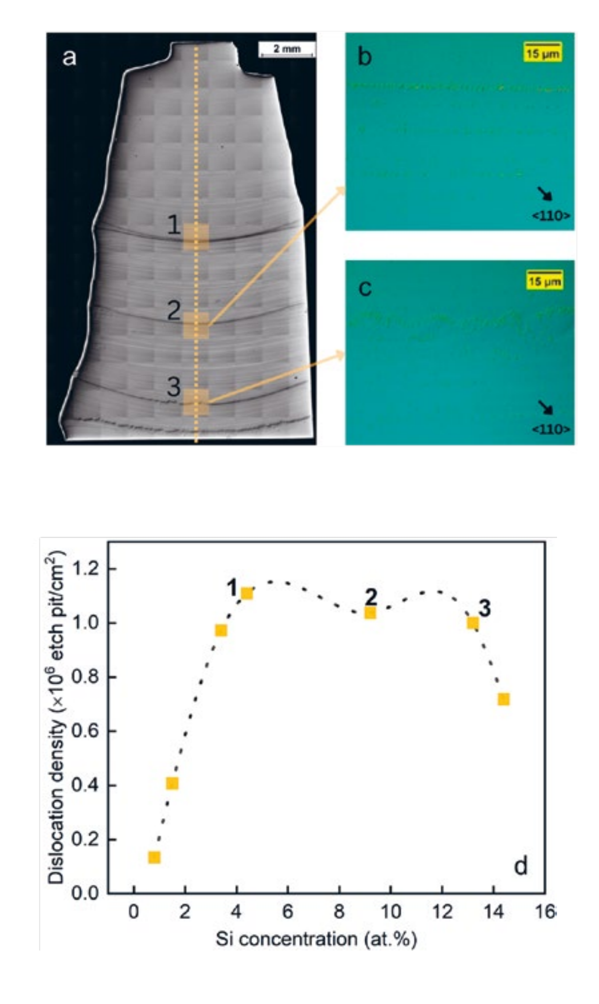

Fig. 2 Etch pit density measurements: (a) position of the dislocations quantified along the centre of the etched longitudinal cut (b) magnified image of position 2 (c) magnified image of position 3 showing the sudden shift to a multi-crystalline regime and then back to single crystalline (d) graph comparing the quantified dislocation density vs the Si concentration along the length of the longitudinal sample shown in (a)

Crystal characterization employed micro-X-ray fluorescence (µ-XRF), rocking-curve imaging (RCI), white-beam x-ray topography (WB-XRT), four-point-probe resistivity measurements (4PP), and etch-pit-density analysis (EPD) to assess composition, homogeneity, electrical purity, and defect density. Along the crystal length, the Si concentration increases from nearly 0 at the seed end to about 19 at.% Si near the tail (Fig. 1 b), broadly following a simple Scheil segregation-based model. The measured profile deviates slightly from the model, indicating non-uniform Si dissolution in the melt, but the agreement remains sufficient for designing future experiments. To assess compositional homogeneity, a wafer was cut from a region containing approximately 16 at.% Si. RCI reveals Si concentrations > 16 at.% across the single-crystalline region, reaching > 16.6 at.% near the centre [2]. In the central region, the local Si fluctuation is only about 0.4 at.%, markedly lower than the roughly 1 at.% undulation amplitude typical of cross-hatch in comparable strain-relaxed SiGe buffers.

Resistivity increases from 40 to 600 Ω·cm, reflecting reduced carrier mobility while indicating a low net carrier density of ~10^{13} cm⁻³. This purity surpasses that of typical graded epitaxial substrates and may provide an advantage for quantum devices by reducing background charge disorder.

EDLM and WB-XRT reveal a homogeneous central crystal region, while the edges show small-angle grain boundaries and higher defect densities. The pure-Ge seed-end remains dislocation-free, but dislocations emerge > ~1 at.% Si, initially at densities of ~10³ cm⁻², and increase with further Si incorporation (as shown in Fig. 2 a, b and c). The significant increase in dislocation density coincides with abrupt Si concentration jumps, which likely destabilize the melt–crystal interface and promote misfit-dislocation formation.

The wafer-level analysis highlights both the current progress and the remaining limitations. In the central wafer region, the dislocation density is about 2×10⁵ cm⁻², while higher values occur near the crystal edge due to thermal stress introduced during the cooling down phase. In some high-Si regions, dislocation densities < 10⁵ cm⁻² are observed (Fig. 2 d), demonstrating the potential for low-defect growth even above 18 at.% Si.

In conclusion, the results demonstrate the feasibility of Cz-grown Ge-rich SiGe bulk crystals as substrates for strained Ge quantum-well heterostructures. The main challenges remain slow and inhomogeneous Si dissolution, oxide formation, abrupt Si jumps, and growth-process control. Overall, this work demonstrates the potential of bulk-grown Ge-rich SiGe wafers with high purity, reduced compositional variation, and locally low dislocation density as an alternative to graded epitaxial buffers.

References

[1] Scappucci, G. et al. Nat. Rev. Mater. 6, 926–943 (2020). https://doi.org/10.1038/s41578-020-00262-z

[2] Subramanian, A. N. et al. J. Appl. Phys. 137, (2025). https://doi.org/10.1063/5.0238533

Yttrium scandium gallium aluminum garnet (YSGAG) single crystals *Photo: IKZ*

C. GUGUSCHEV (1), C. DUBS (2), R. BLUKIS (1), R. KOC (1), C. RHODE (1), K. BERGER (1), O. SURZHENKO (2), C. RICHTER (1), K. MESHRAM (1), N. DROPKA (1), D. PULMANNOVÁ (1), M. BRÜTZAM (1), C. BERRYMAN (1), M. BICKERMANN (1), R. O. SERHA (3), J. SCHÄFER (4), M. WEILER (4), P. PIRRO (5), A. V. CHUMAK (3)

(1) Leibniz-Institut für Kristallzüchtung, Berlin, Germany
(2) INNOVENT e.V. Technologieentwicklung, Jena, Germany
(3) University of Vienna, Faculty of Physics, Vienna, Austria
(4) RPTU Kaiserslautern-Landau, Kaiserslautern, Germany

Novel diamagnetic garnet-type substrate single crystals for yttrium iron garnet $Y_3Fe_5O_{12}$ films with ultralow-damping at cryogenic temperatures

Yttrium iron garnet (YIG) is a cornerstone material in spintronics and magnonics due to its exceptionally low magnetic damping, which allows the propagation of spin waves and their quasiparticles, magnons, over long distances. For applications in radio-frequency technology and magnon-based unconventional or quantum information processing, YIG must be fabricated as thin single-crystal films with thicknesses ranging from tens of nanometers to several micrometers. For room temperature applications, gadolinium gallium garnet (GGG) has long been the standard substrate for epitaxial YIG growth, providing excellent lattice matching and film quality. However, the ferromagnetic resonance (FMR) linewidth of YIG films grown on GGG substrates is significantly affected by stray fields originating from the partially magnetized paramagnetic GGG at low temperatures under externally applied magnetic fields. Together with a resulting magnetic coupling between magnetized substrate and film, this introduces additional dissipation channels, drastically shortening magnon lifetimes and making such systems unsuitable for quantum experiments. This long-standing bottleneck in quantum magnonics – a field exploring the quantum properties of magnons and their application in quantum information technology – has now been overcome by a collaborative international effort. Our novel diamagnetic yttrium scandium gallium aluminum garnet (YSGAG) solid solution single crystals eliminate magnetization issues at millikelvin temperatures. The current Czochralski-grown YSGAG crystals with cubic crystal structure [1] have diameters up to about 30 mm and total lengths up to about 100 mm (Fig. 1). Substrates with high chemical homogeneity and diameters up to 1 inch were prepared at the institute (Fig. 2). Rocking curve measurements on polished sections revealed typical FWHM values of about 22 arcsec, which is indicative of relatively high structural quality for a solid-solution crystal. The composition of the crystals can be finely tuned to precisely adjust the lattice parameter in the range of 12.362 to 12.426 Å, which allows a perfect match with the lattice parameter of YIG (a ~ 12.376 Å).

Analysis of YSGAG substrates using powder X-ray diffraction (XRD) demonstrated that a perfect lattice match to YIG has indeed been achieved (Fig. 3a). To enable the growth of high-quality crystals with minimized internal stresses, simulations of the growth process are also performed (Fig. 3c), however, these require thermodynamic input parameters. To provide these, thermal analysis using differential thermal analysis (DTA) and thermogravimetry (TG) were performed (Fig. 3b). Due to the high melting point of YSGAG, determined as 1851 °C, the measurements were challenging due to atmosphere restrictions of the equipment. By comparing melting peak areas of YSGAG, YAG reference and compensating for Ga evaporation enthalpy of melting could be determined as 641 kJ mol^{-1}. This is the first such determination of thermodynamic parameters experimentally in this solid solution system.

Such novel solid-solution substrate crystals are the foundation toward ultralong-lived magnons in thin films and pave the way for scalable quantum magnonic devices with coherent magnon transport, strong magnon–phonon and magnon–qubit coupling and for the development of integrated quantum networks. Initial results from FMR measurements at low temperatures at the University of Vienna for non-optimized YIG films, which were grown at INNOVENT on non-optimized YSGAG substrates, revealed an absolute FMR linewidth of 2.3 Oe at 30 mK and 5 GHz. This is the lowest value ever achieved for YIG layers at cryogenic temperatures [2].

Acknowledgments: The work is supported by the Federal Ministry of Research, Technology and Space (BMFTR) under the reference numbers (13N17108, 13N17109 and 13N17110) within a collaborative project "Low-loss materials for integrated magnonic-superconducting quantum technologies (MagSQuant)". This research was funded in part by the Austrian Science Fund (FWF) project Paramagnonics (10.55776/6568).

Fig. 1 Novel YSGAG solid solution substrate single crystals

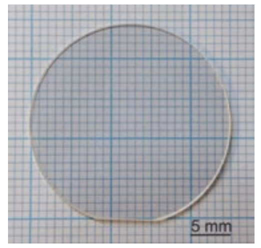

Fig. 2 Both-sided chemical-mechanical polished 1-inch YSGAG substrate

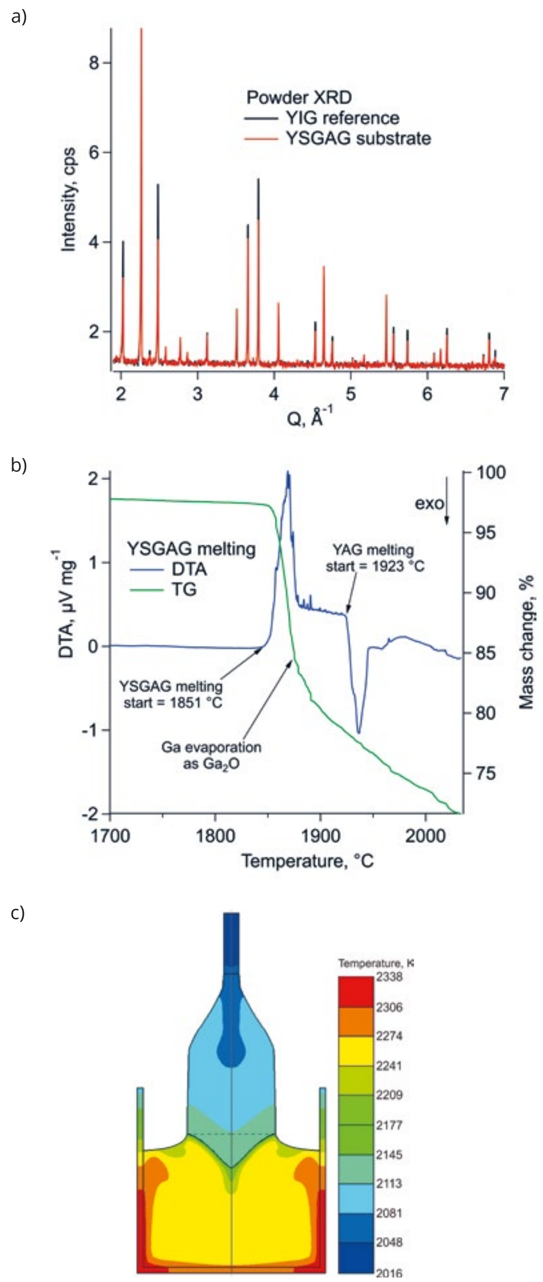

Fig. 3 Powder XRD patterns (a) of YIG and YSGAG showing perfect reflection peak position match. Reflection intensities do differ due to different chemical compositions. Thermal analysis (b), DTA and TG of YSGAG. Initial numerical calculations of the crystal growth process (c).

References

[1] C. Guguschev, C. Dubs, R. Blukis, O. Surzhenko, M. Brützam, R. Koc, C. Rhode, K. Berger, C. Richter, C. Berryman, R. O. Serha, A. V. Chumak, https://doi.org/10.48550/arXiv.2508.18101

[2] R. O. Serha, C. Dubs, C. Guguschev, B. Aichner, D. Schmoll, J. Schäfer, J. Panda, M. Weiler, P. Pirro, M. Urbánek, A. V. Chumak, Communications Materials, 7, 134 (2026). https://doi.org/10.1038/s43246-026-01146-5

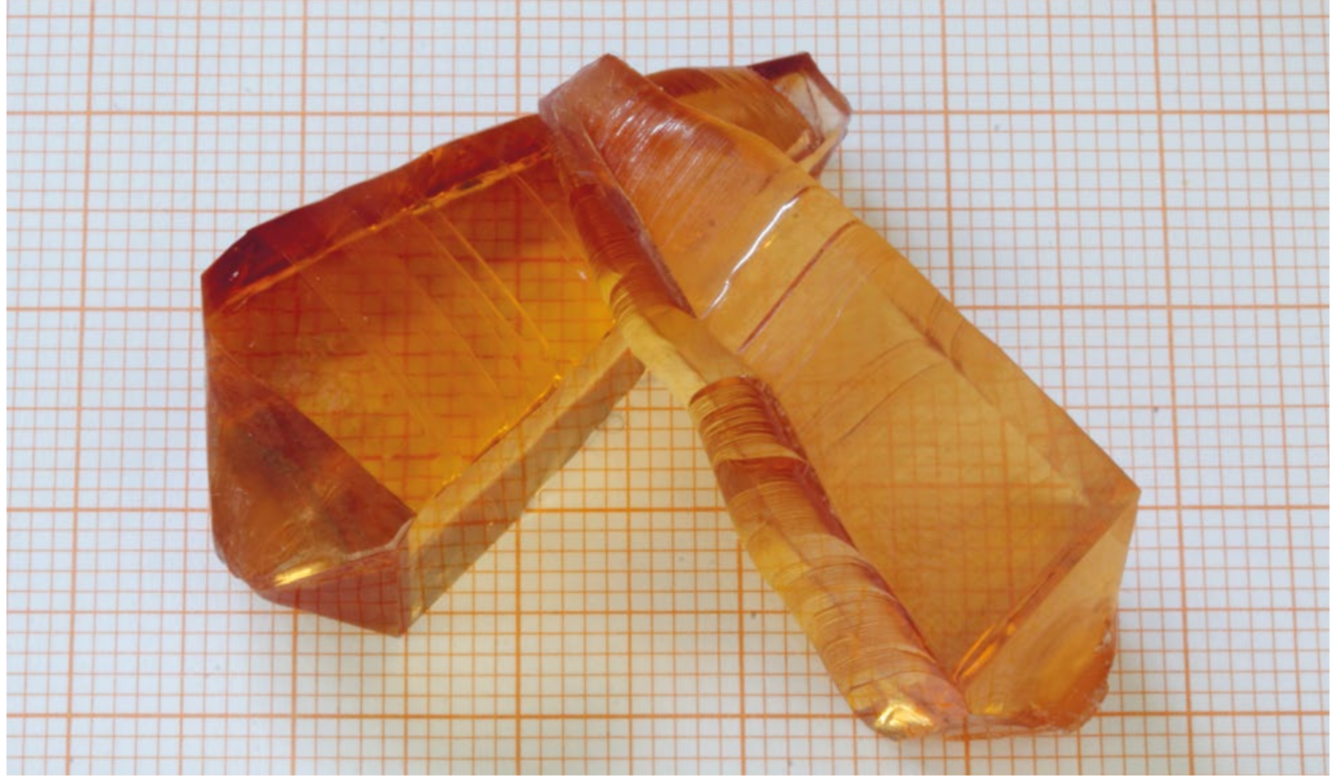

r-GeO_2 single crystals *Photo: Zbigniew Galazka*

Z. GALAZKA, S. BIN ANOOZ, A. FIEDLER, R. BLUKIS, S. GANSCHOW, A. KWASNIEWSKI, M. ALBRECHT, U. JUDA, K. STOLZE, M. IMMING-FRIEDLAND, T. SCHULZ, M. SÜNDERMANN, T. WURCHE, M. HANDWERG, M. PIETSCH, T. SCHRÖDER, M. BICKERMANN

Leibniz-Institut für Kristallzüchtung (IKZ), Berlin, Germany

Rutile-GeO_2 single crystals: growth, wafers, and properties

A continuous search for new ultra-wide bandgap (UWBG) oxide compounds enabling next generation power electronic materials revealed in recent years rutile-phase of GeO_2 (r-GeO_2) as a promising candidate for that purpose. Theoretical work showed promising physical properties of r-GeO_2 : a direct bandgap of 4.6 eV, capability of obtaining bipolar doping with high electron mobility (> 350 $cm^2V^{-1}s^{-1}$ at room temperature (RT)), high Baliga Figure of Merit, and high thermal conductivity of 58 $Wm^{-1}K^{-1}$. Additionally, the low melting point of GeO_2 (1115°C) enables low growth costs of bulk r-GeO_2 single crystals by avoiding Ir crucibles, using cheap thermal insulation, and low energy consumption. Further, the tetragonal crystal system, high hardness, and resistance to many acids make r-GeO_2 a suitable material for wafer fabrication and application in harsh environment.

GeO_2 is an excellent glass former, therefore crystallizing r-GeO_2 requires a glass network breaker (solution). Further, the first phase that crystallizes is an alpha-quartz (trigonal) analog, which is water soluble. The rutile phase crystallizes at yet lower temperature (~1050°C), so the solution must also lower the melting point. This is why so far only small crystals (a few mm in size) have been demonstrated by the hydrothermal, top-seeded solution growth (TSSG), and other flux methods, which are of poor structural quality, contaminated with impurities, and not suitable for wafer fabrication. As a result, thin-film growth activity is carried out using heteroepitaxy with difficulties in obtaining a pure rutile phase. At IKZ we are developing bulk crystal growth of r-GeO_2 single crystals [1,2] by a significantly modified TSSG method [3]. The development was accompanied by extensive thermodynamical studies, comprehensive growth experiments, and systematic characterization. For crystal growth, we investigated different solutions at different concentrations, a wide range of O_2 concentrations in the growth atmosphere, proper melt preparation (mechanical mixing, heating, overheating, cooling, and soak times), various dopants (towards n- and p-type conductivities), and different growth parameters (growth and rotation rates, temperature control, seeding temperature, etc.). We found optimal conditions for solution composition of $K_2CO_3 + Na_2CO_3$ (2.5 – 5 mol.%), O_2 concentration (about 2 – 4 vol.%), growth rate (0.1 – 0.2 mm/h), and rotation rate (10 – 20 rpm), and a growth direction along the [001] axis. Also, some of the crystals have been intentionally doped with Sb, F, Al, or Ga.

Examples of the obtained undoped r-GeO_2 single crystals of diameter 10 – 15 mm and length of 25 mm are shown in Fig. 1a. The crystals have a clear appearance with no inclusions, grains, or cracks. From the crystals, epi-ready wafers 5 × 5 mm^2 or 10 × 10 mm^2 in size with different orientation were fabricated at IKZ, with the surface chemo-mechanically polished, as shown in Fig. 1b. Sb-doped n-type conductive r-GeO_2 wafers (Fig. 1c) were prepared for electrical characterization and device fabrication. X-ray rocking curves (Fig. 2a) show very narrow reflexes across different orientations (FWHM = 13 – 26 arcsec), and atomic force microscopy (AFM) evidenced very good flatness (Fig. 2b) with RMS roughness of 100 – 150 pm, which was further improved even down to 70 pm after annealing. Further, transmission electron microscopy (TEM) investigation did not show any structural defects, indicating their density in the samples is low.

Ellipsometry measurements revealed direct bandgaps of 5.1 (E⊥c) and 5.6 eV (E||c), transmittance spectra showed a full transparency in the visible and NIR spectral regions, while photoluminescence exhibited a very intense luminescence peaking at 520 nm. Thermal conductivity at RT was measured as 45 $WK^{-1}m^{-1}$ along the [001] direction. We have shown for the first time that doping with Sb can lead to very high free electron concentrations of 8×10^{19} – 2.2×10^{20} cm^{-3} with at the same time considerable electron mobilities of 35 – 50 $cm^2V^{-1}s^{-1}$, rendering the crystals well suited for vertical power devices, where the current flows through the substrate. Fluorine doping also induces electrical conductivity. In contrast, simple doping with Al and/or Ga did not induce p-type conductivity. Other approaches need to be applied towards p-type doping, which are currently under study.

The r-GeO_2 wafers will be used for development of thin-film homoepitaxy by MOVPE at IKZ in the near future. In the meantime, wafers were successfully utilized to demonstrate first r-GeO_2 MOSFET transistors by ion implantation at FBH [4].

This work was funded by the Leibniz Association in the frame of the Leibniz Competition under grant number K417/2021.

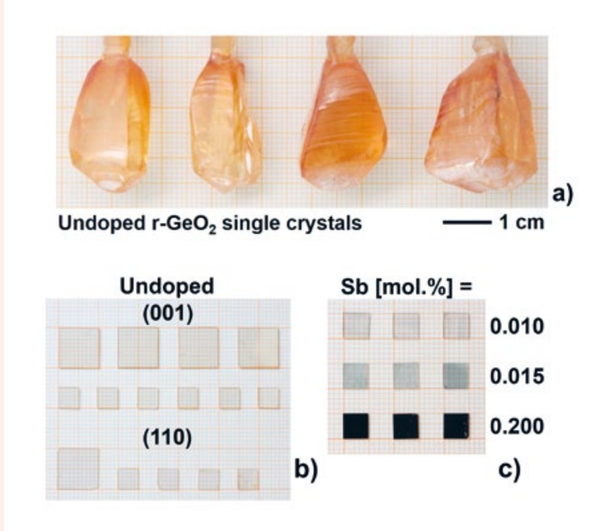

Fig. 1 (a) undoped r-GeO_2 single crystals grown by the TSSG; (b) undoped r-GeO_2 wafers; (c) Sb-doped r-GeO_2 wafers. (reprinted from [2] under CC BY 4.0)

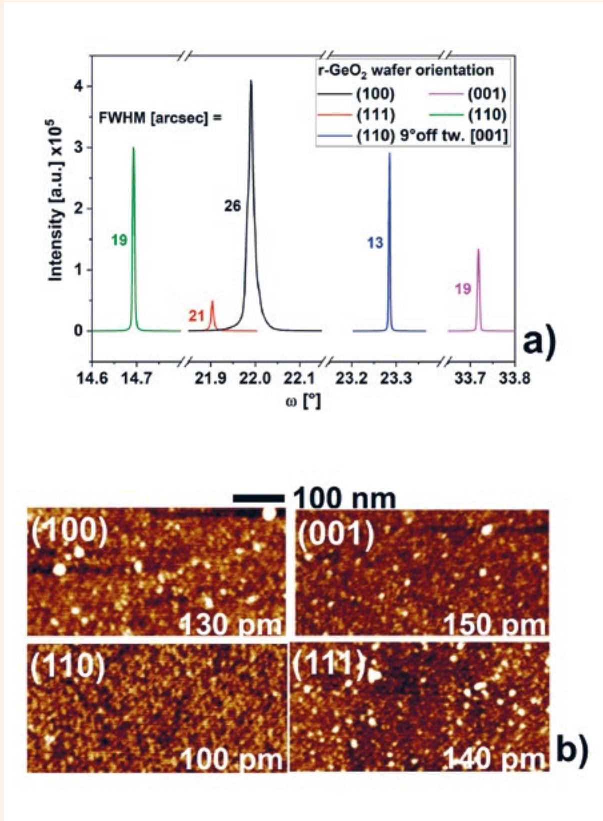

Fig. 2 (a) X-ray rocking curves and (b) AFM images of differently oriented r-GeO_2 wafers prepared from as-grown single crystals shown in Fig. 1. (reprinted from [2] under CC BY 4.0)

References

[1] Z. Galazka, R. Blukis, A. Fiedler, S. Bin Anooz, J. Zhang, M. Albrecht, T. Remmele, T. Schulz, D. Klimm, M. Pietsch, A. Kwasniewski, A. Dittmar, S. Ganschow, U. Juda, K. Stolze, M. Suendermann, T. Schroeder, M. Bickermann; Phys. Status Solidi (b) 262 (2024) 2400326. https://doi.org/10.1002/pssb.202400326

[2] Z. Galazka, S. Bin Anooz, S. Ganschow, A. Kwasniewski, U. Juda, M. Imming-Friedland, T. Wurche, A. Fiedler, T. Schroeder, M. Bickermann; Cryst. Res. Technol. 61 (2026) e70072. https://doi.org/10.1002/crat.70072

[3] Z. Galazka, S. Ganschow, T. Schroeder, M. Bickermann; PCT patent application no. PCT/EP2025/076985 (2025).

[4] K. Tetzner, Z. Galazka, A. Thies, A. Külberg, O. Hilt; IEEE Electron Device Lett. 47 (2026) 566-569. https://doi.org/10.1109/LED.2025.3638262

Research highlights

Nanostructures & Layers

Section Semiconductor Nanostructures
Section Thin Oxide Films

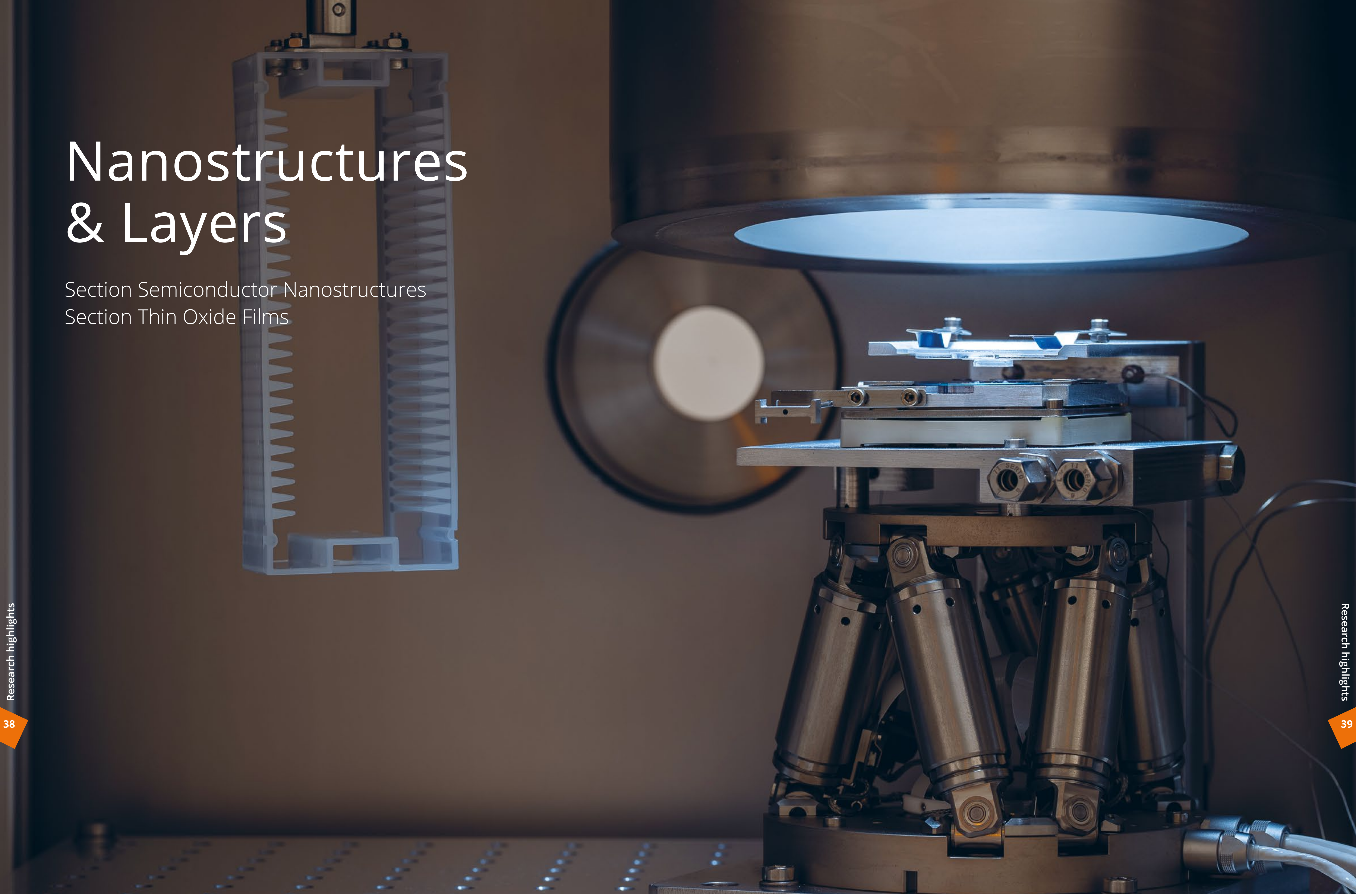

Research highlights

IKZ Annual Report 2025

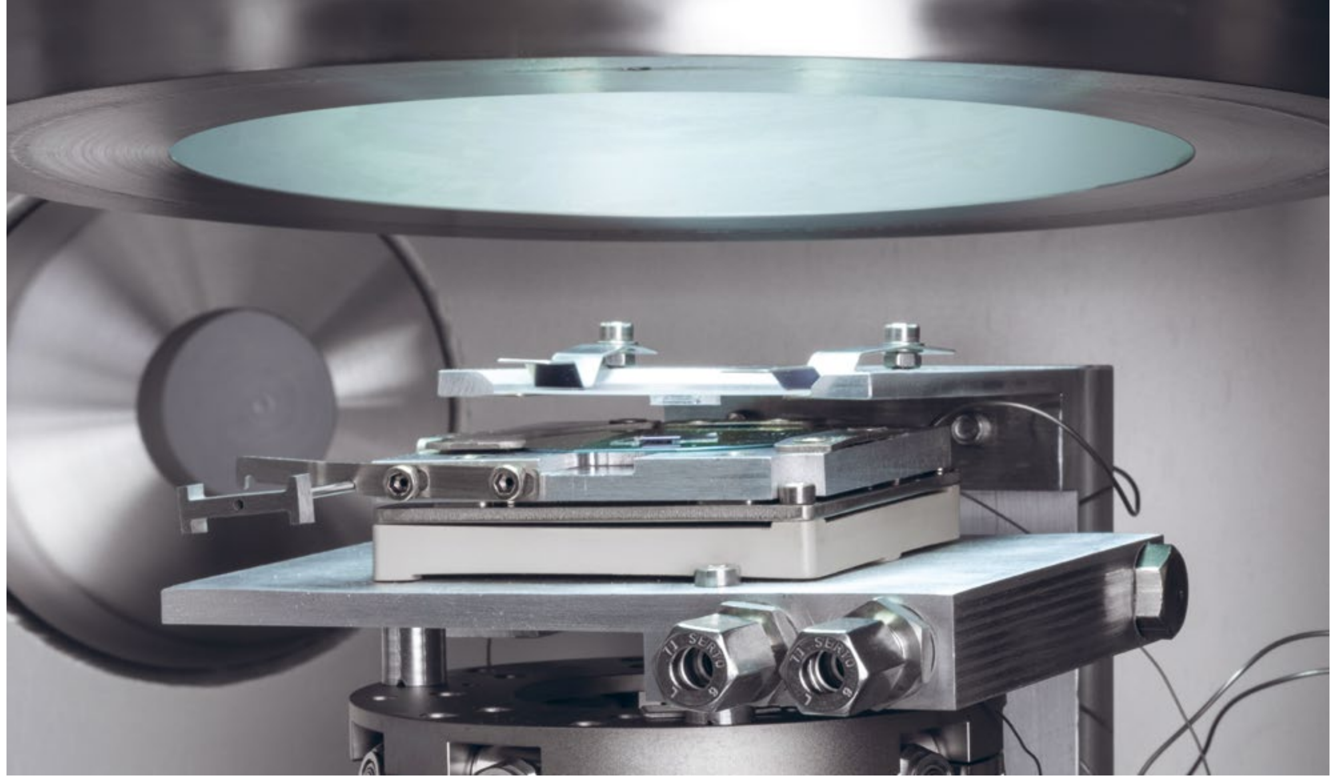

Layer transfer station to place thin crystalline membranes onto arbitrary substrates, for example 2D-MoS_2 on top of a plasmonic structure.
Photo: Simon Eichmann

N. ZORN MORALES (2), D. STEFFEN RÜHL (2), S. SADOFEV (1), E. LIST-KRATOCHVIL (2), S. BLUMSTENGEL (2)

(1) Leibniz-Institut für Kristallzüchtung (IKZ), Berlin, Germany
(2) Department of Chemistry & Center for the Science of Materials Berlin, Humboldt-Universität zu Berlin, Germany

Plasmon-mediated hybridization of Wannier-Mott and Frenkel excitons in a monolayer WS_2–J-aggregate hybrid system

Hybrid light-matter states, also called polaritons, are of great interest due to their unique physical properties and potential applications in physics and chemistry. While initial research interest was triggered by applications ranging from low-threshold power lasers in semiconductors to photonic quantum information, in recent years the possibility of manipulating material properties such as charge and energy transport in organic materials and chemical reactivity has been discovered and is now being intensively researched. The most important prerequisites for achieving the strong coupling regime of hybrid light-matter states are intense narrowband electronic or vibrational transitions and a reduction of the effective mode volume for photons. In practice, surface plasmon polaritons, i.e., electromagnetic excitations propagating at the interface between dielectric and metal, allow for strong electromagnetic field confinement and local field enhancement. Two-dimensional (2D) transition metal dichalcogenides (TMDCs) and molecular J-aggregates are particularly suited since they both exhibit narrow excitonic transitions with large oscillator strengths and exciton binding energies, allowing excitons to persist up to room temperature.

We are interested in the investigation of room-temperature hybridization of dissimilar excitons, namely "large" weakly bound Wannier-Mott-excitons where the diameter exceeds interatomic or intermolecular distances and "small" tightly bound Frenkel-excitons which are confined to individual molecules. For this purpose, a tuneable plasmonic platform consisting of a thin silver film, a dielectric spacer, and a monolayer (1L) of WS_2 in close contact with molecular J-aggregates is fabricated [1].

Large-area 1L-WS_2 (1 cm^2) was obtained by pulsed thermal deposition (PTD) and subsequent polymer-based wet transfer. PTD is a versatile and easy to implement method which demonstrated the fabrication of large-area ternary $(Mo,W)S_2$ monolayers as well as heterostructures involving metallic TaS_2 [2]. 5,5',6,6'-tetrachloro-1,1'-diethyl-3,3'-di(4-sulfobutyl)-benzimid-azolocarbocyanine (TDBC) has been selected on the organic side of the hybrid stack. TDBC is a thoroughly studied cyanine dye, which shows J-aggregation both in solution and in solid state.

The plasmonic platform allows room-temperature hybridization of dissimilar Wannier–Mott excitons (WMX) in 1L-WS_2 and Frenkel excitons (FX) in molecular J-aggregates through strong coupling (SC) to surface plasmon polaritons (SSPs) of the Ag-film. We employ angle-dependent total internal reflection ellipsometry (TIRE) and construct the exciton and polariton dispersion by varying the angle of incidence. We detect three coupled resonances by the observation of double Rabi splitting, indicating hybridization of WMX and FX with SPP in the SC regime (see Fig. 1).

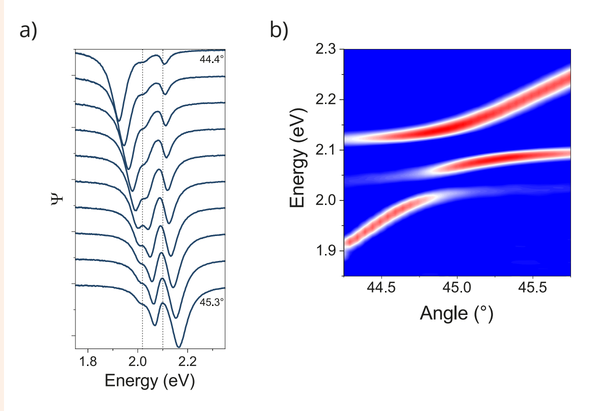

Fig. 1 a) Angle-dependent TIRE Ψ spectra of the hybrid stack. The red dashed line shows a fit of the spectrum at 44.9° to derive the absorption coefficient spectra depicted in Figure 1b. b) Density plot of the complex Fresnel reflection coefficients for p- and s-polarized light versus photon energy and incident angle constructed from the TIRE data. For better contrast, the second derivative $\partial^2/\partial E^2|r_p/r_s|$ is plotted (reprinted from [1] under CC BY 4.0).

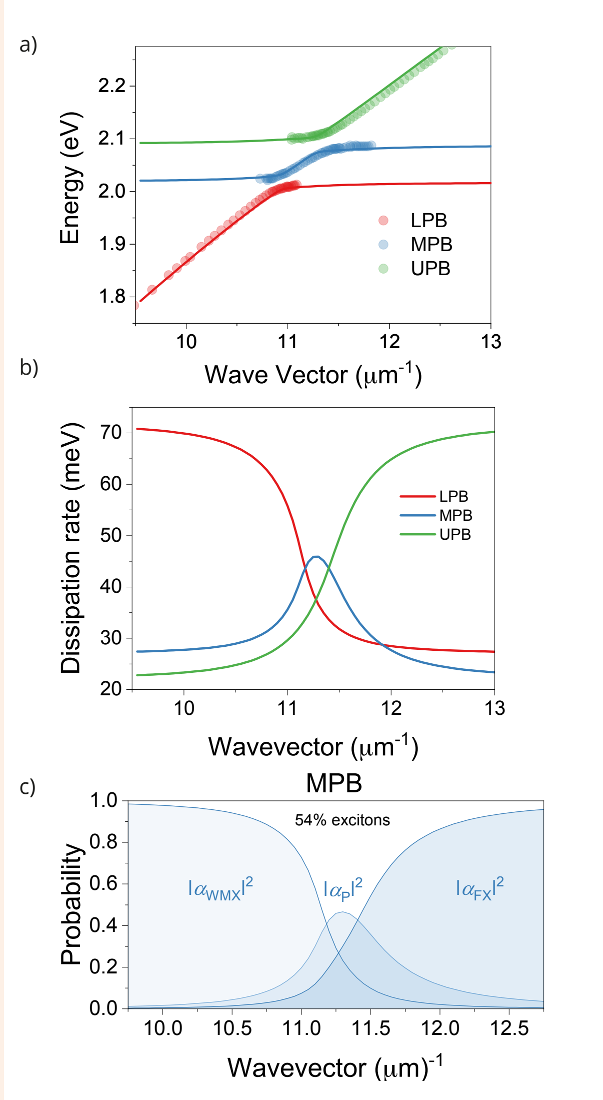

Fig. 2 a) Dispersion relation E versus k‖ of the coupled WMX–FX–SPP resonances of the hybrid stack. The symbols represent the energetic positions of the minima in the |rp/rs| spectra. The solid line is a fit to the data using the coupled oscillator model. b) Derived dissipation rates [Im(E)] of the three polariton branches. c) Hopfield coefficients of the middle polariton branch (MPB) (reprinted from [1] under CC BY 4.0)

The coupling between the excitons and the SPPs is analyzed by a coupled oscillator model, allowing us to derive the coupling strengths and Hopfield coefficients (see Fig. 2). The wave number dependence, i.e. angle dependence in corresponding ellipsometry measurements, demonstrates the modulation of the polariton characteristic by the number of molecules involved. The achieved Rabi splitting is 51 meV and 76 meV at the WMX and FX resonances, correspondingly. Via changing the number of molecules participating in the coupling, the character of the polariton mode can be changed from more photon- to more exciton-like and consequently the dissipation rate controlled.

This study demonstrates a simple plasmonic platform for hybridizing excitons of different materials, enabling improved control over energy losses and modulation parameters. In principle, the interaction between WMX and SPPs can be controlled by electrostatic gating. This becomes particularly appealing when direct coupling between the FX and WMX resonances is present. In this case, the observed mode splitting at the aggregates FX resonance could be remotely controlled via gating of the TMDC and the interaction switched between the weak and SC regimes.

References

[1] N. Zorn Morales, D.S. Rühl, S. Sadofev, E. List-Kratochvil, S. Blumstengel, 2025. Plasmon-Mediated Hybridization of Wannier–Mott and Frenkel Excitons in a Monolayer WS2–J-Aggregate Hybrid System. physica status solidi (RRL)– Rapid Research Letters, 19(6), p.2400417. https://doi.org/10.1002/pssr.202400417

[2] N. Mutz, T. Meisel, H. Kirmse, S. Park, N. Severin, J.P. Rabe, E. List-Kratochvil, N. Koch, C.T. Koch, S. Blumstengel, S. Sadofev, 2019. Pulsed thermal deposition of binary and ternary transition metal dichalcogenide monolayers and heterostructures. Applied Physics Letters, 114(16). https://doi.org/10.1063/1.5088758

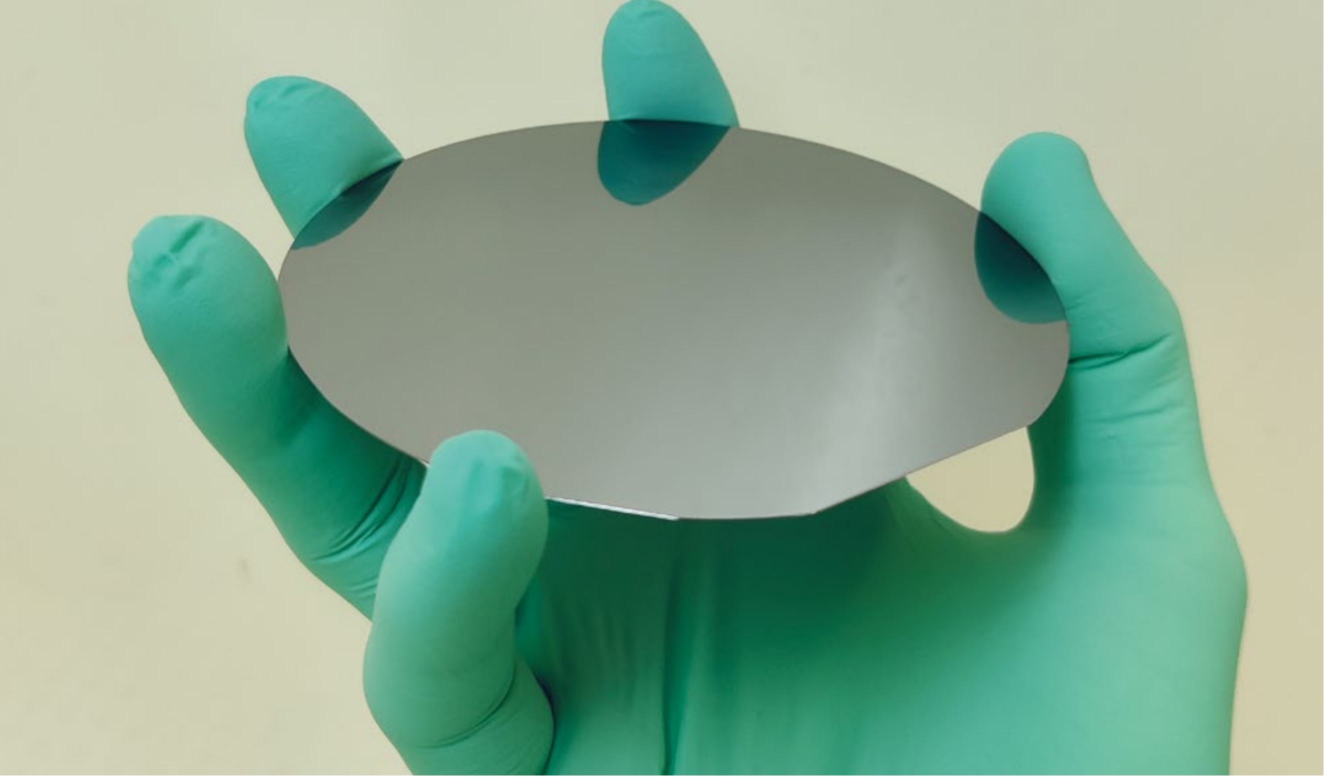

4" Si wafer with SiGe heterostructure *Photo: Kevin Gradwohl*

K.-P. GRADWOHL (1), L. CVITKOVICH (2), C.-H. LU (1), S. KOELLING (3), M. OEZKENT (1), Y. LIU (1), D. WALDHÖR (2), T. GRASSER (2), Y.-M. NIQUET (4), M. ALBRECHT (1), C. RICHTER (1), O. MOUTANABBIR (3), J. MARTIN (1)

(1) Leibniz-Institut für Kristallzüchtung (IKZ), Berlin, Germany
(2) Institute for Microelectronics, Technische Universität Wien, Vienna, Austria
(3) École Polytechnique de Montréal, Montréal, Québec, Canada
(4) Univ. Grenoble Alpes, CEA, IRIG-MEM-L Sim, Grenoble, France

SiGe Wiggle Quantum Wells by MBE

Gate-defined quantum dots in isotopically engineered SiGe heterostructures are a fast developing and promising material platform for quantum computing. These heterostructures consist of strained Si quantum well layers coherently grown on relaxed $Si_{0.7}Ge_{0.3}$, where the strain partially lifts conduction band valley degeneracy. However, the remaining two-fold band energy degeneracy poses a challenge. A reliable integration of a big number of qubits in this material platform will require a technology that allows for a large and controllable valley splitting.

Several approaches to achieve this have been proposed and explored in the past, including atomically-flat interfaces and modifications of the quantum well barriers. However, most recently, an oscillating Ge concentration in the quantum well, a so-called wiggle quantum well (WQW), was proposed and demonstrated to achieve a large and tunable valley splitting in heterostructures grown by chemical vapor deposition (CVD) [2]. Here we demonstrate and investigate the potential of growing such $_{28}$SiGe WQW test structures by molecular beam epitaxy (MBE), which allows for growth at lower temperatures and better compositional control.

WQWs with MBE

The realization of a WQW with enhanced valley splitting requires pronounced Ge concentration oscillations. Precise control of Ge segregation is therefore essential. One effective strategy to suppress Ge segregation is the reduction of the growth temperature. We successfully implemented SiGe growth with such a controlled temperature variation. Figure 1 compares a reference sample grown at constant temperature with a heterostructure fabricated using an optimized oscillating temperature profile. The corresponding time-dependent temperature modulation, together with the Si and Ge shutter configuration, is also shown. The rapid Ge oscillations required for the proposed WQW heterostructures represent a significant technological challenge. Due to the limited heating and cooling ramp rates achievable in MBE, extremely low growth rates are necessary. This, in turn, demands highly controlled growth conditions, particularly with respect to vacuum stability. For the heterostructure shown in Figure 1, evaporation rates as low as 0.001 nm/s (approximately 0.1 monolayers per minute) were employed.

A comparison of ADF-STEM images of the two heterostructures reveals a pronounced difference in Z contrast and, consequently, in the Ge concentration modulation. The corresponding Ge concentration profiles along the WQW, extracted from the STEM images under identical measurement conditions, are presented in Figure 1c. The reduced growth temperature significantly suppresses Ge segregation, enabling substantially lower average Ge concentrations within the WQW. It remains unclear to what extent the residual Ge concentration observed in the valleys of the WQW reflects a physical effect or results from contrast-related artifacts in the TEM analysis.

From the concentration profiles, maximum gradients of approximately 10%/nm are obtained for a constant growth temperature of 500 °C, whereas values of up to 30%/nm are achieved with oscillating temperature growth. The latter clearly demonstrates the high efficiency of segregation suppression by temperature-modulated growth.

Valley splitting simulations

Based on experimentally realistic MBE material parameters (maximum Ge concentration gradients of 30%/nm and finite heating/cooling ramps), tight-binding simulations were performed to evaluate the achievable valley splitting in WQW heterostructures. Representative Ge oscillation profiles with peak concentrations of 10–20% and periods between 1.76 nm and 2.31 nm were considered, corresponding to four to five Ge maxima within a 10 nm Si quantum well.

The simulations show a pronounced enhancement of the valley splitting compared to structures with the same average but homogeneously distributed Ge content. A benchmark value of 200 µeV, considered sufficient for stable spin qubit operation, can be exceeded for optimized oscillatory profiles. For experimentally realized profiles with concentration slopes of 22%/nm, median values slightly above 200 µeV are obtained. For further optimized profiles with sharp peaks and slopes up to 30%/nm, median values around 310 µeV are predicted, with reduced variability expected for realistic, laterally extended quantum dots. Additional variations of the Ge profile (e.g., rounded or spike-like peaks, residual Ge in the valleys) reveal only minor changes in valley splitting, indicating that the WQW concept is robust with respect to profile details.

Hence, with this work we show that with MBE it is possible to achieve sufficient modulation of the Ge concentration to significantly enhance valley splitting. Therefore, WQWs might constitute a promising approach to enhance performance of Si-based electronic qubits.

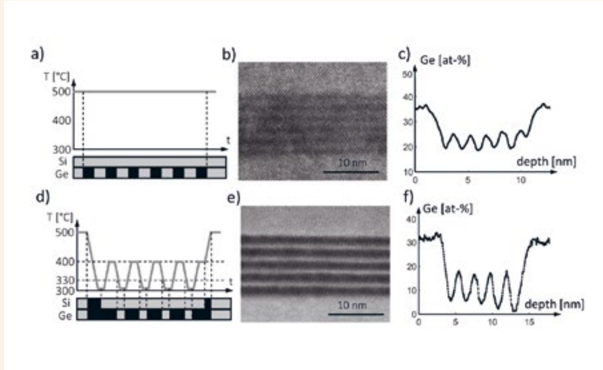

Fig. 1 Comparison of two heterostructures grown at constant temperature (a, b, c) and oscillation growth temperature (d, e, f), respectively. a) and d) show the nominal growth temperature over time together with the Si and Ge shutter configurations where black indicates a closed shutter, with the Si and Ge source kept at the same rate as for the barrier growth. b) and e) the atomic-resolution ADF-STEM images of the heterostructures, and c) and f) the Ge concentration along the heterostructure (reprinted from [2] under CC BY 4.0).

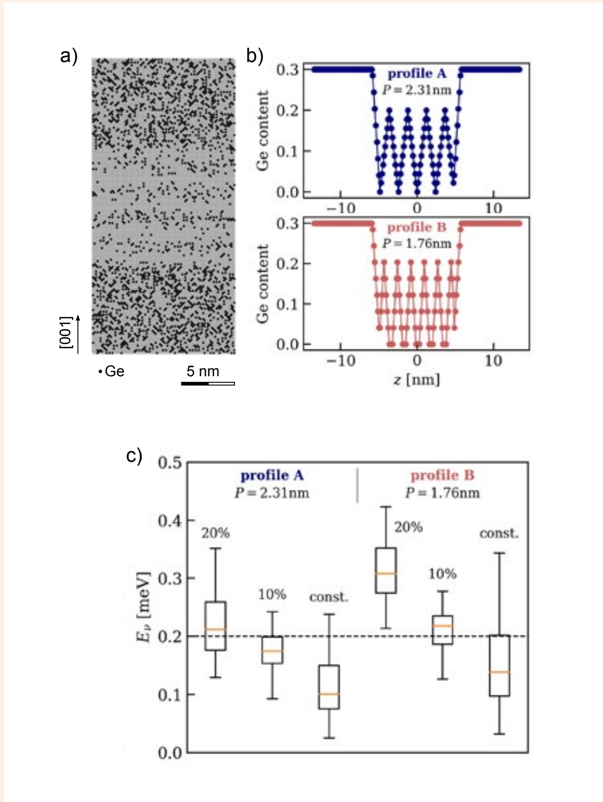

Fig. 2 TB model and valley splitting results. a) Side view of the simulation cell consisting of 230k atoms, where the atoms in black represent Ge. b) Investigated Ge profiles. The length of one oscillation period is given by P. The profile in the top panel is inspired by the Ge profiles in this work. The lower panel shows a Ge profile with a Ge oscillation with wave vector q = 3.5 nm-1. c) Results for valley splittings obtained by sp3d5s* TB calculations for the profiles shown in b) at an electric field of Ez = 5 mV/nm. For each Ge profile, the valley splitting of 50 configurations of Ge atoms were calculated and the median values are given by orange lines, the boxes represent the 25 to 75 percentile ranges, and the whiskers show the full range of data points (reprinted from [2] under CC BY 4.0).

References

[1] I. Fernández de Fuentes, E. Raymenants, B. Undseth, O. Pietx-Casas, S. Philips, M. Mądzik, L. Vandersypen, PRX Quantum 7 (2026), 010308. https://doi.org/10.1103/f285-l2v5

[2] T. McJunkin, B. Harpt, Y. Feng, M.P. Losert, R. Rahman, J.P. Dodson, M.A. Wolfe, D.E. Savage, M.G. Lagally, S.N. Coppersmith, M. Friesen, R. Joynt, M.A. Eriksson, Nat. Commun. 13.1 (2022), 1-7. https://doi.org/10.1038/s41467-022-35510-z

[3] K.-P. Gradwohl, L. Cvitkovich, C.H. Lu, S. Koelling, M. Oezkent, Y. Liu, D. Waldhör, T. Grasser, Y.-M- Niquet, M. Albrecht, C. Richter, O. Moutanabbir, J. Martin, Nano Lett. 25 (2025), p. 4204-4210. https://doi.org/10.1021/acs.nanolett.4c05326

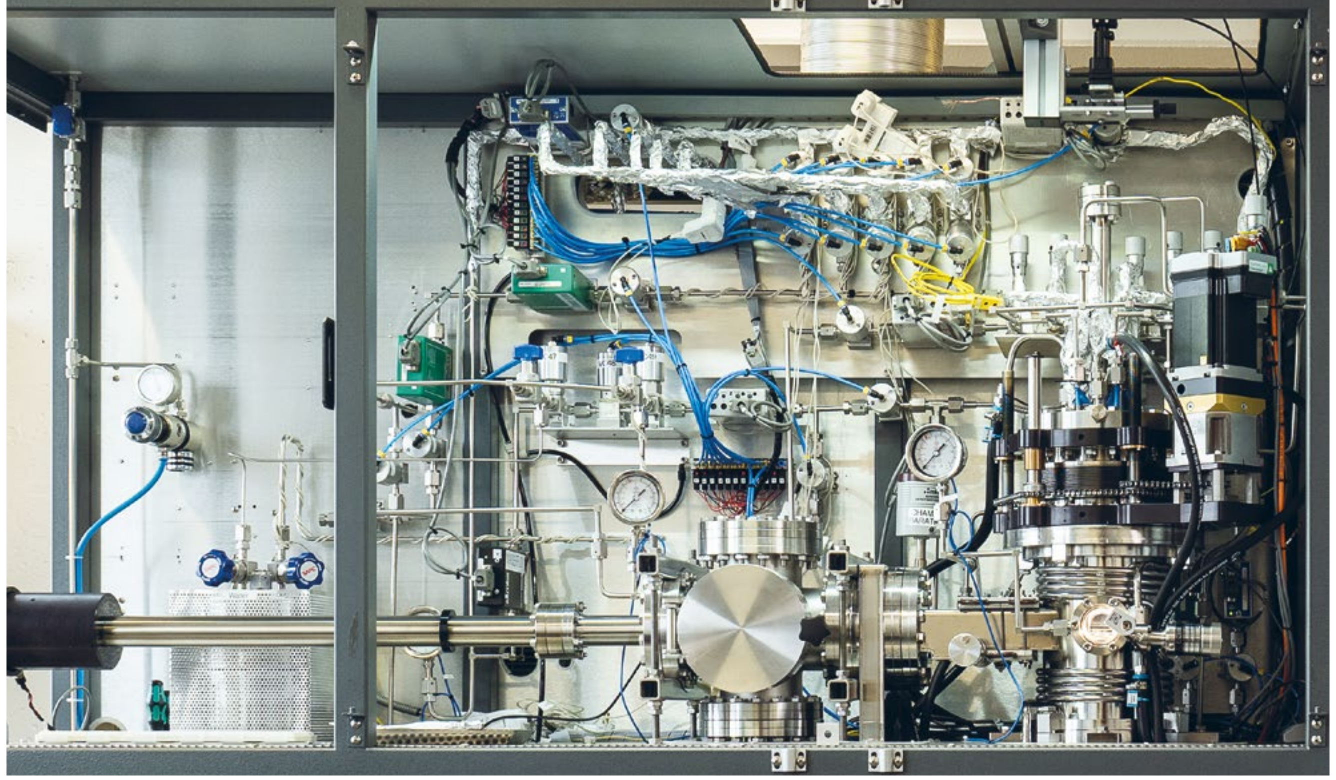

MOVPE reactor for thin-film growth *Photo: HORNNISSEN*

S. B. ANOOZ, T.-S. CHOU, A. AKHTAR, J. REHM, H.-H. CHEN, Z. GALAZKA, M. SCHMIDBAUER, M. ALBRECHT, A. FIEDLER, A. POPP

Leibniz-Institut für Kristallzüchtung (IKZ), Berlin, Germany

First β-Ga_2O_3 thin films grown on β-$(Al_xGa_{1-x})_2O_3$ substrates via MOVPE

Applications for β-Ga_2O_3 are in power electronics, deep-ultraviolet photodetectors, and electronics designed for harsh environments. However, the practical realization of such devices depends on the ability to grow high-quality thin films. One of the key challenges is understanding how strain, which naturally arises when a thin film is grown on a substrate with slightly different lattice parameters, which affects the material's structure, surface quality, and electronic behavior. Strain can be both beneficial and detrimental: it can be used deliberately to tailor material properties, but excessive or uncontrolled strain may lead to defects that degrade device performance.

In this study, we employ metal-organic vapor phase epitaxy (MOVPE), a widely used industrial growth technique, to deposit β-Ga_2O_3 thin films on (100) β-$(Al_xGa_{1-x})_2O_3$ (x = 0.1, 0.15 and 0.2) substrates. By systematically varying the aluminium concentration within the substrate, the degree of lattice mismatch with the epitaxial film can be precisely tuned. This controlled mismatch can induce strain in the β-Ga_2O_3 layers. Structural properties are examined using high-resolution X-ray diffractometry (HR-XRD) technique, which provide insight into lattice parameters, crystal orientation, and strain relaxation. Surface morphology is investigated using atomic force microscopy (AFM). Spectroscopic ellipsometry measurements are employed to determine changes in the band gap.

Increasing aluminum content in the underlying β-$(Al_xGa_{1-x})_2O_3$ substrate substrate reduces the lattice parameters relative to β-Ga_2O_3, thereby inducing compressive strain in the overgrown layer. 2θ–ω scans close to the β-Ga_2O_3 600 Bragg reflection of β-Ga_2O_3 films on (100) on-oriented β-$(Al_xGa_{1-x})_2O_3$ (x = 0.1, 0.15 and 0.2) substrates are shown in figure 1(a).

Thickness fringes were observed, which indicate smooth surfaces and interfaces and a uniform film thickness of about (83 ± 1) nm. The peak separation between the substrate and the film as a function of x shows a consistent shift with increasing x, indicating corresponding variations in the strain values. Reciprocal space mappings (RSM) revealed that all β-Ga_2O_3 films are coherently grown onto the β-$(Al_xGa_{1-x})_2O_3$ substrates (Fig. 1b shows the RSM of a representative film grown on the x = 0.2 substrate). The out-of-plane elastic strain of β-Ga_2O_3 films grown on β-$(Al_xGa_{1-x})_2O_3$ substrates (x = 0.1, 0.15, and 0.2) was determined from 2θ–ω scans to be 0.44%, 0.68%, and 0.91%, respectively, calculated directly from the shift in peak positions between the fully strained and relaxed states.

AFM imaging (a representative example is shown in Fig. 1c for the film grown on the x = 0.2 substrate) reveals that surface roughness remains consistent regardless of the strain levels or aluminium content in the substrate. With a root mean square (RMS) roughness maintained at approximately 0.3 nm, it is evident that the applied strain does not produce a noticeable change in the surface morphology of β-Ga_2O_3.

From spectroscopic ellipsometry experimental data for ψ (amplitude ratio) and Δ (phase shift), the optical constants of the β-Ga_2O_3 thin films were extracted by using a Tauc-Lorentz dispersion formula. The refractive index (n) and the extinction coefficient (k) along the c-direction of the compressively strained β-Ga_2O_3 films grown on β-$(Al_xGa_{1-x})_2O_3$ (x = 0.1, 0.15 and 0.2) are shown in figures 2(a) and (b), respectively.

While the refractive index behaves similarly across most energy levels except near the absorption edge, the extinction coefficient shows a blue shift as strain increases, indicating an expansion of the band gap. In the transparent region our experimental values of n for the β-Ga_2O_3 films are in good agreement with that reported in Ref. [2]. For a more comprehensive examination of this issue, the band gap values of the β-Ga_2O_3 films grown on β-$(Al_xGa_{1-x})_2O_3$ substrates with x = 0.1, 0.15 and 0.2 (obtained from the onset of the main electronic absorption (Tauc–Lorentz) for the films) are presented in figure 2(c). For the film grown under compressive strain -0.44% the band gap is comparable to that of bulk β-Ga_2O_3. However, the films grown under compressive strain -0.68% and -0.91% showed a slightly larger (0.1 eV) band gap than that of bulk β-Ga_2O_3 crystal.

Future research building on this study may explore how strain influences electrical transport properties, such as carrier mobility and conductivity anisotropy. Another promising direction involves integrating strained β-Ga_2O_3 layers into full device architectures to directly correlate materials properties with device metrics such as breakdown voltage, switching speed, and thermal stability.

The publication demonstrates that structural strain potentially offers the possibility in β-Ga_2O_3 heteroepitaxy to adjust the material's properties. This work is an important step toward developing high-efficiency, high-voltage electronic systems that can reduce energy losses in power conversion and operate reliably in demanding environments.

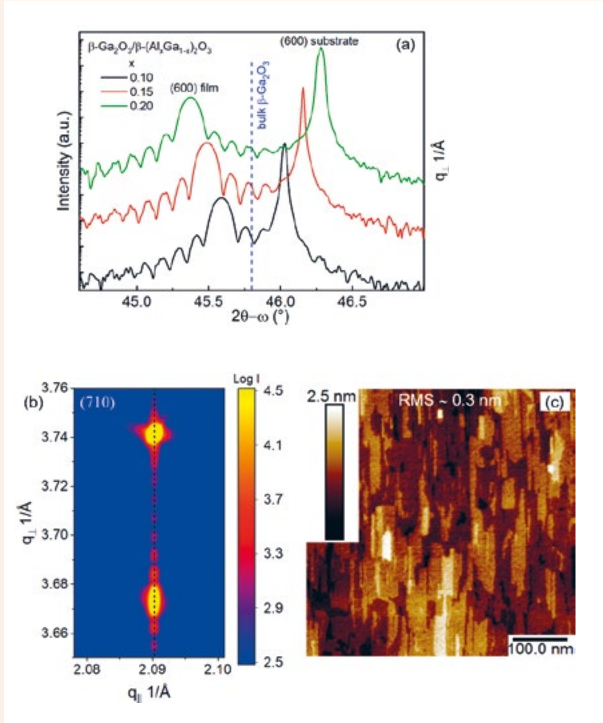

Fig. 1 (a) HR-XRD 2θ–ωscans of β-Ga_2O_3 thin films grown on β-$(Al_xGa_{1-x})_2O_3$ (x = 0.1, 0.15 and 0.2) substrates, (b) X-ray reciprocal space maps in the vicinity of the asymmetrical (710) Bragg wreflection and (c) AFM images of epitaxial β-Ga_2O_3 thin films on substrate with x = 0.2.

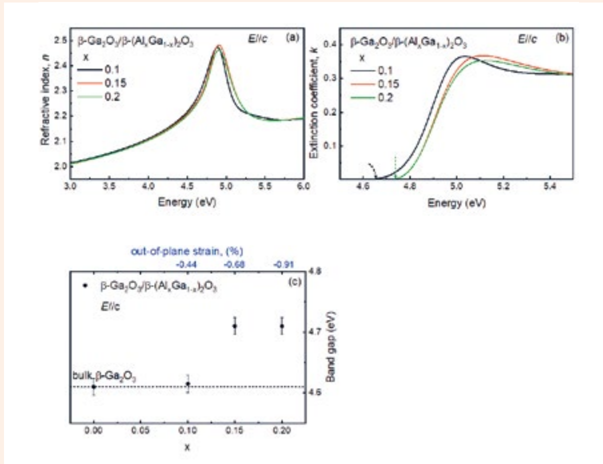

Fig. 2 (a) Refractive index (n), (b) extinction coefficient (k) of β-Ga_2O_3 thin films grown on (100) on β-$(Al_xGa_{1-x})_2O_3$ (x = 0.1, 0.15 and 0.2) substrates, (c) band gap versus Al composition x of β-$(Al_xGa_{1-x})_2O_3$ substrates.

References

This report is based on the following publication [1].

[1] S. Bin Anooz, T.-S. Chou, A. Akhtar, J. Rehm, H.-H. Chen, Z. Galazka, M. Schmidbauer, M. Albrecht, A. Fiedler, A. Popp, J. Phys. D: Appl. Phys., 59 (2025) 015308. https://doi.org/10.1088/1361-6463/ae2aec

[2] T. Onuma, S. Saito, K. Sasaki, T. Masui, T. Yamaguchi, T. Honda, A. Kuramata, M. Higashiwaki, Jap. J. Appl. Phys., 55 (2016) 1202B1202. https://doi.org/10.7567/jjap.55.1202b2

[3] R. Zhang, M. Li, G. Wu, L. Li, Z. Zhang, K. Liang, W. Shen, Results Phys., 52 (2023) 106916. https://doi.org/10.1016/j.rinp.2023.106916

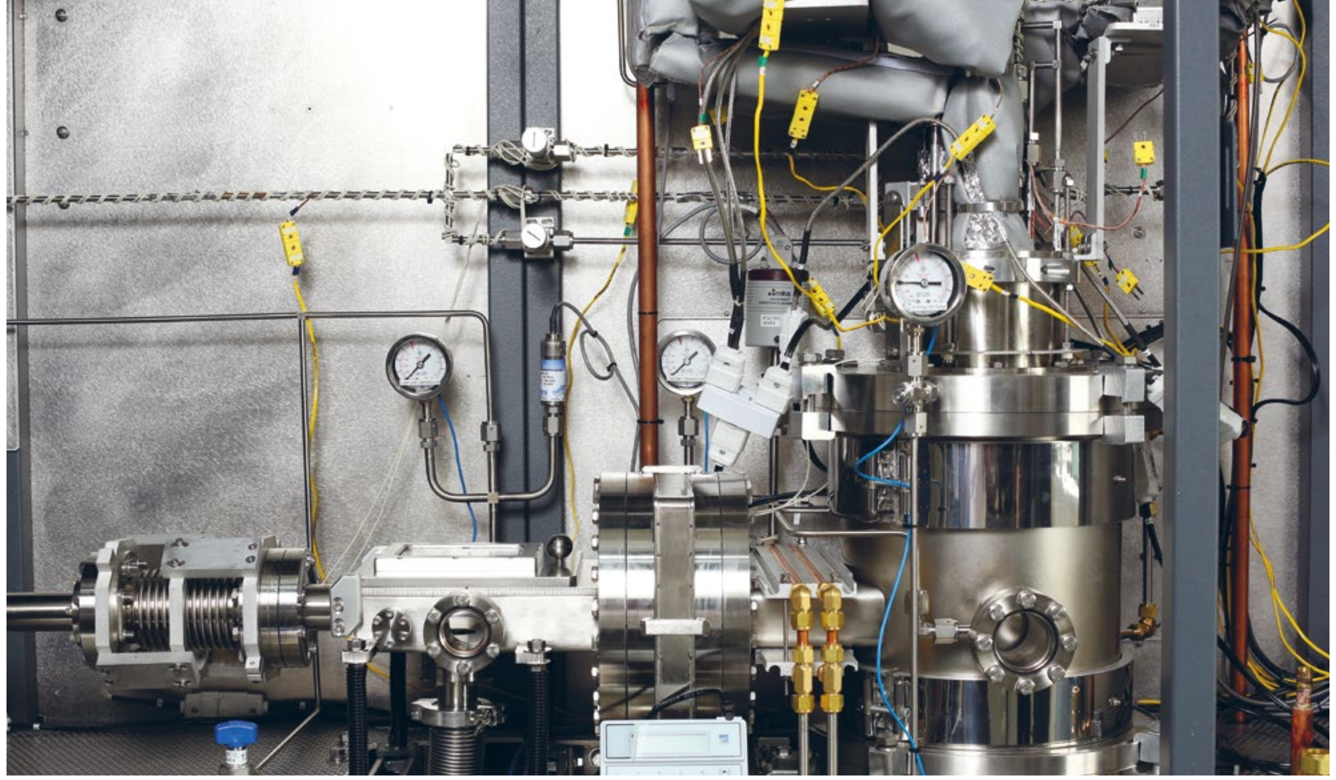

MOVPE reactor *Photo: Matthias Kern*

M. ABDELDAYEM, C.-M. LIU, I.-A. SHAH, A. FIEDLER, D. KLIMM, M. ALBRECHT, J. SCHWARZKOPF

Leibniz-Institut für Kristallzüchtung (IKZ), Berlin, Germany

$CaTiO_3$ thin films for potential applications in memristive devices grown by MOVPE

Perovskite oxide films continue to attract considerable interest due to their diverse functional properties, including ferroelectricity, mixed ionic–electronic transport, and resistive switching. These phenomena are highly sensitive to lattice distortions, strain, and (point) defects, making epitaxial thin films an ideal platform for property engineering. In particular, resistive switching materials are being explored intensively for non-volatile memory concepts such as resistive random-access memory (ReRAM) and for neuromorphic computing architectures that emulate synaptic behavior.

Calcium titanate ($CaTiO_3$) is an incipient ferroelectric perovskite oxide like $SrTiO_3$. But in contrast to the cubic symmetry of $SrTiO_3$, $CaTiO_3$ crystallizes in an orthorhombically distorted perovskite structure (Pbnm). Furthermore, among the alkaline-earth titanates, $CaTiO_3$ remains comparatively less investigated than $SrTiO_3$ or $BaTiO_3$, especially in the context of strain-modified electrical functionality. Theoretical and experimental studies have shown that tensile lattice strain in $CaTiO_3$ induces polar instabilities or relaxor-like behavior with a signifcant impact on charge transport and switching mechanisms.

The aim of the work was to investigate the influence of a targeted stoichiometry deviation on the resistive switching behavior in $CaTiO_3$ thin films [1]. The liquid-delivery spin metal-organic vapor phase epitaxy (MOVPE) method was used for this purpose, because compared to physical vapor deposition methods, MOVPE allows film growth at substantially higher oxygen partial pressures and facilitates stoichiometric films as well as films with a controlled cation off-stoichiometry via the precursor supply rates. Moreover, the technique offers scalability relevant for technological implementation.

Before establishing a feasible growth window for the $CaTiO_3$ films, a detailed thermal analysis of the metal-organic (MO) precursors was carried out. Based on thermogravimetric measurements of the Ca and Ti metal-organic compounds, suitable flash-evaporation temperatures of 210 °C and 250 °C for the Ti and the Ca precursor, respectively, have been fixed. Stoichiometric, 16 - 24 nm thin, epitaxial $CaTiO_3$ films with high structural order and smooth surfaces were realized at a substrate temperature of 740 °C, an O_2/Ar flow ratio of 3.3 and a process pressure of 15 mbar. With the ratio of the Ca and Ti precursors in the source solutions ($(Ca/Ti)_{liq}$), both stoichiometric ($(Ca/Ti)_{liq}$ = 0.494) and deliberately off-stoichiometric $CaTiO_3$ films were realized. High-resolution X-ray diffraction confirms coherent epitaxial growth without plastic relaxation of the imposed tensile lattice strain caused by the lattice mismatch to the $NdGaO_3$ substrates.

For an 18 nm thick, stoichiometric film, high resolution transmission electron microscopy (HRTEM) reveals a sharp and well-defined interface between film and substrate (Fig. 1a). No extended defects or secondary phases are observed within the resolution limits. The lattice continuity across the interface demonstrates high crystalline quality and homogeneous strain incorporation.

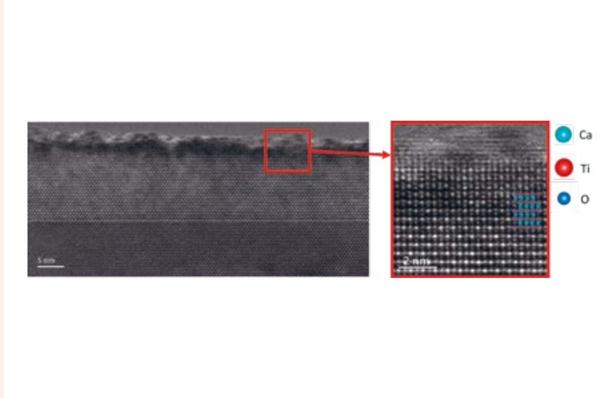

Fig. 1 HRTEM image of an 18 nm $CaTiO_3$ film grown on a $NdGaO_3$ substrate with a (Ca/Ti)liq ratio of 0.494. The interface between the film and substrate is highlighted by a dashed-and-dotted white line. On the right side, a high-magnification HRTEM image of a selected region within the film (indicated by the red box) is shown with the simulated $CaTiO_3$ crystal structure.

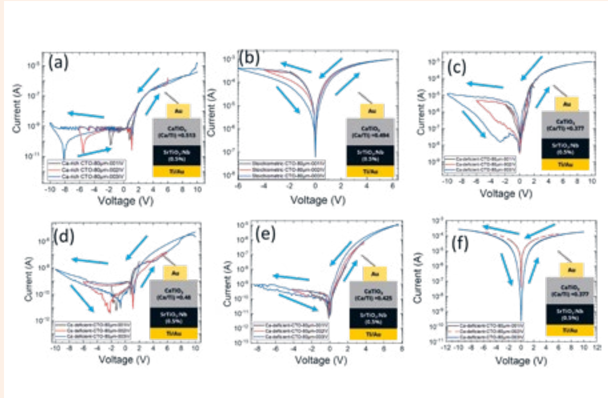

Fig. 2 . I–V characteristics for $CaTiO_3$ films with varying (Ca/Ti)liq ratios: (a) 0.513 (Ca-rich), (b) 0.494 (stoichiometric), (c) 0.480 (slightly Ca-deficient), (d) 0.457 (Ca-deficient), (e) 0.425 (Ca-deficient), and (f) 0.377 (Ca-deficient). The metal-insulator-semiconductor (MIS) device structure is illustrated next to the I–V curves. Current–voltage measurements were conducted in the voltage range of −10 to 10 V, with the measurement directions indicated by the blue arrows on each graph (reprinted from [1] under CC BY ND 4.0).

Systematic variation of the precursor ratio $(Ca/Ti)l_{iq}$ enables the growth of films with a targeted off-stoichiometry on the Ca site, while no significant amount of oxygen vacancies can be observed in the films. Ca-rich films exhibit an enlarged vertical lattice parameter due to additional CaO-related planar faults, whereas Ca-deficient films develop surface roughening, increased lattice parameters and consequently lower tensile lattice strain due to Ca vacancies.

Current–voltage measurements were performed on those stoichiometric and off-stoichiometric $CaTiO_3$ thin films grown on conductive Nb-doped $SrTiO_3$ substrates using a vertical MIS device geometry (Fig. 2).

Strongly Ca-deficient films (Figs. 2(e) and (f)) exhibit a diode-like rectification or nearly ohmic conduction without switching, while all other films reveal a stable switching between high-resistance and low-resistance states over multiple voltage cycles. Most pronounced hysteretic behavior is observed for slightly Ca-deficient $CaTiO_3$ films grown with $(Ca/Ti)_{liq}$ = 0.480 (Fig. 2(c)).

Obviously, there is a notable difference in resistive switching behavior depending on film composition compared to $SrTiO_3$ films in previous work [2]. In homoepitaxially grown $SrTiO_3$ films, switching only occurs in off-stoichiometric, Ti-rich films and was associated with a defect-induced mechanism based on the formation polar Ti anti-sites. In contrast, $CaTiO_3$ films also exhibit resistive switching behavior when they have been grown stoichiometrically. It has to be noted that $CaTiO_3$ cannot be grown homoepitaxially and growth on $SrTiO_3$ substrate inherently results in tensile lattice strain. The presence of this strain, even in stoichiometric films, leads to lattice distortions causing local polar defects. Such polar nanoregions are known to be the origin of relaxor behavior in perovskite oxides, which is assumed to contribute to the switching mechanism in strained films. Therefore, not only defect chemistry influences the electrical properties of dielectric oxide films, the data also indicate that lattice strain is a decisive parameter in $CaTiO_3$ to specifically modify electrical properties. These results are published in Ref. [1].

Future work will focus on disentangling strain- and defect-driven contributions to the switching mechanism and on optimizing device architectures for stable long-term operation.

References

[1] M. Abdeldayem, C.M. Liu, I.A. Shah, A. Fiedler, D. Klimm, M. Albrecht, J. Schwarzkopf, Cryst. Growth Des. 25 (2025) 3654. https://doi.org/10.1021/acs.cgd.4c01412

[2] A. Baki, J. Stöver, T. Schulz, T. Markurt, H. Amari, C. Richter, J. Martin, K. Irmscher, M. Albrecht, J. Schwarzkopf, Sci. Rep. 11 (2021) 1, https://doi.org/10.1038/s41598-021-87007-2

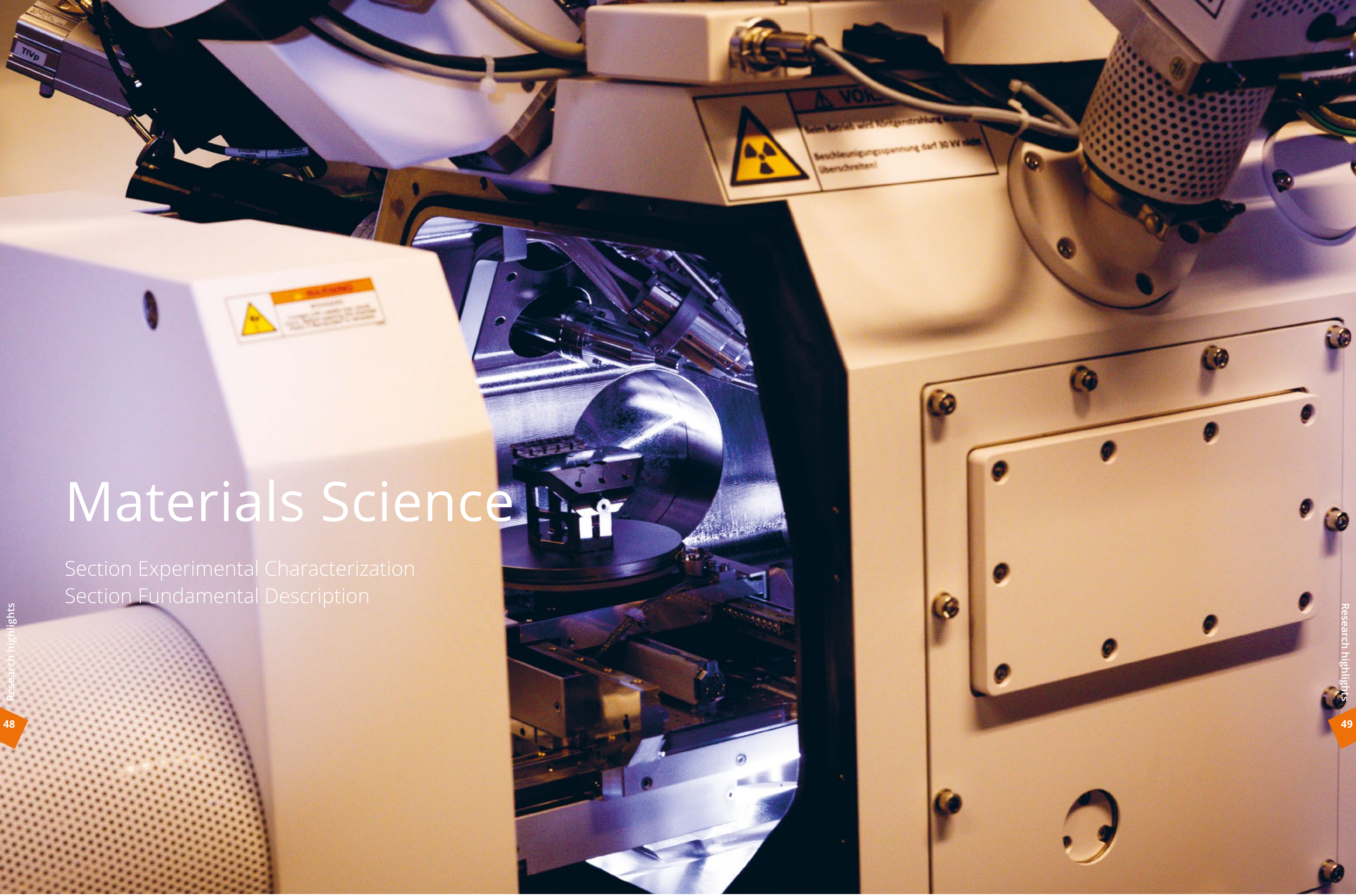

Materials Science

Section Experimental Characterization
Section Fundamental Description

Research highlights

IKZ Annual Report 2025

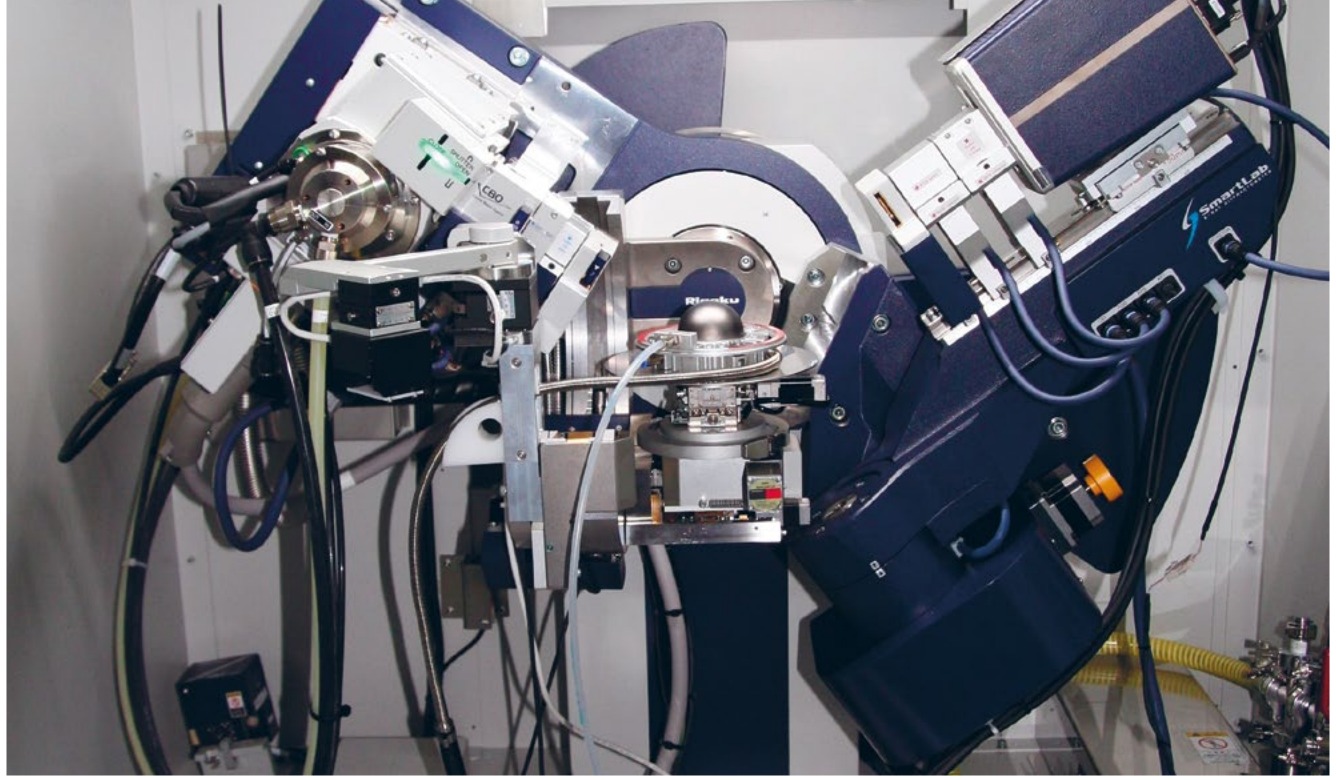

SmartLab X-ray diffractometer *Photo: IKZ*

M. DE OLIVEIRA GUIMARAES (1), C. RICHTER (1), J. SCHWARZKOPF (1), M. ENGL (2), S. SLESAZECK (2), M. SCHMIDBAUER (1)

(1) Leibniz-Institut für Kristallzüchtung (IKZ), Berlin, Germany
(2) NaMLab gGmbH, Dresden, Germany

Ferroelectric switching and temperature-dependent electrical properties of (K,Na)NbO_3 capacitor devices

In ferroelectric thin films, the switching of electrical polarization is a fundamental phenomenon that enables a wide range of technological applications. However, the ferroelectric properties depend strongly on the microscopic switching mechanism and the electrostatic boundary conditions. We have investigated strained, lead-free potassium-sodium-niobate (K,Na)NbO_3 films as ferroelectric material grown by metal-organic vapor phase epitaxy (MOVPE) close to thermodynamic equilibrium and at comparatively high oxygen partial pressures. This results in extremely perfect thin films with low defect density and virtually exact stoichiometric composition, as well as smooth surfaces and interfaces.

By growing these film epitaxially on different rare-earth scandate substrates, the strain state can be tuned in order to obtain the desired ferroelectric phase. As demonstrated by high-resolution X-ray diffraction [1], compressively strained ferroelectric $K_{0.7}Na_{0.3}NbO_3$ thin films grown on orthorhombic (110) $TbScO_3$ substrates occur in the vertically inclined monoclinic M_C phase and exhibit a very regular ferroelectric domain pattern (Fig. 1a). The monoclinic symmetry is of particular technological interest, as the electric polarization vector is able to rotate continuously within a specific symmetry plane of the monoclinic unit cell when an external electric field is applied, resulting in enormous piezoelectric responses. However, despite the high quality and the well-ordered monoclinic domains, ferroelectric switching has been hindered so far by high leakage currents, high coercive fields and large (µm-range) film thickness. Therefore, key ferroelectric properties, e.g. electrical polarization, endurance, and temperature dependence remain largely unknown.

In our newest publication [2], we successfully demonstrate stable ferroelectric switching in fully strained $K_{0.7}Na_{0.3}NbO_3$ based vertical capacitor devices and have undertaken detailed electrical characterization. In contrast to capacitor structures using metal top electrodes (Pt and Au), which lead to high leakage currents and poor ferroelectric response, using epitaxial $SrRuO_3$ top and bottom electrodes (Fig. 1b), fabricated by pulsed laser deposition (PLD), resulted in reliable capacitor performance .

At room temperature, our capacitor devices exhibit a high electrical polarization at zero voltage of around 20 µC/cm^2, comparable to much thicker $K_{0.7}Na_{0.3}NbO_3$ films. Hysteresis measurements revealed reliable ferroelectric behavior up to at least 10^7 cycles (Fig. 2a) without showing any considerable fatigue, increase in leakage current or degradation. In particular, a characteristic double-peak (labeled P1/P2 and P3/P4) switching behavior was observed. These evolve into a single peak with cycling with a gradual increase in polarization, representing a wake-up effect analogous to that reported in doped hafnium oxide [3] and lead zirconate titanate systems [4]. The observed double-peak behavior is attributed primarily to domain-wall pinning/de-pinning and back-switching, rather than charge-trapping or field-induced phase transitions. This is supported by the suppression of back-switching peaks at low temperatures down to 100 K (not shown here) and their occurrence only after the device has been pre-poled. This interpretation is also confirmed by the observed frequency behavior between 1 kHz and 20 kHz (Fig. 2b): At low frequencies, the switching current peaks (P1–P4) appear sharp and well defined, while at higher frequencies they broaden and shift toward larger absolute voltage values. Supplementary capacitance-voltage measurements reveal an increased dielectric response at higher temperatures (Fig. 3), consistent with enhanced domain wall mobility. The asymmetry in coercive voltages additionally points to internal bias fields likely arising from electrode interfaces.

Our results provide a comprehensive overview of the switching dynamics of strained $K_{0.7}Na_{0.3}NbO_3$ epitaxial films and demonstrate ferroelectricity in the monoclinic M_C phase. The combination of film thickness, switching voltages below 2 V, and cycling endurance above 10^7 cycles make such devices promising as candidates for next-generation, lead-free nonvolatile memories.

The present study was carried out in collaboration with NaMLab gGmbH (Dresden) in the framework of the joint DFG project "FeDiBiS" (SCHM 1515/3-1, SL 305/3-1). We also thank ERDF (Project No. 1.8/15) for funding. Our special thanks go to Saud Bin Anooz and Yankun Wang for film growth, and to Andreas Fiedler for fruitful discussions. The $TbScO_3$ substrates were grown at the IKZ in the group of S. Ganschow.

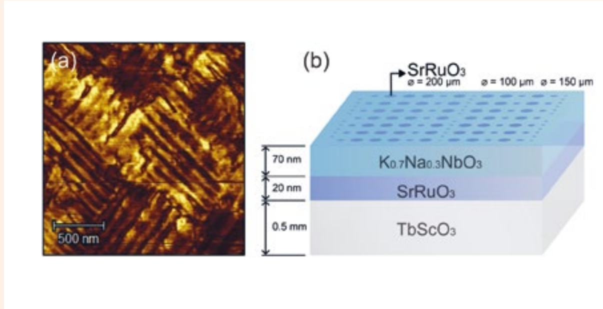

Fig. 1 (a) Lateral piezoresponse force micrograph (2 µm x 2 µm) of a K0.7Na0.3NbO3/SrRuO3/ (110) TbScO3 thin film showing a highly regular domain pattern as a typical characteristic of the monoclinic MC phase. (b) Sample structure of K0.7Na0.3NbO3/SrRuO3/(110) TbScO3 with SrRuO3 top electrodes of different diameters (reprinted from [2] under CC BY 4.0).

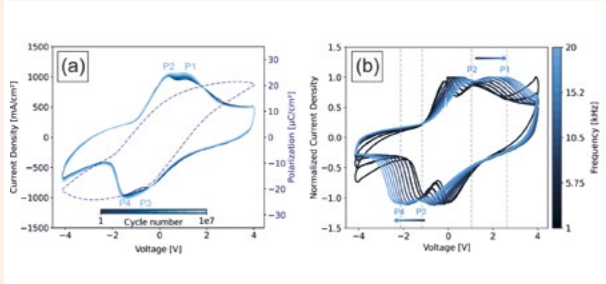

Fig. 2 Room temperature electrical measurements for the sample shown in Fig.1. (a): Polarization-voltage hysteresis loop (dashed line) at 7 kHz for the initial cycle, and current-voltage dependence on cycling (blue shades), showing characteristic ferroelectric switching up to 10^7 cycles with a gradual increase in polarization; (b): Frequency dependency between 1 kHz and 20 kHz (reprinted from [2] under CC BY 4.0).

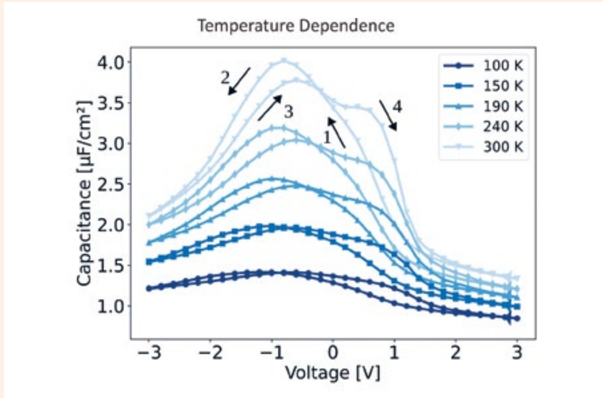

Fig. 3 Capacitance-voltage (C-V) characteristics for various temperatures, with labeled peaks (P1–P4) corresponding to the switching processes. Butterfly peaks increase with temperature, suggesting enhanced domain wall mobility (reprinted from [2] under CC BY 4.0).

References

[1] L. von Helden, M. Schmidbauer, S. Liang, M. Hanke, R. Wördenweber, J. Schwarzkopf, Nanotechnology 29, 415704 (2018) https://doi.org/10.1088/1361-6528/aad485

[2] M. de Oliveira Guimarães, C. Richter, J. Schwarzkopf, M. Engl., S. Slesazeck, M. Schmidbauer, Phys. Rev. Materials 10, 014413 (2026) https://doi.org/10.1103/ht3s-gvnm

[3] M. Lederer, R. Olivo, D. Lehninger, S. Abdulazhanov, T. Kämpfe, S. Kirbach, C. Mart, K. Seidel, L. M. Eng, Phys. Status Solidi (RRL) 15, 2100086 (2021). https://doi.org/10.1002/pssr.202100086

[4] T. M. Kamel and G. de With, J. Appl. Phys. 102, 044118 (2007). https://doi.org/10.1063/1.2767188

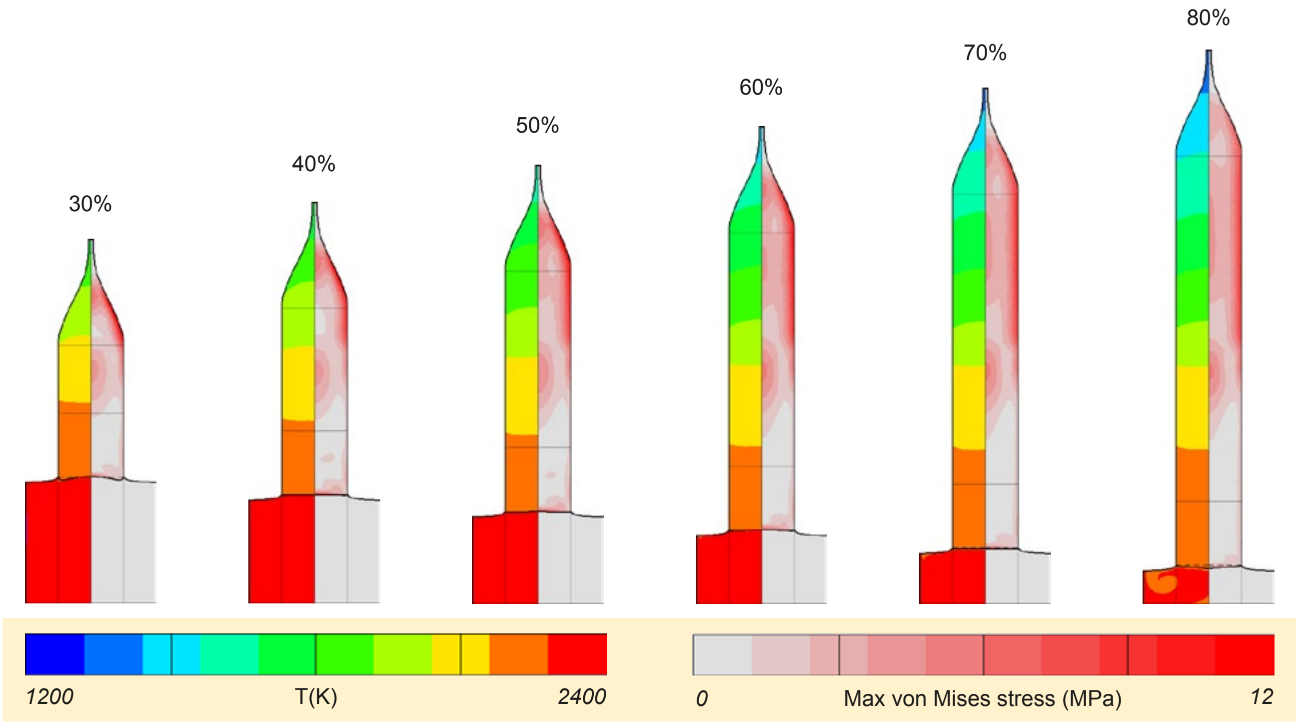

Fig. 3 CFD snapshots of temperature and von Mises stress fields for the optimized Cz-YAG recipe from 30-80% crystallization. Reprinted from [1] under CC BY 4.0. *Image: IKZ*

KUNAL MESHRAM (1), MILENA PETKOVIC (1), MARTIN HOLENA (2), NATASHA DROPKA (1)

(1) Leibniz-Institut für Kristallzüchtung (IKZ), Berlin, Germany
(2) Institute of Computer Science, Czech Academy of Sciences, Prague, Czech Republic

Machine learning framework for derivation and optimization of Cz-YAG crystal growth recipe

Undoped yttrium aluminum garnet (YAG) is a key optical oxide whose Czochralski (Cz) growth is governed by strong radiative heat transfer and nonlinear melt convection. These couplings govern interface morphology, axial temperature gradients, and thermoelastic stress. Conventional optimization via experiment or full computational fluid dynamics (CFD) is slow and costly.

We developed a surrogate-assisted multi-objective optimization (MOO) framework for dynamic Cz-YAG recipe generation [1]. High-fidelity steady-state CFD simulations were performed at 25%, 50% and 75% crystallization using a fully coupled axisymmetric furnace model (melt flow, induction heating, radiation, thermoelasticity). A two-stage design of experiments (DOE) ensured broad and physically meaningful coverage of the ten-dimensional input space. In stage 1, Latin Hypercube Sampling (LHS) was applied to systematically stratify each parameter range into equiprobable intervals, guaranteeing uniform marginal distributions while minimizing clustering in multidimensional space. This approach efficiently captured nonlinear parameter interactions with a limited number of simulations. In stage 2, stratified-quota sampling expanded geometric variation (crystal and crucible diameters). After convergence screening, 423 CFD cases formed the training dataset spanning ten input variables (geometry, melt charge, rotation rate, pulling rate, heater position, absorption, crystallized fraction).

Four outputs were extracted: heater power (y_0), interface deflection ΔZ (y_1), axial gradient gradT (y_2), and maximum von Mises stress $\sigma_{VM,max}$ (y_3).

Symbolic regression (SISSO++) [2] provided interpretable expressions and showed highest accuracy for power and gradT (R^2 test up to 0.99 and 0.91). Artificial neural network (ANN) ensembles better captured nonlinearities in ΔZ and $\sigma_{VM,max}$ (R^2 test up to 0.95 and 0.83) and were therefore embedded into NSGA-II MOO [3]. Surrogate evaluation reduced computation time from ~8–10 h per CFD case to milliseconds, enabling rapid exploration of process space across 30–80% crystallization.

The optimization targeted $|\Delta Z| \rightarrow 0$, gradT → 1 K mm^{-1} and minimum $\sigma_{VM,\,max}$. The statistical effect of MOO is most clearly visible in the distribution analysis (Fig. 1): compared with the original CFD dataset, optimized solutions show markedly narrower distributions centered around $\Delta Z \approx 0$ mm, gradT ≈ 1 K mm^{-1} and lower $\sigma_{VM,\,max}$. The violin plots demonstrate that high crystal quality is not achieved by isolated parameter extremes, but by coordinated adjustment of rotation rate, pulling rate and heater distance. At the same time, input distributions remain within realistic experimental bounds, confirming manufacturability of the optimized process windows.

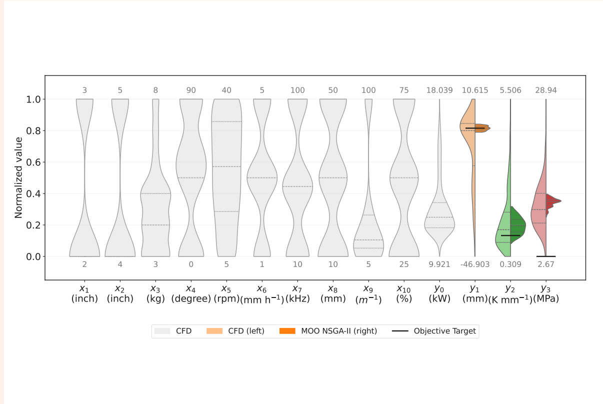

Fig. 1 Comparison of normalized input and output parameters before (original CFD data) and after MOO (reprinted from [1] under CC BY 4.0).

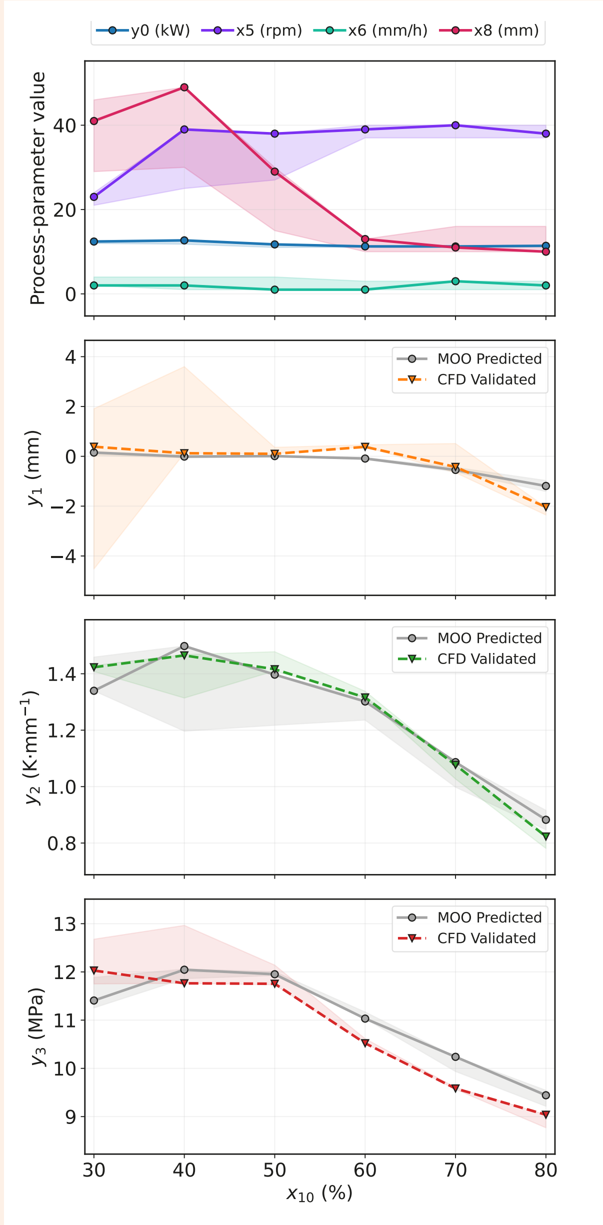

Fig. 2 Stagewise dynamic recipe and CFD validation from 30-80% crystallization. Shaded regions indicate Pareto-optimal process windows; symbols show CFD-validated operating points. Reprinted from [1] under CC BY 4.0.

Spatial CFD validation (Fig. 3) confirms the physical realism of the surrogate-derived recipes. Across 30–80% crystallization, the solid-liquid interface remains nearly flat and centered, avoiding curvature reversal. Temperature fields exhibit uniform axial alignment consistent with the targeted gradient, while stress maps show decreasing $\sigma_{VM,\,max}$ with increasing crystallized fraction due to reduced melt height and improved thermal relaxation. The absence of localized stress spikes or asymmetric temperature distortions demonstrates that the optimized settings preserve thermo-mechanical stability throughout growth.

For direct implementation, the stagewise dynamic recipe is summarized in Fig. 2 using CFD-validated Pareto solutions [3]. The recipe prescribes increasing rotation rate (23 → 38–40 rpm) to compensate for weakening buoyancy convection, moderate pulling rates (1-3 mm h^{-1}) to stabilize axial gradients, and reduced heater distance (41 → 10 mm) as the melt column shrinks. Heater power decreases steadily (12.4 → 11.4 kW), consistent with classical energy balance considerations. Resulting CFD values maintain ΔZ within ±0.4 mm over most of the window, gradT near 1-1.5 K mm^{-1}, and $\sigma_{VM,\,max}$ decreasing from ~12 MPa to ~9 MPa at late stages.

Together, Figs. 1-3 demonstrate that the surrogate-MOO-CFD loop produces statistically robust, spatially consistent and experimentally actionable dynamic growth recipes. The framework preserves essential physics while reducing computational cost by orders of magnitude, establishing a scalable digital-twin strategy for adaptive oxide crystal manufacturing.

References

[1] K. Meshram, M. Petkovic, M. Holena, N. Dropka, Machine learning framework for derivation and optimization of Cz-YAG crystal growth recipe, J. Cryst. Growth 676 (2026) 128451. https://doi.org/10.1016/j.jcrysgro.2025.128451.

[2] L.M. Ghiringhelli, J. Vybiral, S.V. Levchenko, C. Draxl, M. Scheffler, Big data of materials science: Critical role of the descriptor, Phys. Rev. Lett. 114 (2015) 105503. https://doi.org/10.1103/PhysRevLett.114.105503.

[3] K. Deb, A. Pratap, S. Agarwal, T. Meyarivan, A fast and elitist multiobjective genetic algorithm: NSGA-II, IEEE Trans. Evol. Comput. 6 (2002) 182–197. https://doi.org/10.1109/4235.996017.

[4] C.M. Fonseca, P.J. Fleming, Multiobjective optimization and multiple constraint handling with evolutionary algorithms. I. A unified formulation, IEEE Trans. Syst. Man Cybern. Part A 28 (1998) 26–37. https://doi.org/10.1109/3468.650319.

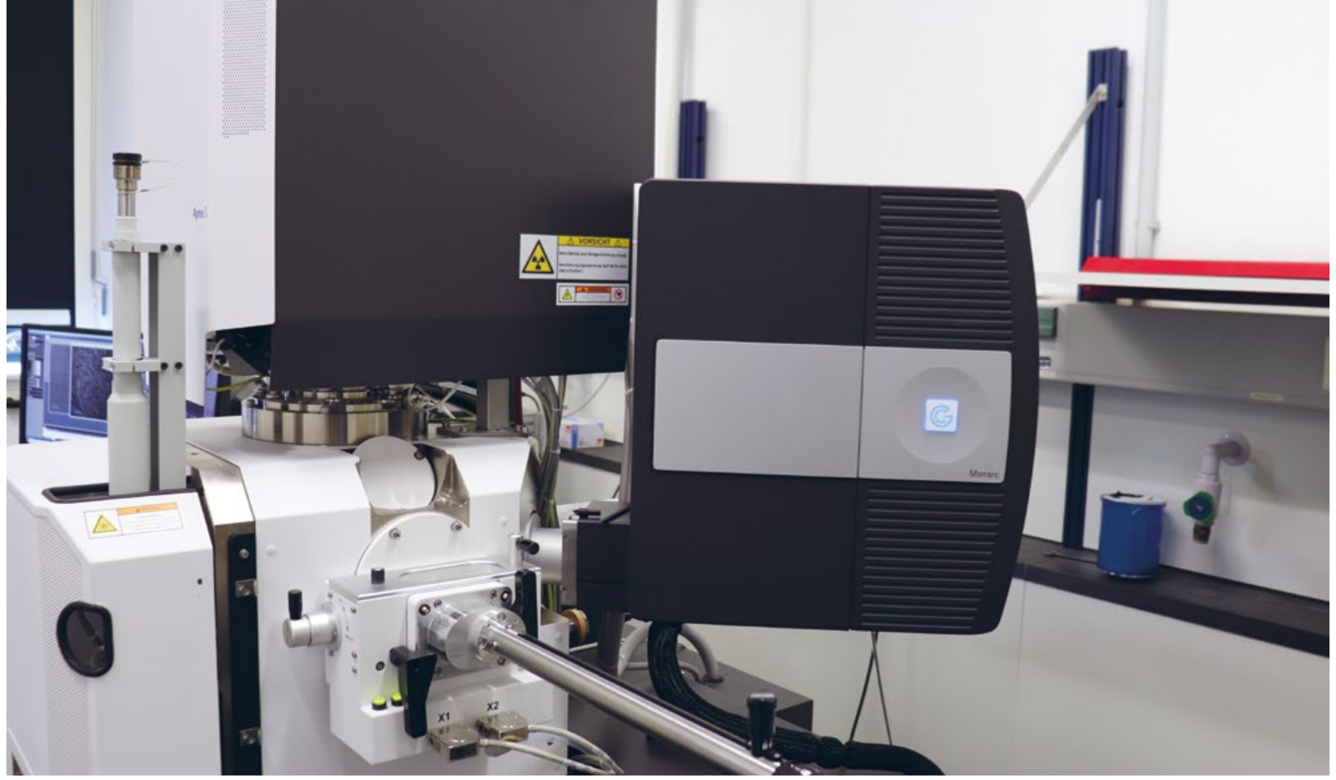

Cathodolumineszenz spectrometer at IKZ *Photo: IKZ*

T. SCHULZ, A. LACHOWSKI, R. KERNKE, M. ALBRECHT

Leibniz-Institut für Kristallzüchtung (IKZ), Berlin, Germany

Cathodoluminescence in a scanning electron microscope operated in transmission mode

Cathodoluminescence (CL) examines the light emission of materials under electron beam excitation, providing valuable information about its optical properties, structural defects, and chemical composition. Owing to the use of an electron beam rather than optical excitation, CL allows analyses with spatial resolution far beyond the diffraction limit of light.

Cross-sectional samples enable detailed investigation of individual layers in epitaxial films. The highest spatial resolution is achieved using electron-transparent specimens, where the electron beam passes through the sample while simultaneously exciting CL. The emitted light is collected by a parabolic mirror, and transmitted electrons are detected using a segmented STEM detector. Such experiments are commonly performed in a transmission electron microscope (TEM). However, apart from the higher cost, the high acceleration voltages available in a TEM often cannot be fully exploited for CL because they may damage beam-sensitive materials and degrade their optical properties.

Modern scanning electron microscopes (SEMs) provide a cost-effective alternative. Despite being limited to acceleration voltages of 30 keV, such systems can achieve sub-nanometer probe sizes and are often equipped with STEM detectors that simultaneously acquire bright-field (BF), dark-field (DF), and high-angle annular dark-field (HAADF) signals alongside with CL, providing complementary structural information.

The following section demonstrates some of the possibilities of CL in a SEM, operated in transmission mode, to study the structural properties of an (Al,Ga)N /AlN epilayer stack. This material is currently intensively investigated for application in light emitting diodes in the ultraviolet range (UV-LEDs), in particular for disinfection applications. To achieve electron transparency, the samples were prepared by mechanical polishing followed by ion milling.

Figure 1(a) shows a STEM bright-field (BF) image of the sample oriented along <1-100> (bottom) and <11-20> (top), displayed on a logarithmic intensity scale. For such thin specimens, the STEM detector provides significantly higher image quality compared to in-lens or chamber detectors. In the (Al,Ga)N layer, the BF image reveals stripe-like structures perpendicular to the growth direction. Notably, in the <1-100> orientation, the stripes are slightly inclined relative to the AlN / (Al,Ga)N interface, while they appear nearly parallel in the <11-20> direction. These contrast features are characteristic of compositional variations along the growth direction, associated with an undesired growth mode known as step bunching. In addition, the BF image also reveals strain-related contrast caused by threading dislo-

Research highlights 54

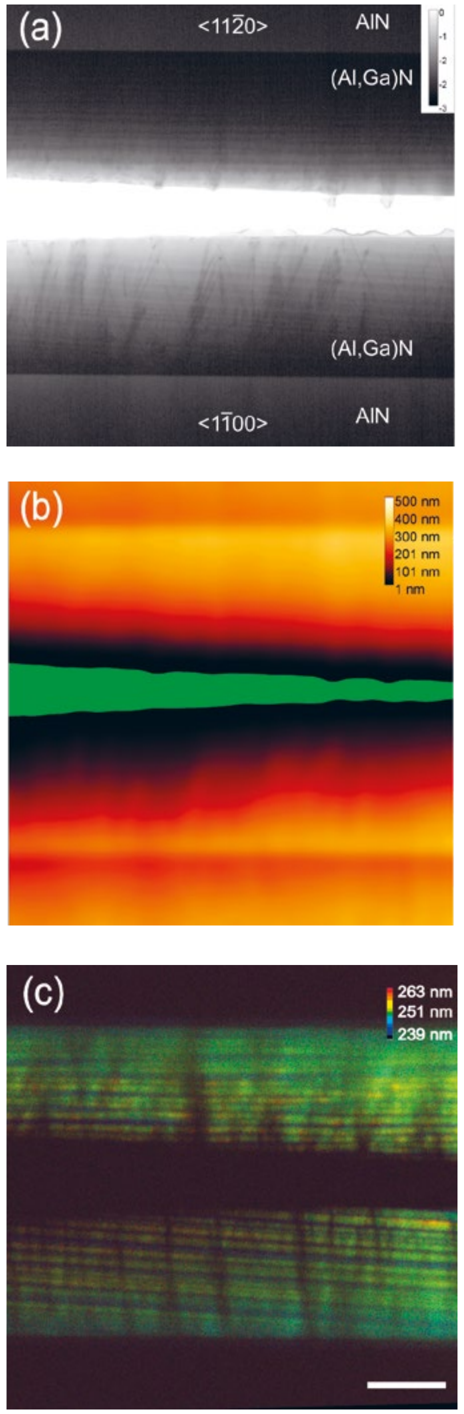

Fig. 1 (a) BF STEM image displayed on logarithmic intensity scale. Beam settings were 30 keV, 1.6 nA, and a dwell time of 64 µs. Lower sample piece corresponds to the <1-100> zone axis, upper to the <11-20> zone axis. (b) Thickness estimation from the quantified BF intensity in combination with Monte Carlo Simulations. The indicator equals 1 µm. (c) Reconstructed false-color RGB image from a series of 20 monochromatic images, each having a 2 nm bandpass, recorded in a spectral range between 230 nm and 270 nm.

cations emerging from the AlN / (Al,Ga)N interface toward the surface.

Before analyzing the optical properties of these features, the sample thickness was determined by evaluating the absorption of primary electrons within the material. This was accomplished by comparing the measured BF intensity with Monte Carlo simulations of electron transmission. The resulting thickness map in Fig 1(b) reveals the characteristic wedge-shaped geometry of ion-milled samples, with the thickness decreasing toward the glue line where the two sample halves meet.

Thickness values range from below 100 nm in the thinnest regions to several hundred nanometers in thicker areas. By correlating the thickness map with the CL signal, it was found that CL emission becomes negligible for sample thicknesses below approximately 20 nm. This reduction is primarily due to decreased energy deposition by the electron beam and increased non-radiative recombination at the sample surfaces.

Finally, spectrally resolved CL was investigated by recording a series of monochromatic images between 230 nm and 270 nm with a bandpass of 10 nm. From this dataset, a false-color image was reconstructed, as shown in Figure 1(c). On average, the emission occurs is centered at 253 nm, corresponding to an average aluminum content of approximately 65%.

The periodic compositional variations caused by step bunching in the (Al,Ga)N layer cause spectral shifts of the emission. Analyzing the peak shifts reveals composition variations of about ±1% along the growth direction with a periodic spacing of about 100 nm. In addition, the threading dislocations appear as dark lines in the CL maps, since they act as non-radiative recombination centers that locally reduce the CL yield.

Overall, this study demonstrates that cathodoluminescence measurements performed in a SEM operated in transmission mode provide a powerful approach for the correlative analysis of optical, structural, and compositional properties. Combining CL with transmitted electron signals, such as BF imaging, allows to identify defects, estimate sample thickness, and analyze compositional variations of epitaxial layers. This methodology extends the capabilities of conventional SEM instruments and offers a flexible alternative to CL measurements in dedicated TEM systems. Future developments will enable in-operando studies, allowing electrical bias and temperature to be applied while monitoring the sample's optical properties.

References

Schulz, T., Lachowski, A., Kernke, R. et al. Cathodoluminescence in a Scanning Electron Microscope Operated in Transmission Mode. J. Electron. Mater. 54, 5058–5065 (2025). https://doi.org/10.1007/s11664-025-11904-9

Research highlights 55

Application Science

Section Crystalline Materials for Photonics
Section Crystalline Materials for Electronics

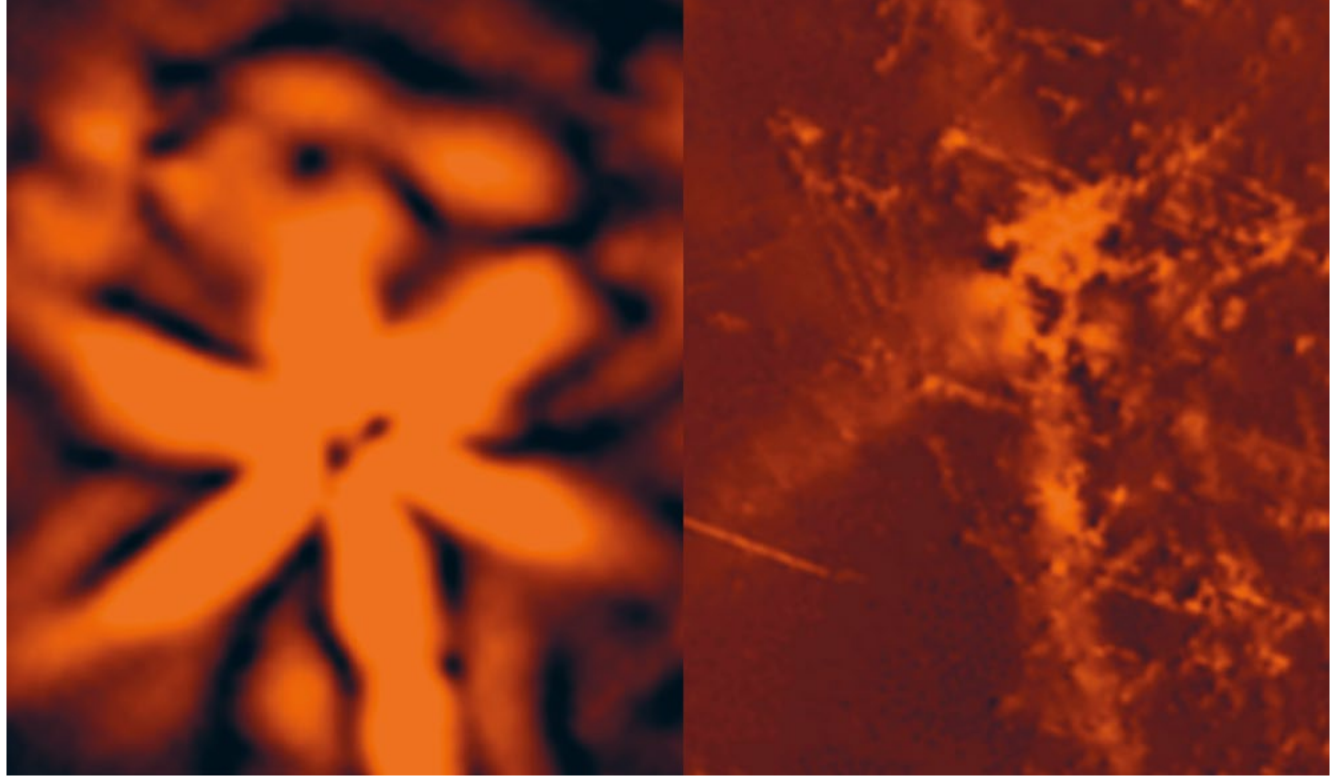

Local dislocation cluster in AlN visualized with Scanning Infrared Depolarization (SIRD, left) and X-Ray Topography (XRT, right) *Photo: IKZ*

M. HERMS (2), M.CP. KABUKCUOGLU (3), C. HARTMANN (1), M. STÖHR (2), M. WAGNER (2), E. HAMANN (3), D. HÄNSCHKE (3), C. RICHTER (2), T. STRAUBINGER (2)

(1) Leibniz-Institut für Kristallzüchtung (IKZ), Berlin, Germany
(2) PVA Metrology & Plasma Solutions GmbH., Wettenberg, Germany
(3) Institute for Photon Science and Synchrotron Radiation (IPS), Karlsruhe, Germany Institute of Technology (KIT), Eggenstein-Leopoldshafen, Germany

Residual stress and defects in single-Crystalline (0001) AlN wafers: Scanning infrared depolarization and white-beam X-ray topography

Scanning infrared depolarization (SIRD) is an efficient method to visualize and quantify local stress in semiconductor substrates and is used for substrate quality control and process monitoring in the semiconductor industry mainly for the materials silicon, gallium arsenide and silicon carbide. The depolarization measured by SIRD can be directly converted to maps of shear stress.

In the present work [1] the method is evaluated for the material aluminium nitride (AlN) in comparison with X-ray Diffraction Tomography (XRT) [2].

Fig. 1 (left) shows the shear stress in an AlN substrate (wafer A) with 1-inch diameter which was prepared from a crystal grown with comparatively high lateral temperature gradients dT (5 K/cm). The maximal stress around 6 MPa and the hexagram pattern in the shear stress mapping calculated after high pass filtering (Fig. 1 right) are in good agreement with a previous work [3] in which the hexagram pattern observed in XRT images is explained by dislocation multiplication during glide processes in m- and c-planes.

XRT images of wafer A corresponding to different reflexes reveal that the hexagram pattern is formed of a-type dislocations which are mostly inclined to the rim in growth direction inside the m-glide planes (Fig. 2). The inclination increases the closer the dislocations are to the edge of the crystal. At the 6 corners of the hexagram corresponding to m-directions (Fig. 2 left – orange surroundings) the dislocation density is comparatively high and the dislocations are parallel to the c-plane.

In the image corresponding to the 0-110 reflex (Fig. 2 left) the dislocations inclined in the 0-110 plane (Fig. 2 right – blue colour) show a weaker contrast compared to the other two dislocation groups corresponding to the 1-100 (Fig. 2 right – green colour) and 10-10 planes (Fig. 2 right – black colour) due to the extinction rule $g \cdot b=0$.

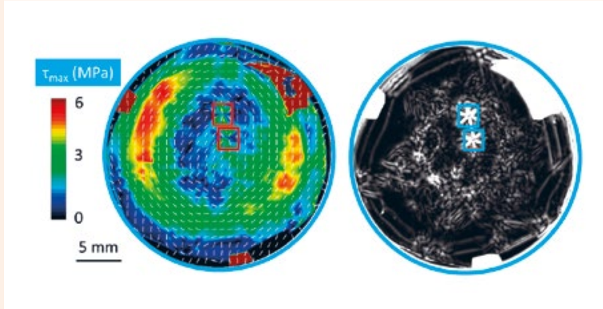

Fig. 1 AlN substrate (wafer A) with 1-inch diameter grown with high temperature gradients. Maps of shear stress maximum calculated from single shear stress equivalent maps as measured (left) and from those after high-pass-filtering (right).

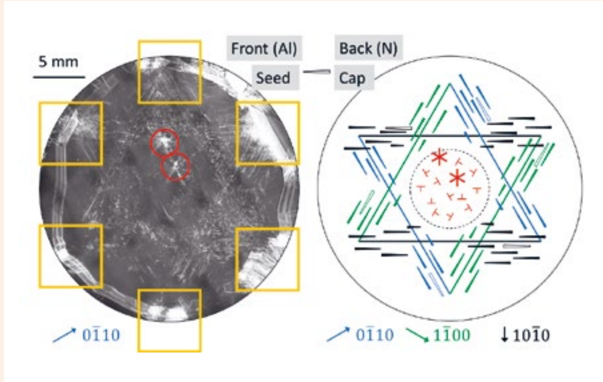

Fig. 2 AlN substrate (wafer A) with 1-inch diameter grown with high temperature gradients. Left: XRT image corresponding to the 0-110 reflex with hexagram pattern and dislocation clusters at the m-edges (orange surroundings) and in the centre (red surroundings). Right: Schematic drawing of dislocation distribution for 3 x 2 equivalent a-type burgers vectors in the c-plane.

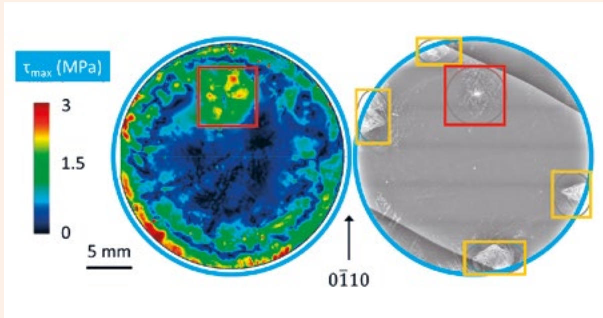

Fig. 3 AlN substrate (wafer B) with 1-inch diameter grown with low temperature gradients. Left: Map of shear stress maximum calculated from single shear stress equivalent maps as measured. Right: WB-XRT mapping corresponding to the 0-110 reflection without global hexagram-shaped pattern, dislocation clusters with lines parallel to the c-plane at the m-edges (orange surroundings) and one cluster with dislocation lines perpendicular to the c-plane in the central area (red surrounding). The diagonal straight lines at the top and bottom of the image are caused by the wafer holder and do not represent features of the crystal.

The observed dislocation distribution is attributed to the formation of dislocations at the crystal edges of the hexagonal shaped crystal growing in c-direction as well as in m-directions and subsequent gliding of dislocations through m-planes into the crystal volume. The dislocation movement was driven by thermoelastic stress that was relieved at the growth temperature and can be indirectly observed in SIRD-measurements after cool down to room temperature ("frozen dislocations").

In the crystal centre the dislocations are aligned along the c-direction and their density is generally low ($< 10^2$ cm^{-2}). Two small clusters with locally high dislocation density (Fig. 2 left – red surroundings) are present which are probably inherited from the seed.

The SIRD-based shear stress mapping of a wafer B (Fig. 3 left) grown with lower lateral temperature gradients around 3 K/cm shows significantly lower stress around 3 MP compared to wafer A and no hexagram pattern is observed in the XRT image corresponding to the 0-110 reflex while still clusters with locally high density of dislocations with dislocation lines parallel to the c-plane are present.

The conditions at the crystal corners along the m-directions remain favorable for dislocation formation; however, the reduced thermoelastic stress is insufficient to activate dislocation migration in m-planes or along the a-directions into the crystal volume.

In summary, SIRD represents a powerful and reliable tool for the efficient, non-destructive detection of structural defects in aluminium nitride substrates and for quantitative stress analysis. Anyway, for a deeper analysis of dislocation distributions and evolution XRT is better suited.

The presented work also showed that low lateral temperature gradients are key to realize aluminium nitride substrates with low dislocation densities.

1" prototype substrates [4] are available via the IKZ webpage. (ikz-berlin.de/en/offer/aluminum-nitride).

References

[1] Herms et al., Phys. Status Solidi A, 2025, 222, 2400787. https://doi.org/10.1002/pssa.202400787

[2] Straubinger et al., Cryst. Growth Des., 2023, 23, 1538-1546. https://doi.org/10.1021/acs.cgd.2c01131

[3] Hu et al., J. of Cryst. Growth 2022, 584, 126548. https://doi.org/10.1016/j.jcrysgro.2022.126548

[4] Hartmann et al., Appl. Phys. Express, 2023, 16, 075502. https://doi.org/10.35848/1882-0786/ace60e

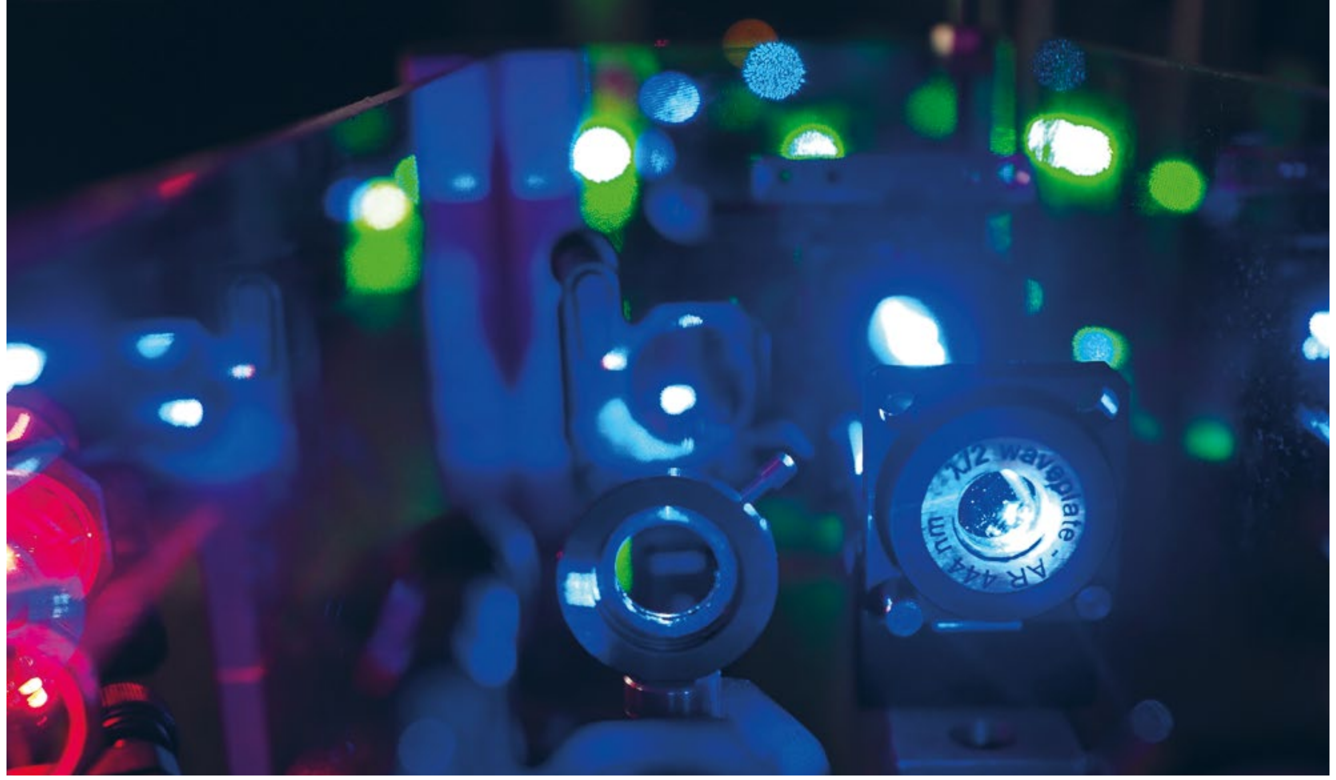

Impression of a visible praseodymium laser setup in the ZLM Laboratory at IKZ *Photo: Christian Kränkel*

C. KRÄNKEL, M. BADTKE, H. TANAKA, S. PÜSCHEL, AND S. KALUSNIAK

Leibniz-Institut für Kristallzüchtung (IKZ), Berlin, Germany

Thulium lasers at 820 nm: Compact alternative to Ti:sapphire

Laser light at wavelengths around 820 nm is crucial in modern science and technology, with applications in quantum research, precision measurements, spectroscopy, and advanced optical experiments. Today, this wavelength range is typically covered by titanium-sapphire (Ti:sapphire) lasers, which are highly versatile, but complex, expensive, and limited in output power. This can restrict their practical use in many laboratories and industrial settings.

Researchers at IKZ's Center for Laser Materials, (Zentrum für Lasermaterialien, ZLM), in collaboration with the fluoride growth group, have now demonstrated a promising alternative using a fluoride crystal doped with the rare-earth element thulium. Using a thulium-doped yttrium lithium fluoride (Tm:YLF) crystal grown at IKZ (Fig. 1, right), we achieved efficient continuous-wave laser operation at room temperature between 804 nm and 834 nm for the first time. The laser reached 1.1 W of output power at 820 nm with a slope efficiency of 62 %, surpassing the highest efficiency ever reported with Ti:sapphire lasers. The laser also operated at several nearby wavelengths, between 804 nm and 834 nm, demonstrating the flexibility of this new approach.

Trivalent thulium ions (Tm^{3+}) are established active ions in infrared solid-state lasers around 2 µm, typically pumped by laser diodes near 780 nm into to an energy level far above the 2-µm emitting level. This indirect pumping allows a single absorbed photon to excite two ions by an efficient energy-transfer process between neighboring thulium ions. This "two-for-one" pumping scheme enables highly efficient laser operation.

Recently, researchers have revisited other transitions in thulium which could generate laser light at shorter wavelengths. One particularly attractive transition is found between 800 nm and 840 nm (see Fig. 1, left), a region currently dominated by Ti:sapphire lasers. Efficient Tm^{3+} lasers in this range could provide a simple and compact alternative for many scientific and technological applications.

Achieving efficient laser operation at this transition is not straightforward. To avoid the two-for-one process removing excitation energy from the upper laser level of the 820-nm transition, low doping concentrations are required to reduce energy exchange between thulium ions. Another challenge is that thulium ions accumulate in a long-lived intermediate energy level. Ions trapped in this state no longer contribute to 820-nm laser emission, reducing the optical gain and limiting the laser efficiency. Understanding and mitigating this effect is key to unlocking the full potential of thulium-based lasers at shorter wavelengths.

To investigate these phenomena, we carried out detailed spectroscopic studies on Tm^{3+}-doped YLF crystals. We measured absorption and emission across the relevant wavelength range and conducted numerical simulations of the evolution of different energy-level populations under optical pumping. These revealed that the material exhibits broad and smooth gain spectra from roughly 800 nm to 850 nm, allowing for broad wavelength tuning and supporting ultrashort laser pulses. At the same time, the simulations indicated that under strong pumping, more than 60 % of excited ions could be trapped in the intermediate level. This significantly limits the number of ions available for lasing and therefore reduces efficiency.

Based on these findings, we built a proof-of-concept laser using an YLF crystal doped with only 1% of Tm^{3+}. It was placed inside a laser resonator and pumped with a Ti:sapphire laser at 781 nm, where Tm:YLF absorbs best. We achieved 1.1 W of output power with 62 % slope efficiency at a laser wavelength of 820 nm (see Fig. 2). By exchanging the mirrors of the resonator, laser emission was also demonstrated at multiple wavelengths between 804 nm and 834 nm (see Fig. 3), highlighting the potential for wavelength-tunable operation or the generation of ultrafast pulses. All details of the laser experiments can be found in [1].

While this proof-of-concept setup relied on a Ti:sapphire laser for pumping, the long-term goal is to develop directly diode-pumped systems. Diode-pumped solid-state lasers (DPSSL) are compact, efficient, and comparably inexpensive, making them practical for laboratory and industrial use. Efficiency improvements are anticipated by minimizing the population trapped in the intermediate energy level through optimized crystal compositions, additional laser transitions (co-lasing), or advanced cavity designs. Modifying parameters such as the thulium concentration, crystal length, and mirror coatings could further enhance output power and overall performance, enabling more robust and versatile laser systems.

Efficient high-power laser sources in the 800-850 nm wavelength range are particularly valuable for quantum technologies. The 813.4 nm "magic wavelength" is needed for optical lattice clocks based on strontium atoms, which are among the most precise timekeeping devices ever developed, and essential for precision metrology and fundamental physics. Laser light around 820 nm can also be frequency-doubled into ultraviolet radiation near 410 nm, useful for experiments with cold trapped ions such as ytterbium, which is relevant for quantum computing.

The demonstration of efficient room-temperature operation of thulium around 820 nm is a significant step toward a new class of solid-state laser sources. With further development, thulium-based lasers could become compact, efficient, and scalable alternatives to Ti:sapphire systems in the 800 nm to 850 nm spectral region. This would make high-performance lasers in this wavelength range more accessible for various applications including quantum technologies.

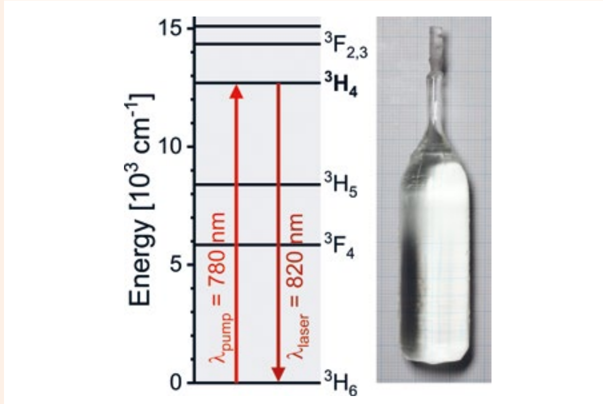

Fig. 1 Energy level scheme of Tm^{3+} with the transitions relevant for the 820 nm laser (left), photo of an as-grown Tm:YLF crystal (right).

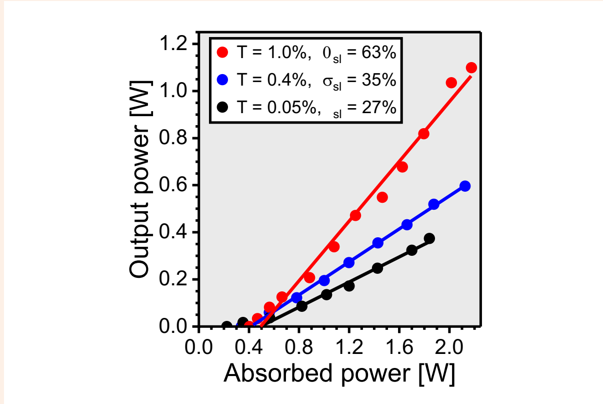

Fig. 2 Laser characteristics of Tm(1%):YLF around 820 nm using different output coupler transmissions.

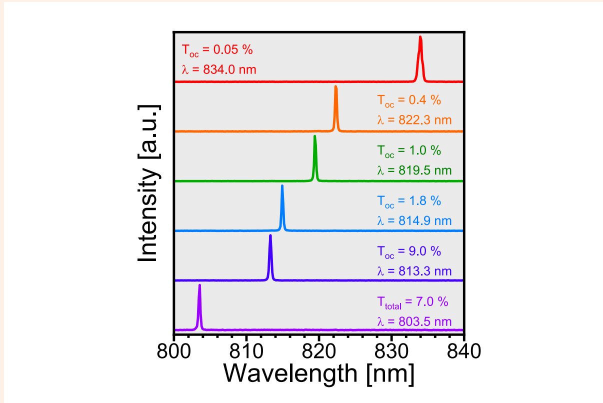

Fig. 3 Laser spectra of Tm:YLF for different output coupler transmissions.

References

[1] M. Badtke, H. Tanaka, S. Püschel, C. Kränkel, S. Kalusniak, "Efficient room temperature continuous wave laser operation of Tm:YLF around 820 nm," Opt. Lett. 50 (12), 3994 (2025).

Appendix

Publications

M. Abdeldayem; C. M. Liu; I. A. Shah; A. Fiedler; D. Klimm; M. Albrecht; J. Schwarzkopf, Epitaxial Growth of $CaTiO_3$ Thin Films by Metal Organic Vapor Phase Epitaxy for Potential Applications in Memristive Devices. Crystal Growth & Design; 25 (2025), 3654-3664 https://doi.org/10.1021/acs.cgd.4c01412.

K. Akkiraju; D. Y. Kuo; C. J. Eom; R. R. Rao; J. N. Nelson; E. Crumlin; K. M. Shen; D. G. Schlom; J. Suntivich; Y. Shao-Horn, Low-temperature oxidation of methane and methanol on iridium oxides. Cell Reports Physical Science; 6 (2025), 103023 https://doi.org/10.1016/j.xcrp.2025.103023.

S. P. Alaei; R. Raj; S. Channa; L. Takana; D. O'Mahoney; X. Y. Zheng; E. E. Fleck; T. Y. Chen; Z. Galazka; A. D. Kent; K. A. Mkhoyan; Y. Suzuki, Efficient spin transport across a disordered interface in a low damping magnetic insulator/heavy metal bilayer. Applied Physics Letters; 127 (2025), 262403 https://doi.org/10.1063/5.0294600.

M. Albrecht; O. Bierwagen; C. Draxl; K. Tetzner; H. von Wenckstern, Advances in Gallium Oxide-from Fundamental Materials Science to Device Implementation. Physica Status Solidi B-Basic Solid State Physics; 262 (2025), 2500299 https://doi.org/10.1002/pssb.202500299.

O. Altaher; K. Hasse; S. Suntsov; H. Tanaka; C. Kränkel; I. Bányász; R. Miksová; D. Kip, Ion-Implanted Diamond Blade Diced Ridge Waveguides in Pr:YLF-Optical Characterization and Small-Signal Gain Measurement. Applied Sciences-Basel; 15 (2025), 4956 https://doi.org/10.3390/app15094956.

B. Andriyevsky; L. Bychto; A. Patryn; U. Schade; L. Puskar; A. Veber; N. Abrosimov; A. I. Kashuba, Investigations of free electrons in doped silicon crystals derived from Fourier transformed infrared measurements and ab initio calculations. Opto-Electronics Review; 33 (2025), e153756 https://doi.org/10.24425/opelre.2025.153756.

A. Ardenghi; P. Mazzolini; G. Wagner; Z. Galazka; O. Bierwagen, Carrier Concentration-Dependent Seebeck Coefficient in β-Ga_2O_3. Physica Status Solidi B-Basic Solid State Physics; 262 (2025), 2400641 https://doi.org/10.1002/pssb.202400641.

E. L. Arnold; J. M. Riley; L. B. Duffy; A. I. Figueroa; R. Held; K. M. Shen; D. G. Schlom; P. D. C. King; M. Hoesch; G. van der Laan; T. Hesjedal, Magnetic x-ray spectroscopy of Gd-doped EuO thin films. Physical Review Materials; 9 (2025), 024410 https://doi.org/10.1103/PhysRevMaterials.9.024410.

D. Avadanii; S. Ganschow; M. Stypa; S. Müller; S. B. A. Lang; D. Kramer; C. Kirchlechner; R. Mönig, Disconnected Lithium Metal Damages Solid-State Electrolytes. Acs Energy Letters; 10 (2025), 2061-2067 https://doi.org/10.1021/acsenergylett.5c00101.

M. Badtke; S. Kalusniak; S. Püschel; H. Tanaka; C. Kränkel, Prospects of UV and blue laser emission from the 5D3 level in Tb^{3+}:$LiYF_4$. Journal of Luminescence; 280 (2025), 121061 https://doi.org/10.1016/j.jlumin.2025.121061.

M. Badtke; S. Kalusniak; S. Püschel; H. Tanaka; C. Kränkel, Temperature-Dependent Spectroscopy and Laser Performance of Yellow Tb:YLF Lasers with 36% Slope Efficiency at Room Temperature and 61% at 100 K. Laser & Photonics Reviews; 19 (2025), 2402019 https://doi.org/10.1002/lpor.202402019.

M. Badtke; S. Kalusniak; H. Tanaka; C. Kraenkel, Tb:YLF laser at 412.7 nm and 435.1 nm. Optics Letters; 50 (2025), 3421-3424 https://doi.org/10.1364/ol.553252.

M. Badtke; S. Püschel; Z. Liestmann; H. Tanaka; C. Kränkel; S. Kalusniak, Highly efficient continuous-wave Tm^{3+}:YLF cascade laser operating at telecommunication wavelengths. Optics Express; 33 (2025), 14340-14349 https://doi.org/10.1364/oe.559428.

M. Badtke; H. Tanaka; S. Püschel; C. Kränkel; S. Kalusniak, Efficient room temperature continuous wave laser operation of Tm:YLF around 820 nm. Optics Letters; 50 (2025), 3994-3997 https://doi.org/10.1364/ol.563752.

D. Barbalas; R. Romero, III; D. Chaudhuri; F. Mahmood; H. P. Nair; N. J. Schreiber; D. G. Schlom; K. M. Shen; N. P. Armitage, Energy Relaxation and Dynamics in the Correlated Metal Sr_2RuO_4 via Terahertz Two-Dimensional Coherent Spectroscopy. Physical Review Letters; 134 (2025), 036501 https://doi.org/10.1103/PhysRevLett.134.036501.

I. R. Berkman; A. Lyasota; G. G. de Boo; J. G. Bartholomew; S. Q. Lim; B. C. Johnson; J. C. McCallum; B. B. Xu; S. Y. Xie; N. V. Abrosimov; H. J. Pohl; R. L. Ahlefeldt; M. J. Sellars; C. M. Yin; S. Rogge, Long optical and electron spin coherence times for erbium ions in silicon. Npj Quantum Information; 11 (2025), 66 https://doi.org/10.1038/s41534-025-01008-x.

S. Chae; S. M. Lee; A. Park; M. K. I. Senevirathna; Y. F. Feng; V. Kanneboina; V. A. Ha; Y. Q. Hu; C. J. Du; M. Barone; V. Protasenko; Y. E. Li; N. Podraza; K. Johnson; D. Jena; H. G. Xing; X. Q. Pan; K. Cho; F. Giustino; M. D. Williams; D. G. Schlom, Controlling the p-type conductivity of α-SnO thin films by potassium doping. Apl Materials; 13 (2025), 101114 https://doi.org/10.1063/5.0288742.

S. Channa; H. Sabri; X. Y. Zheng; T. Y. Chen; H. W. Ren; Q. C. Wu; K. Wang; Y. T. Li; Z. Galazka; I. R. Fisher; X. Hong; A. D. Kent; J. D. Zang; Y. Suzuki, Signatures of Fluctuation-Driven Magnetic Topological Charge in Pt-Ferromagnetic Insulator Bilayers. Physical Review Letters; 135 (2025), 096702 https://doi.org/10.1103/r5pw-sqk2.

G. K. Chappa; M. Petkovic; N. Dropka, Data-driven feasibility study of VGF β-Ga_2O_3 growth under traveling magnetic fields. Journal of Crystal Growth; 652 (2025), 128049 https://doi.org/10.1016/j.jcrysgro.2024.128049.

T. S. Chou; S. Bin Anooz; N. Dropka; H. H. Chen; Z. Galazka; M. Albrecht; A. Fiedler; A. Popp, Optimizing the morphology transition on MOVPE-grown (100) β-Ga_2O_3 film between step-flow growth and step-bunching: A machine learning-assisted approach. Apl Materials; 13 (2025), 051110 https://doi.org/10.1063/5.0261944.

T. S. Chou; S. Bin Anooz; Z. Galazka; M. Albrecht; A. Fiedler; A. Popp, In-situ reflectance analysis of Si-doped β-Ga_2O_3 films grown by MOVPE: The influence of doping concentration and substrate conductivity. Journal of Applied Physics; 137 (2025), 095703 https://doi.org/10.1063/5.0251523.

T. S. Chou; J. Rehm; S. Bin Anooz; C. Wouters; O. Ernst; A. Akhtar; Z. Galazka; M. Albrecht; A. Fiedler; A. Popp, Impurity-induced step pinning and recovery in MOVPE-grown (100) β-Ga_2O_3 film. Applied Physics Letters; 126 (2025), 022101 https://doi.org/10.1063/5.0242301.

T. S. Chou; T. T. V. Tran; H. Peelaers; K. Tetzner; O. Hilt; J. Rehm; S. Bin Anooz; A. Fiedler; Z. Galazka; M. Albrecht; A. Popp, Out-Diffusion and Uphill-Diffusion of Mg in Czochralski-Grown (100) β-Ga_2O_3 Under High-Temperature Annealing and Its Influence on Lateral MOSFET Devices. Advanced Electronic Materials; 11 (2025), 2400342 https://doi.org/10.1002/aelm.202400342.

I. N. Demchenko; Y. Syryanyy; A. Shokri; Y. Melikhov; J. Domagala; R. Minikayev; A. Derkachova; F. Munnik; U. Kentsch; M. Zajac; A. Reck; N. Haufe; Z. Galazka, Local structure modification around Si atoms in Si-implanted monocrystalline β-Ga_2O_3 (100) under heated substrate conditions. Acta Materialia; 292 (2025), 121036 https://doi.org/10.1016/j.actamat.2025.121036.

N. Dropka; M. Petkovic; C. Frank-Rotsch; D. Linke; M. Holena, Toward a Universal Czochralski Growth Model Leveraging Data-Driven Techniques. Advanced Theory and Simulations; 8 (2025), e01159 https://doi.org/10.1002/adts.202501159.

F. E. El Azzouzi; D. Klimm; A. Kapp; L. M. Verhoff; N. A. Schäfer; S. Ganschow; K. D. Becker; S. Sanna; H. Fritze, Evolution of the Electrical Conductivity of $LiNb_{1-x}Ta_xO_3$ Solid Solutions across the Ferroelectric Phase Transformation. Physica Status Solidi a-Applications and Materials Science; 222 (2025), 2300966 https://doi.org/10.1002/pssa.202300966.

J. Feldl; R. Gillen; J. Maultzsch; A. Papadogianni; J. Kler; Z. Galazka; O. Bierwagen; M. Ramsteiner, Unravelling the oxygen influence in cubic bixbyite In_2O_3 on Raman active phonon modes by isotope studies. Journal of Materials Chemistry C; 13 (2025), 23545-23553 https://doi.org/10.1039/d5tc02566d.

S. Foroushani; A. Wintzer; F. M. Kiessling; K. Dadzis, Heating efficiency and energy saving potential of Czochralski crystal growth furnaces. Journal of Crystal Growth; 662 (2025), 128106 https://doi.org/10.1016/j.jcrysgro.2025.128106.

P. Gaczynski; Y. Suhak; S. Ganschow; S. Sanna; H. Fritze; K. D. Becker, A High-Temperature Optical Spectroscopy Study of the Fundamental Absorption Edge in the $LiNbO_3$-$LiTaO_3$ Solid Solution. Physica Status Solidi a-Applications and Materials Science; 222 (2025), 2300972 https://doi.org/10.1002/pssa.202300972.

Z. Galazka, Current Status of Bulk β-Ga_2O_3 and β-$(Al_xGa_{1-x})_2O_3$ Crystal Growth. Ieee Transactions on Semiconductor Manufacturing; 38 (2025), 796-802 https://doi.org/10.1109/tsm.2025.3603605.

Z. Galazka; R. Blukis; A. Fiedler; S. Bin Anooz; J. J. Zhang; M. Albrecht; T. Remmele; T. Schulz; D. Klimm; M. Pietsch; A. Kwasniewski; A. Dittmar; S. Ganschow; U. Juda; K. Stolze; M. Suendermann; T. Schroeder; M. Bickermann, Bulk Single Crystals and Physical Properties of Rutile GeO_2 for High-Power Electronics and Deep-Ultraviolet Optoelectronics. Physica Status Solidi B-Basic Solid State Physics; 262 (2025), 2400326 https://doi.org/10.1002/pssb.202400326.

Z. Galazka; A. Fiedler; M. Pietsch; A. Kwasniewski; A. Dittmar; R. Blukis; S. Ganschow; U. Juda; T. Schroeder; M. Bickermann, Incorporation of divalent transition-metal ions in bulk In_2O_3 single crystals grown from the melt and their impact on optical and electrical properties. Journal of Applied Physics; 138 (2025), 025104 https://doi.org/10.1063/5.0273999.

Z. Galazka; A. Fiedler; A. Popp; P. Seyidov; S. B. Anooz; R. Blukis; J. Rehm; K. Tetzner; M. Pietsch; A. Dittmar; S. Ganschow; A. Akhtar; T. Remmele; M. Albrecht; T. Schulz; T. S. Chou; A. Kwasniewski; M. Suendermann; T. Schroeder; M. Bickermann, Solid-Solution Limits and Thorough Characterization of Bulk β-$(Al_xGa_{1-x})_2O$ Single Crystals Grown by the Czochralski Method. Advanced Materials Interfaces; 12 (2025), 2400122 https://doi.org/10.1002/admi.202400122.

K. M. Gambaryan; O. Ernst; T. Boeck; O. Marquardt, Energy level alignment of confined hole states in $InAs_{1-x-y}Sb_xP_y$ asymmetric double quantum dots for single-photon energy up- and downconversion. Applied Physics Letters; 126 (2025), 061102 https://doi.org/10.1063/5.0244778.

J. Gollwitzer; J. Z. Kaaret; Y. E. Suyolcu; G. Khalsa; R. C. Fernandes; O. Gorobtsov; S. Buchenau; C. J. You; J. Higgins; R. S. Russell; Z. M. Shao; Y. A. Birkhölzer; T. Sato; M. Chollet; G. Coslovich; M. Brützam; C. Guguschev; J. W. Harter; A. S. Disa; D. G. Schlom; N. A. Benedek; A. Singer, Picosecond Expansion in $LaAlO_3$ Resonantly Driven by Infrared-Active Phonons. Physical Review Letters; 135 (2025), 116906 https://doi.org/10.1103/vzkw-n2bm.

K. P. Gradwohl; L. Cvitkovich; C. H. Lu; S. Koelling; M. Oezkent; Y. J. Liu; D. Waldhör; T. Grasser; Y. M. Niquet; M. Albrecht; C. Richter; O. Moutanabbir; J. Martin, Enhanced Nanoscale Ge Concentration Oscillations in Si/SiGe Quantum Well through Controlled Segregation. Nano Letters; 25 (2025), 4204-4210 https://doi.org/10.1021/acs.nanolett.4c05326.

I. Grants; J. Pal; I. Tsiapkinis; S. Eckert; G. Gerbeth; D. Raebiger; K. Dadzis, Flow instability caused by temperature boundary conditions in a model of Czochralski crystal growth. Physics of Fluids; 37 (2025), 024106 https://doi.org/10.1063/5.0250371.

N. K. Gupta; R. T. Gong; Y. Wu; M. G. Kang; C. T. Parzyck; B. Z. Gregory; N. Costa; R. Sutarto; S. Sarker; A. Singer; D. G. Schlom; K. M. Shen; D. G. Hawthorn, Anisotropic spin stripe domains in bilayer $La_3Ni_2O_7$. Nature Communications; 16 (2025), 6560 https://doi.org/10.1038/s41467-025-61653-w.

I. A. Harris; S. Husain; P. Meisenheimer; M. Ramesh; H. W. Park; L. Caretta; D. G. Schlom; Z. Yao; L. W. Martin; J. iñiguez-González; S. K. Kim; R. Ramesh, Symmetry-Based Phenomenological Model for Magnon Transport in a Multiferroic. Physical Review Letters; 134 (2025), 016703 https://doi.org/10.1103/PhysRevLett.134.016703.

D. L. Helis; P. Camiti; E. Celi; D. Chiesa; J. Corbett; Dafinei; P. Di Stefano; F. Ferella; Z. Galazka; S. Ghislandi; C. Gotti; R. Knobel; J. Kotila; J. Kostensalo; S. Nagorny; S. Nisi; L. Pagnanini; G. Pessina; S. Pirro; S. Pozzi; A. Puiu; S. Quitadamo; J. Suhonen; Y. Zhu; Current Status and Perspectives of the ACCESS project; Workshop On The Calculation Of Double-Beta-Decay Matrix Elements, Medex'22; 3143 (2025) https://doi.org/10.1063/5.0250148

M. Hennecke; D. Schick; T. P. H. Sidiropoulos; J. X. Lin; Z. X. Guo; G. Malinowski; M. Mattern; L. Ehrentraut; M. Schmidbauer; M. Schnuerer; C. V. Schmising; S. Mangin; M. Hehn; S. Eisebitt, Transient domain boundary drives ultrafast magnetisation reversal. Nature Communications; 16 (2025), 8233 https://doi.org/10.1038/s41467-025-63571-3.

F. V. E. Hensling; C. T. Parzyck; B. Cromer; M. A. Al Mamun; Y. E. Suyolcu; L. Kalaydjian; I. Subedi; J. Park; K. Azizie; Q. Song; P. A. Van Aken; N. J. Podraza; K. Cho; D. Jena; H. G. Xing; K. M. Shen; D. G. Schlom; P. Vogt, Growth of tetragonal PtO by molecular-beam epitaxy and its integration into β-Ga_2O_3 Schottky diodes. Apl Materials; 13 (2025), 111108 https://doi.org/10.1063/5.0274229.

F. V. E. Hensling; P. Vogt; J. Park; S. L. Shang; H. C. Ye; Y. M. Wu; K. Smith; V. Show; K. Azizie; H. Paik; D. Jena; H. G. Xing; Y. E. Suyolcu; P. A. van Aken; S. Datta; Z. K. Liu; D. G. Schlom, Fully Transparent Epitaxial Oxide Thin-Film Transistor Fabricated at Back-End-of-Line Temperature by Suboxide Molecular-Beam Epitaxy. Advanced Electronic Materials; 11 (2025), 2400499 https://doi.org/10.1002/aelm.202400499.

F. Herklotz; I. Chaplygin; E. V. Lavrov; V. V. Melnikov; Z. Galazka; L. Vines, Transition metal-hydrogen complexes in SnO_2. Physical Review B; 111 (2025), 195208 https://doi.org/10.1103/PhysRevB.111.195208.

M. Herms; M. P. Kabukcuoglu; C. Hartmann; M. Stöhr; M. Wagner; E. Hamann; D. Hänschke; C. Richter; T. Straubinger, Comparative Study of Residual Stress and Defects in Single-Crystalline (0001) AlN Wafers by Scanning Infrared Depolarization and White-Beam X-ray Topography. Physica Status Solidi a-Applications and Materials Science; 222 (2025), 2400787 https://doi.org/10.1002/pssa.202400787.

M. Hollenbach; N. Klingner; P. Mazarov; W. Pilz; A. Nadzeyka; F. Mayer; N. V. Abrosimov; L. Bischoff; G. Hlawacek; M. Helm; G. V. Astakhov, Programmable Activation of Quantum Emitters in High-Purity Silicon with Focused Carbon Ion Beams. Advanced Quantum Technologies; 8 (2025), 2400184 https://doi.org/10.1002/qute.202400184.

W. T. Hou; S. Kalusniak; S. Püschel; H. Tanaka; J. Xu; J. Tang; C. Kränkel, Spectroscopy and efficient OPSL-pumped laser operation of Er:BaF_2 crystal at 2.8 µm. Optics Express; 33 (2025), 6799-6807 https://doi.org/10.1364/oe.550678.

N. Kafi; A. Rodrigues; I. Häusler; H. R. Ma; C. Netzel; A. Hammud; O. Skibitzki; M. Schmidbauer; F. Hatami, Broadband light emission from GaAsP and GaInP islands grown on silicon nanotip wafer via nanoheteroepitaxy. Applied Physics Letters; 127 (2025), 191106 https://doi.org/10.1063/5.0285546.

S. Kalusniak; C. Guguschev; R. Koc; R. Blukis; C. Rhode; J. Cejka; A. Dittmar; D. G. Schlom; C. Kränkel, Growth, spectroscopy, and laser operation of Yb:$LaLuO_3$. Optical Materials Express; 15 (2025), 1924-1938 https://doi.org/10.1364/ome.565169.

Y. Kaneda; H. Tanaka; V. Temyanko, Diode-pumped Sm:YLF laser at 605 nm and 648 nm. Optics Express; 33 (2025), 8903-8910 https://doi.org/10.1364/oe.554022.

F. Kannari; T. Ishikawa; H. Tanaka; Y. Shioya; R. Yasuhara, 544-nm Tb^{3+}-doped $LiYF_4$ laser pumped by 488-nm InGaN laser diodes and high peak power operation with cavity-dumped Q-switching. Applied Optics; 64 (2025), 83-90 https://doi.org/10.1364/ao.543155.

A. Klump, C. Hartmann, M. Bickermann, T. Straubinger; Prediction of impurity concentrations in AlN single crystals by absorption at 230 nm using random forest regression; CrystEngComm; 27 (2025) 184-190. https://doi.org/10.1039/d4ce00813h

C. Kofahl; L. Dörrer; S. Ganschow; H. Wulfmeier; H. Fritze; H. Schmidt, Hydrogen and lithium tracer diffusivities as a function of hydrogen concentration in Li(Nb,Ta)O_3 single crystals. Solid State Ionics; 429 (2025), 116968 https://doi.org/10.1016/j.ssi.2025.116968.

C. Kofahl; J. Uhlendorf; B. A. Muscutt; M. N. Pionteck; S. Sanna; H. Fritze; S. Ganschow; H. Schmidt, Oxygen Diffusion in Li(Nb,Ta)O_3 Single Crystals. Physica Status Solidi a-Applications and Materials Science; 222 (2025), 2300959 https://doi.org/10.1002/pssa.202300959.

B. Koppitz; S. Ganschow; M. Rüsing; L. M. Eng, Ferroelectric Hysteresis Measurement in the Lithium Niobate-Lithium Tantalate Single-Crystalline Family: Prospects for Lithium Niobate-Tantalate. Physica Status Solidi a-Applications and Materials Science; 222 (2025), 2300967 https://doi.org/10.1002/pssa.202300967.

B. Koppitz; T. Saxena; F. Bernhardt; S. Ganschow; S. Sanna; M. Ruesing; L. M. Eng, Second harmonic generation contrasts of ferroelectric domain structures and composition in lithium niobate-tantalate mixed crystals. Journal of Applied Physics; 138 (2025), 034101 https://doi.org/10.1063/5.0276183.

L. Kotov; Y. Kaneda; S. Püschel; H. Tanaka; J. Hair; A. Nehrir; V. Temyanko, Continuous-wave and Q-switched Tb:YLF lasers at 587 nm. Optics Express; 33 (2025), 3950-3956 https://doi.org/10.1364/oe.549208.

P. Kruszewski; A. Fiedler; Z. Galazka, The electric field influence on EC-0.18 eV electron trap level in (100)-oriented β-Ga_2O_3 crystals grown by the Czochralski method. Applied Physics Letters; 126 (2025), 062110 https://doi.org/10.1063/5.0251567.

S. W. Li; S. Kalusniak; A. Mounérat; S. Ganschow; I. Arlt; C. Kränkel, Growth, spectroscopy, and laser operation of Ho^{3+}:$YScO_3$. Optical Materials Express; 15 (2025), 698-710 https://doi.org/10.1364/ome.557704.

Y. E. Li; J. Shine; C. Guguschev; M. Brützam; D. G. Schlom; N. Ravi, Corroborating the magnetic easy axis of epitaxial (100) α-iron and (0001) $BaFe_{12}O_{19}$ thin films by ^{57}Fe Mössbauer spectroscopy. Aip Advances; 15 (2025), 015323 https://doi.org/10.1063/5.0244334.

A. Maity; K. Habicht; M. Merz; A. H. Said; C. Guguschev; D. Kojda; B. Ryll; J. E. Hoffmann; A. Dittmar; T. Keller; F. Weber, Soft phonon and the central peak at the cubic-to-tetragonal phase transition in $SrTiO_3$. Physical Review B; 111 (2025), 134108 https://doi.org/10.1103/PhysRevB.111.134108.

S. Michler; Y. Hamdaoui; S. Thapa; G. Schwalb; S. Besendörfer; K. Ziouche; M. Albrecht; F. Brunner; F. Medjdoub; E. Meissner, Epitaxy of >7 µm Thick GaN Drift Layers on 150 mm Si(111) Substrates Realizing Vertical PN Diodes with 1200 V Breakdown Voltage. Physica Status Solidi a-Applications and Materials Science; 222 (2025), 2400544 https://doi.org/10.1002/pssa.202400544.

N. Z. Morales; D. S. Rühl; S. Sadofev; E. List-Kratochvil; S. Blumstengel, Plasmon-Mediated Hybridization of Wannier-Mott and Frenkel Excitons in a Monolayer WS_2-J-Aggregate Hybrid System. Physica Status Solidi-Rapid Research Letters; 19 (2025), 2400417 https://doi.org/10.1002/pssr.202400417.

A. Mrokon; H. Kraft; D. Shin; H. Tanaka; S. J. Herr; K. Buse; I. Breunig, Electrically induced resonance shifts of whispering gallery resonators made of barium magnesium fluoride. Apl Photonics; 10 (2025), 096109 https://doi.org/10.1063/5.0274891.

M. Münchhalfen; J. Schreuer; C. Rhode; C. Guguschev, Single-crystal thermoelastic behavior of magnetoplumbite-type (Mg,Zr):$SrGa_{12}O_{19}$ and Pr:$SrAl_{12}O_{19}$ between 103 and 1573 K. Aip Advances; 15 (2025), 025120 https://doi.org/10.1063/5.0252715.

S. K. Ojha; P. Pal; S. Prokhorenko; S. Husain; M. Ramesh; X. Y. Li; D. Kang; P. Meisenheimer; D. G. Schlom; P. Stevenson; L. Caretta; Y. Nahas; Y. M. Han; L. W. Martin; L. Bellaiche; C. B. Eom; R. Ramesh, Morphogenesis of spin cycloids in a noncollinear antiferromagnet. Proceedings of the National Academy of Sciences of the United States of America; 122 (2025), e2423298122 https://doi.org/10.1073/pnas.2423298122.

V. B. Oliva; E. Robin; S. Hagedorn; H. Kirmse; J. L. Rouviere; H. Okuno; B. Damilano; A. Michon; T. Remmele; T. Schulz; H. Amari; M. Albrecht; P. Vennéguès, Polarity Inversions in AlN Films on Sapphire Exploiting Silicon and Oxygen Diffusion during High-Temperature Annealing. Crystal Growth & Design; 25 (2025), 5697-5708 https://doi.org/10.1021/acs.cgd.4c01641.

P. C. Palleti; A. Gybin; S. Bergmann; U. Juda; M. Albrecht; R. R. Sumathi, Development and morphological analysis of the zone refining process for high purity germanium. Materials Science in Semiconductor Processing; 185 (2025), 108924 https://doi.org/10.1016/j.mssp.2024.108924.

Y. Pan; X. Z. Liu; S. Y. Zhen; J. X. Zhao; Y. H. Wang; M. S. Ge; J. R. Zhang; Y. Pan; L. Gu; L. Zhang; D. Zhou; D. Su, Alloying Effects on Iron Oxide Redox Pathways: Insights into Sustainable Hydrogen-Based Reduction. Journal of Physical Chemistry Letters; 16 (2025), 5506-5514 https://doi.org/10.1021/acs.jpclett.5c00954.

Y. Pan; S. Y. Zhen; X. Z. Liu; M. S. Ge; J. X. Zhao; L. Gu; D. Zhou; L. Zhang; D. Su, Looping metal-support interaction in heterogeneous catalysts during redox reactions. Nature Communications; 16 (2025), 8627 https://doi.org/10.1038/s41467-025-63646-1.

C. T. Parzyck; Y. Wu; L. Bhatt; M. Kang; Z. Arthur; T. M. Pedersen; R. Sutarto; S. Fan; J. Pelliciari; V. Bisogni; G. Herranz; A. B. Georgescu; D. G. Hawthorn; L. F. Kourkoutis; D. A. Muller; D. G. Schlom; K. M. Shen, Superconductivity in the Parent Infinite-Layer Nickelate $NdNiO_2$. Physical Review X; 15 (2025), 021048 https://doi.org/10.1103/PhysRevX.15.021048.

A. Paskin; T. Couasnon; R. Blukis; J. P. H. Perez; S. Reinsch; V. Roddatis; M. Syczewski; L. G. Benning, Temperature-Induced Phase Transitions of Vivianite: In Situ Analysis of a Redox-Driven Crystallization. Inorganic Chemistry; 64 (2025), 18227-18236 https://doi.org/10.1021/acs.inorgchem.5c02399.

A. Paul; Z. Liestmann; S. Zaenker; K. Vogel; T. Broszies; M. Ostermann, How reliable is the X-ray fluorescence-based differentiation between glass wool and rock wool and the age classification of rock wool? X-Ray Spectrometry; 54 (2025), 224-234 https://doi.org/10.1002/xrs.3451.

S. G. Pavlov; A. N. Subramanian; R. R. Sumathi; S. B. Anooz; N. V. Abrosimov; M. Sidorova; H.-W. Hübers; Infrared Spectroscopy of Heavily Doped Germanium Crystals; META Conference Proceedings; (2025) 1850. ISSN 2429-1390

M. Petkovic; N. Dropka, SyMO: A Hybrid Approach for Multi-Objective Optimization of Crystal Growth Processes. Advanced Theory and Simulations; 8 (2025), e00677 https://doi.org/10.1002/adts.202401361.

M. Petkovic; N. Dropka; X. Tang; J. Zittel, Leveraging Transfer Learning to Overcome Data Limitations in Czochralski Crystal Growth. Advanced Theory and Simulations; 8 (2025), https://doi.org/10.1002/adts.202500677.

M. Petkovic; L. Vieira; N. Dropka, Machine learning in crystal growth: A review of methods, data, and applications. Progress in Crystal Growth and Characterization of Materials; 71 (2025), 100689 https://doi.org/10.1016/j.pcrysgrow.2025.100689.

N. Pieczulewski; K. T. Smith; C. M. Efaw; A. Singh; C. A. Gorsak; J. T. Buontempo; J. Wensel; K. Azizie; K. Gann; M. O. Thompson; D. G. Schlom; F. Rana; H. P. Nair; S. M. Hues; E. Graugnard; P. H. Davis; D. Jena; H. G. Xing; D. A. Muller, Achieving 0.05 Ω-mm contact resistance in non-alloyed Ti/Au ohmics to β-Ga_2O_3 by removing surface carbon. Apl Materials; 13 (2025), 061122 https://doi.org/10.1063/5.0276786.

V. Rindert; Z. Galazka; M. Schubert; V. Darakchieva, High-frequency/high-field electron paramagnetic resonance generalized spectroscopic ellipsometry characterization of Cr^{3+} in β-Ga_2O_3. Applied Physics Letters; 126

(2025), 082105 https://doi.org/10.1063/5.0255802.

S. J. Ring; M. J. Henehan; R. Blukis; F. von Blanckenburg, Adsorption pathways of boron on clay and their implications for boron cycling on land and in the ocean. Geochimica Et Cosmochimica Acta; 389 (2025), 74-83 https://doi.org/10.1016/j.gca.2024.08.014.

S. J. Ring; M. J. Henehan; P. J. Frings; R. Blukis; F. von Blanckenburg, Late Cenozoic Rise in Seawater δ^{11}B Not Driven by Increasing Boron Adsorption. Geochemistry Geophysics Geosystems; 26 (2025), e2024GC011911 https://doi.org/10.1029/2024gc011911.

A. Rodrigues; A. Kamath; H. S. Illner; N. Kafi; O. Skibitzki; M. Schmidbauer; F. Hatami, Monolithically Integrated GaAs Nanoislands on CMOS-Compatible Si Nanotips Using GS-MBE. Nanomaterials; 15 (2025), 1083 https://doi.org/10.3390/nano15141083.

F. Sauerwein; N. Dömer; T. Hehemann; M. Huesmann; S. Ganschow; M. Imlau, Lithium Niobate Tantalate Solid Solutions Probed by Luminescence Spectroscopy. Crystals; 16 (2025), 1 https://doi.org/10.3390/cryst16010001.

A. Scheid; T. Heil; Y. E. Suyolcu; Q. Song; N. Enderlein; A. P. N. Tchiomo; P. Ngabonziza; P. Hansmann; D. G. Schlom; P. A. van Aken, Unveiling the Interfacial Reconstruction Mechanism Enabling Stable Growth of the Delafossite $PdCoO_2$ on Al_2O_3 and $LaAlO_3$. Acs Applied Materials & Interfaces; 17 (2025), 24620-24629 https://doi.org/10.1021/acsami.5c03536.

A. Scheid; Q. Song; S. Ribet; C. Ophus; Y. E. Suyolcu; D. G. Schlom; T. Heil; P. A. van Aken, Atomic-Scale Mechanisms in Nucleation and Stabilization in $CuCrO_2$ and $CuFeO_2$ Delafossite Thin Films on Al_2O_3. Advanced Materials Interfaces; 12 (2025), 2500218 https://doi.org/10.1002/admi.202500218.

M. Schilling; C. Hartmann; M. Guttmann; U. Juda; A. Muhin; J. Höpfner; T. Wernicke; T. Straubinger; M. Kneissl, Light Extraction and External Quantum Efficiency of 235 nm Far-Ultraviolet-C Light-Emitting Diodes on Single-Crystal AlN Substrates. Physica Status Solidi a-Applications and Materials Science; 222 (2025), 2400812 https://doi.org/10.1002/pssa.202400812.

M. Schmidbauer; J. Maltitz; F. Stümpel; M. Hanke; C. Richter; J. Schwarzkopf; J. Martin, Periodic lateral superlattice in bonded $SrTiO_3$/$SrTiO_3$ twisted perovskites. Applied Physics Letters; 126 (2025), 101902 https://doi.org/10.1063/5.0251478.

D. Schmidt; D. von Stetten; M. Agthe; D. Hensel; A. R. Pearson; G. S. Beddard; B. A. Yorke; F. Tellkamp; P. Gaal, Demonstration of Advanced Timing Schemes in Time-Resolved X-ray Diffraction Measurements. Acs Omega; 10 (2025), 57703-57710 https://doi.org/10.1021/acsomega.5c09218.

D. Schmidt; J. Wawra; D. Hensel; M. Brede; R. Hühne; P. Gaal, How does picosecond structural deformation of $(Ba,Sr)TiO_3$ relate to the pyroelectric effect? Journal of Alloys and Compounds; 1042 (2025), 183792 https://doi.org/10.1016/j.jallcom.2025.183792.

M. Schroeder, Z. Galazka, TS Chou, C. Hartmann, T. Straubinger, A. Popp, A. Fiedler, M. Bickermann, K. Stolze, T. Schroeder; Wide Bandgap Materials for Next-Generation Power Devices: Progress on AlN and beta-Ga_2O_3 Crystal Growth and Epitaxy at IKZ; IEEE 12th Workshop on Wide Bandgap Power Devices and Applications, WIPDA, 199 (2025); https://doi.org/10.1109/WiPDA63755.2025.11303403

T. Schulz; A. Lachowski; R. Kernke; M. Albrecht, Cathodoluminescence in a Scanning Electron Microscope Operated in Transmission Mode. Journal of Electronic Materials; 54 (2025), 5058-5065 https://doi.org/10.1007/s11664-025-11904-9.

P. Seyidov; J. B. Varley; Y. K. Frodason; D. Klimm; L. Vines; Z. Galazka; T. S. Chou; A. Popp; K. Irmscher; A. Fiedler, Thermal Stability of Schottky Contacts and Rearrangement of Defects in β-Ga_2O_3 Crystals. Advanced Electronic Materials; 11 (2025), 2300428 https://doi.org/10.1002/aelm.202300428.

C. H. Sharma; A. Parvangada; L. Tiemann; K. Rossnagel; J. Martin; R. H. Blick, Resistively detected electron spin resonance and g-factor in few-layer exfoliated MoS_2 devices. Journal of Physics-Condensed Matter; 37 (2025), 185502 https://doi.org/10.1088/1361-648X/adc35d.

L. Y. Shi; Z. Tagay; J. H. Liang; K. Duong; Y. Wu; F. Ronning; D. G. Schlom; K. M. Shen; N. P. Armitage, Low-energy electrodynamics and a hidden Fermi liquid in the heavy-fermion compound CeCoIn5. Physical Review B; 111 (2025), 165113 https://doi.org/10.1103/PhysRevB.111.165113.

S. Slimi; H. H. Yu; H. J. Zhang; C. Kränkel; P. Loiko; R. M. Solé; M. Aguiló; F. Díaz; W. D. Chen; U. Griebner; V. Petrov; X. Mateos, Growth, structure, spectroscopic, and laser properties of Ho-doped yttrium gallium garnet crystal. Optics Express; 33 (2025), 2529-2541 https://doi.org/10.1364/oe.540363.

J. Som; A. J. Reese; L. Mitrovic; R. S. Kim; S. McBride; S. S. Nalawade; S. Aravamudhan; G. Hautier; J. Yano; D. G. Schlom; J. Suntivich, Strained-Induced Morphological Reconstruction of RuO_2(110) Thin-Film Electrocatalysts. Journal of the American Chemical Society; 147 (2025), 37115-37122 https://doi.org/10.1021/jacs.5c08607.

J. Steele; J. Chen; T. Burrell; N. A. Pieczulewski; D. Bhattacharya; K. Smith; K. Gann; M. O. Thompson; H. G. Xing; D. Jena; D. A. Muller; M. D. Williams; M. K. I. Senevirathna; D. G. Schlom, Erratum: "Growth of conductive Si-doped α-Ga_2O_3 by suboxide molecular-beam epitaxy" APL Mater. 13, 101117 (2025). Apl Materials; 13 (2025), 129901 https://doi.org/10.1063/5.0309396.

C. Y. Su; Y. Y. Liang; H. K. Nie; B. T. Zhang; J. Zhang; J. Liu; T. Li; C. Kränkel, All-solid-state continuous-wave mode-locked $Er:Lu_2O_3$ laser at 3 μ m. Optics and Laser Technology; 181 (2025), 111787 https://doi.org/10.1016/j.optlastec.2024.111787.

A. N. Subramanian; M. P. Kabukcuoglu; C. Richter; U. Juda; R. Kernke; F. Bärwolf; E. Hamann; M. Zuber; N. V. Abrosimov; R. R. Sumathi, Growth of Boron-Doped Germanium Single Crystals by the Czochralski Method. Crystal Growth & Design; 25 (2025), 1075-1081 https://doi.org/10.1021/acs.cgd.4c01413.

A. N. Subramanian; C. Richter; A. Gybin; M. P. Kabukcuoglu; E. Hamann; M. Zuber; M. Oezkent; C. Guguschev; U. Juda; T. Schroeder; N. V. Abrosimov; R. R. Sumathi; K. P. Gradwohl, On the Czochralski growth of Si_xGe_{1-x} crystals as substrates for strained Ge quantum well heterostructures. Journal of Applied Physics; 137 (2025), 065704 https://doi.org/10.1063/5.0238533.

Y. W. Sun; Y. Han; D. Zhou; A. S. Galanis; A. Gomez-Perez; K. Wang; S. Nicolopoulos; H. Pérez-Garza; Y. Yang, In situ nanometer-resolution strain and orientation mapping for gas-solid reactions via precession-assisted four-dimensional scanning transmission electron microscopy. Nano Today; 64 (2025), 102784 https://doi.org/10.1016/j.nantod.2025.102784.

K. Surovovs; S. L. Strozevs; M. Surovovs; R. Menzel; G. Ratnieks; J. Virbulis, Calibration of a Melt Flow Model for Silicon Crystal Growth with the Floating Zone Method. Crystals; 15 (2025), 667 https://doi.org/10.3390/cryst15070667.

X. Tang; M. Petkovic; G. K. Chappa; L. Vieira; N. Dropka, Comparative analysis of machine learning approaches for predicting and interpreting Cz-sapphire growth. Journal of Crystal Growth; 664 (2025), 128185 https://doi.org/10.1016/j.jcrysgro.2025.128185.

É. Tichy-Rács; S. Hurskyy; U. Yakhnevych; P. Gaczynski; S. Ganschow; H. Fritze; Y. Suhak, Influence of Li-Stoichiometry on Electrical and Acoustic Properties and Temperature Stability of $Li(Nb,Ta)O_3$ Solid Solutions up to 900 °C. Physica Status Solidi a-Applications and Materials Science; 222 (2025), 2300962 https://doi.org/10.1002/pssa.202300962.

J. Tröger; R. Kersting; B. Hagenhoff; D. Bougeard; N. V. Abrosimov; J. Klos; L. R. Schreiber; H. Bracht, Optimizing time-of-flight secondary ion mass spectrometry depth profiles of semiconductor heterostructures. Journal of Applied Physics; 137 (2025), 025301 https://doi.org/10.1063/5.0232252.

S. Unger; M. Leich, A. Schwuchow; M. Lorenz; R. Müller; A. Pratiwi; J. Kobelke; A. Lorenz; J. Dellith; C. Kränkel; M. Jäger, Absorption and emission properties of thulium doped glasses in optical fibers, Opt. Mat. Express, 15 (3) 446-464 (2025), https://doi.org/10.1364/OME.547199

L. Vieira; R. Menzel; M. Holena; N. Dropka, An Analysis of Elusive Relationships in Floating Zone Growth Using Data Mining Techniques. Advanced Theory and Simulations; 8 (2025), https://doi.org/10.1002/adts.202400781.

H. Voss; S. Zahedi-Azad; O. C. Ernst; J. Lucassen; G. Mann; J. Bonse; T. Boeck; J. Martin; M. Schmid; J. Krüger, Chemical vapor deposition of indium precursors for solar micro-absorbers using continuous laser radiation. Applied Physics a-Materials Science & Processing; 131 (2025), 781 https://doi.org/10.1007/s00339-025-08895-z.

H. H. Wan; F. Ren; T. S. Chou; S. B. Anooz; S. J. Pearton, Al composition dependence of band alignment in $NiO/(Al_xGa_{1-x})_2O_3$ heterojunctions. Journal of Vacuum Science & Technology A; 43 (2025), 063415 https://doi.org/10.1116/6.0005029.

Q. Wang; H. Y. Meng; Y. X. Guo; Y. K. Wang; L. Y. Dai; J. Y. Zhao; L. B. Zhao; Z. D. Jiang; J. Schwarzkopf; S. L. Wu; L. F. Liu; C. M. Wang; Z. M. Wang; F. Chu; Y. Wang; W. Ren; G. Niu, Ultra-thin epitaxial orthorhombic ferroelectric $Hf_{0.97}Y_{0.03}O_2$ films on $La_{2/3}Sr_{1/3}MnO_3$/$SrTiO_3$ substrate with different orientations. Journal of Crystal Growth; 652 (2025), 128043 https://doi.org/10.1016/j.jcrysgro.2024.128043.

A. Wintzer; B. E. Abali; K. Dadzis, Multiphysics simulation of crystal growth with moving boundaries in FEniCS. Computer Methods in Applied Mechanics and Engineering; 437 (2025), 117783 https://doi.org/10.1016/j.cma.2025.117783.

A. Wintzer; I. Tsiapkinis; S. Püschel; C. Guguschev; K. Dadzis, Validation of a numerical model for Czochralski growth of cesium iodide and calcium fluoride. Journal of Crystal Growth; 661 (2025), 128155 https://doi.org/10.1016/j.jcrysgro.2025.128155.

A. Wüthrich; R. Goldhahn; Z. Galazka; M. Feneberg, Optical properties of $ZnGa_2O_4$: Band gaps, plasmonic effects, and phonons. Physical Review Materials; 9 (2025), 064602 https://doi.org/10.1103/PhysRevMaterials.9.064602.

L. Xiao; Z. L. Song; T. Li; Y. R. Yin; Y. Y. Liang; C. Kränkel, Power-scaling of a 3 μm $Er:Lu_2O_3$ laser via amplification of injected 1.6 μm laser radiation. Optics Express; 33 (2025), 46764-46776 https://doi.org/10.1364/oe.578088.

U. Yakhnevych; V. Sargsyan; F. El Azzouzi; A. Kapp; F. Bernhardt; Y. Suhak; S. Ganschow; H. Schmidt; S. Sanna; H. Fritze, Acoustic Loss in $LiNb_{1-x}Ta_xO_3$ at Temperatures up to 900 °C. Physica Status Solidi a-Applications and Materials Science; 222 (2025), 2400106 https://doi.org/10.1002/pssa.202400106.

I. Zaitsev; A. A. Corley-Wiciak; C. Corley-Wiciak; M. H. Zoellner; C. Richter; E. Zatterin; M. Virgilio; B. Martin-Garcia; D. Spirito; C. L. Manganelli; Thermo-opto-mechanical properties of GeSn micro-disks: a comprehensive analysis; 2025 IEEE Silicon Photonics Conference, Siphotonics (2025). https://doi.org/10.1109/SiPhotonics64386.2025.10985018

J. J. Zhang; C. M. Liu; C. Wouters; M. Nofal; P. Mazzolini; O. Bierwagen; M. Albrecht, In situ TEM study of phase transformation in oxide semiconductors. Nano Today; 63 (2025), 102766 https://doi.org/10.1016/j.nantod.2025.102766.

X. Y. Zhang; S. H. Lee; J. E. Ryu; J. M. Suh; T. H. Kim; M. R. Barone; N. A. Parker; G. H. Lee; I. J. Kim; I. J. E. Yeo; J. Shin; J. S. Lee; D. G. Schlom; C. S. Chang; J. S. Seo; S. M. Yu; M. K. Song; J. Kim, Single-crystalline $BaTiO_3$-based ferroelectric capacitive memory via membrane transfer. Science Advances; 11 (2025), eadz2553 https://doi.org/10.1126/sciadv.adz2553.

D. Zhou; R. M. Wang; Y. C. Zhu; H. Pérez-Garza; K. Field, Preface to the special issue on advanced In-Situ transmission electron microscopy for multi-scale manufacturing: Dynamics in matter and process. Nano Today; 63 (2025), 102769 https://doi.org/10.1016/j.nantod.2025.102769.

Talks and presentations

I. Arlt	R. Blukis, S. Ganschow, C. Kränkel,	Investigation of the miscibility gap in the binary Y_2O_3-Sc_2O_3 system and its impact on crystal growth	14th German-French Workshop on Oxides, Dielectrics, and Laser Crystals (WODIL 2025) 24.-25.9.2025, Ettlingen, Germany
M. Badtke	S. Püschel, Z. Liestmann, H. Tanaka, C. Kränkel, S. Kalusniak	Highly efficient Tm^{3+}:LiYF$_4$ cascade laser for telecom wavelengths	Conference on Lasers and Electro-Optics (CLEO/Europe-EQEC) 2027 23.-27.06.2025, Munich, Germany
M. Badtke	H. Tanaka, S. Kalusniak, C. Kränkel	Solid-state lasers with direct emission at 413 nm and 435 nm	Conference on Lasers and Electro-Optics (CLEO/Europe-EQEC) 2026 23.-27.06.2025, Munich, Germany
M. Badtke	S. Kalusniak, H. Tanaka, C. Kränkel	Green Tb:ZBLAN Fiber Laser	Advanced Solid-State Lasers Conference 2025 19-23.10.2025, Prague, Czech Republic
M. Bickermann		AlN and Ga_2O_3 Substrate Solutions for Next Generation Efficient Power Electronics Devices	Workshop on High Voltage Power Components For Defence 11.06.2025 Saint Louis, France
M. Bickermann	Z. Galazka, S. Ganschow, A. Popp, S. Bin Anooz, J. Rehm, A. Fiedler, D. Pfützenreuther, M. Zupancic, R. Blukis, C. Guguschev, T. Schröder	Crystals and Substrates for Next-Generation Oxide Semiconductor Devices	DGKK Annual Meeting (DKT 2025) 05.-07.03.2025, Frankfurt am Main, Germany
M. Bickermann	Z. Galazka, A. Fiedler, R. Blukis, C. Guguschev, S. Ganschow, T. Schröder	Growth of Bulk Oxide Crystals for Next-Generation Oxide Semiconductors	14th German-French Workshop on Oxide, Dielectric, and Laser Single Crystals 2025 (WODIL 2025), 24.-25.09.2025, Ettlingen, Germany
I. Buchovska	R. Menzel, L. Vieira, J. Soerensen, B. Kramm, M. Kraft, J. Winkler	Challenges in Scaling up Floating Zone Silicon Crystal Diameter	DKT 2025 (German-French Crystal Growth Conference), 07.03.2025, Frankfurt, Germany
I. Buchovska	B. Scalise, M. Scheffler, F. Kiessling, K. Schindler, I. Tsiapkinis, R. Menzel, A. Nela, G. Lacaille, K. Haughian, K. Toland, A. Spencer	Float zone silicon fibers for suspension application in Einstein Telescope	Materials for Advanced Detectors 2025 (MAD25), 07.10.2025, Berlin, Germany
K. Dadzis	F. Oesterle, N. Sagias	An experimental setup and numerical simulation for teaching the multiphysics of crystal growth	13th Annual Meeting of the Young Crystal Growers (jDGKK), 04.03.2025, Frankfurt, Germany
K. Dadzis	N. Sagias	Energy consumption and sustainability in crystal growth and other high-temperature processes	MEP 2025 (10th International Scientific Colloquium Modelling for Electromagnetic Processing Hannover), 15.-17.09.2025, Hannover, Germany
K. Dadzis	N. Sagias	Energy consumption and sustainability in crystal growth: insights from experiments and numerical modelling	83rd International Scientific Conference of the University of Latvia, 21.02.2025, Riga, Lettland (online)
N. Dropka		Artificial intelligence in crystal growth	19th International Summer School on Crystal Growth - ISSCG19, 28.07.-02.08.2025, Xi'an, China
N. Dropka	N. Dropka, M. Holena, M. Petkovic, L. Vieira, G. Chappa, K. Meshram, X. Tang	Data Driven Modelling and Optimization of Cz, Fz, and VGF Crystal Growth Processes	4. Internationales Symposium „Modeling of Crystal Growth Processes and Devices“ (MCGPD-2026) und 3. Indo-Japanischer Workshop „Machine Learning for Crystal Growth“(MLCG-2026), 16.-18.02.2025, Chennai, India
N. Dropka	M. Petkovic, C. Frank-Rotsch, D. Linke, M. Holena	Towards a Universal Czochralski Growth Model Leveraging Data-Driven Techniques	21st International Conference on Crystal Growth and Epitaxy (ICCGE-21), 03.-08.08.2025, Xi'an, China
C. Frank-Rotsch	N. Dropka, U. Juda, G. Chappa, O. Root, L. Smejkalova, F. Kießling,	Modern application of traveling magnet fields for semiconductor materials	ICCGE-21, 07.08.2025, Xi'an, China
Z. Galazka		Current status of bulk β-Ga_2O_3 and β-$(Al_xGa_{1-x})_2O_3$ crystal growth	CS MANTECH, 19-22.05.2025, New Orleans, USA
Z. Galazka		Growth and basic physical properties of bulk single crystals of transparent semiconducting oxides	International Workshop on Semiconductor Oxides, 02.-06.03.2025, Tempe, USA
C. Guguschev	C. Hirschle, K. Dadzis, A. Tallaire, U. Waldschlaeger, M. Kabukcuoglu, A. Kwasniewski, M. Schulze, L. Schellkopf, C. Richter	Application of laboratory micro X-ray fluorescence devices for X-ray topography	24th American Conference on Crystal Growth and Epitaxy (ACCGE-24), 13.-18.07.2025, Stevenson, Washington, USA
C. Guguschev	C. Hirschle, K. Dadzis, A. Tallaire, U. Waldschlaeger, M. Kabukcuoglu, A. Kwasniewski, M. Schulze, L. Schellkopf, C. Richter	Application of laboratory micro X-ray fluorescence devices for X-ray topography	DGKK Annual Meeting (DKT 2025), 05.-07. 03. 2025, Frankfurt am Main, Germany
O. Hahn	S. Kalusniak, H. Tanaka, C. Kränkel	Temperature-dependent spectroscopy of Pr^{3+}:LiYF$_4$	Advanced Solid-State Lasers Conference 2025, 19.-23.10.2025, Prague, Czech Republic
C. Hartmann	C. Richter, M. Kabukcuoglu, L. Kirste, M. Bickermann, T. Schroeder, T. Straubinger	Diameter Enlargement of Bulk AlN Crystals up to 2 Inches: Evaluation of the superior structural quality via X-Ray Topography	DGKK Workgroup "Bulk Semiconductors" 12.-13.11.2025, Freiberg, Germany
C. Hartmann	C. Richter, M. Kabukcuoglu, L. Kirste, M. Bickermann, T. Schroeder, T. Straubinger	Efficient Diameter Enlargement of Bulk AlN	CS International 2025 07.-09.04.2025, Brussels, Belgium
S. Kalusniak	M. Badtke, H. Tanaka, C. Kränkel	Cryogenic Cascade Lasing of Tm:YLF with 39 mW Output Power at 450 nm	Advanced Solid-State Lasers Conference 2025, 19-23.10.2025, Prague, Czech Republic
S. Kalusniak	H. Tanaka, C. Kränkel	Violet, Blue and Infrared Cryogenic Lasing from the 5D3 Level in Tb^{3+}	Advanced Solid-State Lasers Conference 2025, 19-23.10.2025, Prague, Czech Republic
S. Kalusniak	S. Kalusniak, M. Badtke, S. Püschel, H. Tanaka, C. Kränkel	Watt-Level Continuous-Wave Ground-State Laser Operation of Tm:YLF at 0.8 µm	Advanced Solid-State Lasers Conference 2025, 19-23.10.2025, Prague, Czech Republic

F. Kannemann	K. Dadzis	Experimental study for the growth of organic crystals from melt	DKT 2025 (German-French Crystal Growth Conference), 05.-07.03., Frankfurt am Main, Germany
F. Kiessling	I. Buchovska, R. Menzel	Growth method dependent purity of silicon crystals for ET	Materials for Advanced Detectors 2025 (MAD25), 06.10.2025, Berlin, Germany
C. Kränkel	I. Arlt, S. Kalusniak	Czochralski-growth and efficient laser operation of rare-earth-doped $YScO_3$ crystals	21st International Conference on Crystal Growth and Epitaxy (ICCGE-21) 2025, 03.-05.08.2025, Xian, China
C. Kränkel	S. Kalusniak, S. Ganschow, M. Stypa, C. Büdenbender,	Nd:LuAP Laser at 1083 nm for Atmospheric Helium LiDAR	Advanced Solid-State Lasers Conference 2025, 19-23.10.2025, Prague, Czech Republic
C. Kränkel	S. Kalusniak, M. Badtke, H. Tanaka	New 'old' laser transitions in Tm3+-doped fluoride crystals	14th German-French Workshop on Oxides, Dielectrics, and Laser Crystals (WODIL 2025), 24.-25.09.2025, Ettlingen, Germany
C. Kränkel		Recent research results at the center for laser materials at the IKZ	Meeting on German-Chinese Research Collaborations, 05.08.2025, Xian, China
C. Kränkel	M. Badtke, H. Tanaka,	Trivalent thulium: Old laser transitions revisited	Advanced Solid-State Lasers Conference 2025, 19-23.10.2025, Prague, Czech Republica
C. Kränkel	S. Kalusniak, I. Arlt	Wavelength Tuning of 253 nm in Czochralski-grown Tm^{3+}:$YScO_3$ around 2.1 µm	Advanced Solid-State Lasers Conference 2025, 19-23.10.2025, Prague, Czech Republic
Z. Liestmann	S. Püschel, S. Kalusniak, C. Kränkel, H. Tanaka	Impact of foreign rare-earth impurities on optical refrigeration of Yb:YLF	SPIE Photonics West 2025, 28.-30.01.2025, San Francisco, USA
Z. Liestmann	S. Kalusniak, C. Kränkel, H. Tanaka	Temperature-Dependent Spectroscopy and Laser Cooling Potential of Tm^{3+}-Doped Fluoride Crystals	Advanced Solid-State Lasers Conference 2025, 1 9-23.10.2025, Prague, Czech Republic
J. Martin		Fabrication pathways for freestanding oxide membranes and novel crystalline interfaces	5th Advanced Epitaxy for freestanding mambranes and 2D materials, 07.- 09.07.2025, Grenoble, France
J. Martin		Periodic lateral superlattice in bonded $SrTiO_3$/$SrTiO_3$ twisted perovskites	DKT 2025 (German-French Crystal Growth Conference), 05.- 07.03.2025, Frankfurt am Main, Germany
R. Menzel	I. Buchovska, K. Dadzis, F. Kiessling	Towards high-purity, large-diameter silicon mirror substrates: A self-crucible growth concept	Materials for Advanced Detectors 2025 (MAD25), 06.10.2025, Berlin, Germany
W. Miller		First results of kinetic Monte Carlo computations for growth of 2D materials	DGKK Workgroup "Kinetics", 15.-16.09.2025, Berlin, Germany
W. Miller		Kinetic Monte Carlo for thin film growth and JuliaMolSimul Ecosystem	MMS days 2025, 2 6.3-28.3.2025, Warnemünde, Germany

A. Popp	A. Popp, T. Chou, S. Bin Anooz, J. Rehm, A. Akhtar, Z. Galazka, A. Fiedler, P. Seyidov, K. Irmscher, M. Albrecht	Homoepitaxialgrowth of β-$Ga_2O_3$by MOVPE	WOCDICE EXMATEC, 18.06.2025, Cadiz, Spain
S. Püschel	Z. Liestmann, C. Kränkel, H. Tanaka	Laser cooling of Yb-doped KY_3F_{10} to 170 K	Conference on Lasers and Electro-Optics (CLEO/Europe-EQEC) 2025, 23.-27.06.2025, München, Germany
R. Radhakrishnan Sumathi		Achieving sustainability in Germanium resources by circular means of Recycling and Reuse	EMRS 2025 Spring Meeting, Symposium W - Circular Economy through Urban Mining, 26.-30.05.2025, Strasbourg, France
C. Richter		X-ray diffraction imaging of lattice defects and strain	Physics Colloquium, TU Bergakademie, 12.02.2025, Freiberg, Germany
S. Sadofiev		"2D materials and "2D goes 3D" strategy at Leibniz-Institut für Kristallzüchtung"	DGKK Workgroup "Kinetics", 15.-16.09.2025, Berlin, Germany
N. Sagias	K. Dadzis	Influence of furnace design on energy consumption and thermal stresses in crystal growth from melt	DKT 2025 (German-French Crystal Growth Conference), 05.-07.03.2025, Frankfurt am Main, Germany
M. Schröder	Z. Galazka, T. Chou, C. Hartmann, T. Straubinger, A. Popp, A. Fiedler, M. Bickermann, K. Stolze, T. Schroeder	Wide Bandgap Materials for Next-Generation Power Devices: Progress on β-Ga_2O_3 and AlN Crystal Growth and Epitaxy at IKZ	2025 IEEE 12TH Workshop on wide bandgap power devices and appli-cation, WIPDA, 10.-12.11. 2025, Fayetteville, USA
T. Schröder	M. Bickermann	IKZ - Modern Crystal Science & Technology in Times of Geopolitical Change	Seminar von Prof. Daniel Vizman, Department of Physics, University of West Timisoara, 23.-24.07. 2025, Timisoara, Rumänien,
J. Schwarzkopf		Growth of complex oxides by MOVPE and the influence lattice strain and off-stoichiometry	Korean-German Oxide Workshop, 03.07.2025, Berlin, Gemany
J. Schwarzkopf		MOVPE of complex oxide thin films and their modification by lattice strain	HINA Seminar, 27.05.2025, online
J. Schwarzkopf		Strain engineering and phase transitions in heteroepitaxially grown (K,Na)NbO_3 films and free-standing membranes	DGKK Workgroup "Kinetics", 15.-16.09.2025, Berlin, Germany
T. Straubinger	C. Hartmann, A. Klump, C. Richter, M. Kabukcuoglu, L. Kirste, M. Bickermann, T. Schröder	AlN Bulk Substrates for UV Emitters	Photonic Days Berlin, 08.10.2025, Berlin, Germany
T. Straubinger	C. Hartmann, C. Richter, M. Kabukcuoglu, L. Kirste, M. Bickermann, T. Schröder	Efficient Diameter Enlargement of Bulk AlN	International Conference on Nitride Semiconductors (ICNS-15), 06.07. - 11.07.2025, Malmö, Sweden
T. Straubinger		Growth of Oxide- & Fluoride Single Crystals & Preparation of Photonic Components	12th European Seminar on Precision Optics Manufacturing 06.05.- 07.05.2025, Teisnach, Germany

T. Straubinger	Z. Galazka, A. Popp, T. Chou, D. Schulz, F. Kannemann, T. Luthardt, M. Bickermann, T. Schröder	2 Zoll Gallium-Oxid Prototyp Substrat: Cz-Züchtung, Wafering und MOVPE	DGKK-Arbeitskreis Herstellung und Charakterisierung von massiven Halbleiterkristallen, 12.11.- 13.11.2025, Freiberg, Germany
H. Tanaka	S. Püschel, Z. Liestmann, C. Kränkel,	Optical refrigeration of ytterbium-doped fluoride crystals: From YLF to novel host materials	SPIE Photonics West 2026, 28.-30.01.2025, San Francisco, USA
I. Tsiapkinis	K. Dadzis	In-situ measurement of melt flows during crystal growth processes, MEP 2025	10th International Scientific Colloquium Modelling for Electromagnetic Processing Hannover), 15.-17.09.2025, Hannover, Germany
I. Tsiapkinis	K. Dadzis	Model experiments with in-situ melt flow measurements for crystal growth processes	DGKK Workgroup "Bulk Semiconductors" 12.-13.11.2025, Freiberg, Germany
I. Tsiapkinis	K. Dadzist	Multiphysical simulation of the Floating Zone process with open-source software	DKT 2025 (German-French Crystal Growth Conference), 05.- 07.03.2025, Frankfurt am Main, Germany

Patents

Semiconductors

J. Boschker, Ch. Frank-Rotsch, M. Zorn, T. Schröder	Semiconductor device and method for producing a substrate for a semiconductor component, and use of indium during production of same	DE102020131850, US 18/039668
K. Stolze, P. Steglich, K, Berger, U. Juda, J. Martin	Method and apparatus for fabricating a semiconductor structure	DE 102022100661.1, EP23151074.4
M. Wünscher, H. Riemann	Device for non-crucible zone pulling of crystal rods	EP 2920342B1
N. Abrosimov, J. Fischer, H. Riemann, M. Renner	Process and apparatus for producing semiconductor single crystals	DE102010005520B4
D. Souptel, D. Sokolov, Ch. Frank-Rotsch, A. Pötzsch, B. Weinert, O. Root, L. Smejkalova	Improved doped InP crystals	DE102024202321, PCT/EP2025/053419

Registered Trademark

KRISTMAG®

Oxides and laser materials

Z. Galazka, R. Uecker, D. Klimm, M. Bickermann	Method for growing beta phase of gallium oxide (ß-Ga_2O_3) single crystals from the melt contained within a metal crucible	EP3242965B1, KR101979130B1, US20170362738A1, JP 2020-164415
Z. Galazka, R. Uecker, R. Fornari	Method and apparatus for growing indium oxide (In_2O_3) single crystals and Crystal growth device and method for growing a semiconductor	DE 102022119343.8, US2024/0044044
C. Guguschev, M. Brützam, D. Schlom, H. Paik	Method and setup for growing bulk single crystals	DE102020114524A1, US20200378030A1, KR1020200138082A

C. Guguschev, E. Haurat, D. Klimm, C. Kränkel, A. Uvarova	Method and device for growing a rare earth sesquioxide crystal	DE102020120715, WO/EP21748512.7
Z. Galazka, S. Ganschow, M. Bickermann, T. Schröder, W. Häckl	Method and apparatus for producing electrically conducting bulk ß-Ga_20_3 single crystals and electrically conducting bulk ß-Ga_20_3 single crystal	EP22154305.1, PCT/EP/2023051212, TW 112102595
Z. Galazka, S. Ganschow, M. Bickermann, T. Schröder	Melt-grown bulk ß-$(Al_xGa_{1-x})_2O_3$ single crystals and method for producing bulk ß-(Al_xGa_{1-x})2O3 single crystals	TW 202432918
Z. Galazka, M. Bickermann, S. Ganschow, T. Schröder	Method and apparatus for growing oxide single crystals from the melt containing at least one glass-forming binary oxide, and oxide single crystals containing at least one glassforming binary oxide	PCT/EP2025/076985

Aluminium nitride

A. Dittmar, C. Hartmann, J. Wollweber, M. Bickermann	(Sc,Y):AlN single crystals for lattice-adapted AlGaN systems	KR1020180048926A1
C. Hartmann, T. Straubinger	Crystal growth device and method for growing a semiconductor	DE 102022119343.8, US2024/0044044

Semiconducting layers and nanostructures

O. Ernst, T. Boeck, F. Lange, H.-P. Schramm, T. Teubner, D. Uebel	Method for microstructuring	DE102020126553
D. Uebel, R. Bansen, T. Boeck, O. Ernst, H.-P. Schramm, T. Teubner	Silicon-based wafers and method for fabricating silicon-based wafers	DE102020132900.8
O. Ernst, D. Uebel, T. Boeck	Process for the preparation of isotope-enriched germanium-hydrogen compounds	DE 102022105177.3, EP 4486690
S. Zahedi-Azad, T. Boeck, O. Ernst, H.-P. Schramm, D. Uebel	Method and growth setup for the fabrication of localized structures	DE 102022116962.6

Oxide layers

M. Albrecht, A. Baki, K. Irmscher, T. Schulz, J. Schwarzkopf, J. Stöver	Method for producing an oxide crystal having a perovskite structure	DE1020132049, EP 4256115
T. Chou, A. Popp, W. Häckl	Method for producing a gallium oxide layer on a substrate	EP 4123061, DE 102020132900.8, TW202305870, CN 117677737A, WO2024052149
S. Bin-Anooz, T.-S. Chou, W. Häckl, A. Popp	Method for growing a gallium oxide layer on a substrate and semiconductor wafer	EP 4335949, WO2024/052149A1, TW 111126459 EP 4123061

X-ray optics

P. Gaal	Providing a transient grid	DE102019132393B4

Memberships in committees

Committees

M. Bickermann	Speaker DGKK workgroup "Crystals for Photonics" Member of Review Panel of "Linköping University Research Evaluation 2025 (LiRE25)"
C. Frank-Rotsch	Secretary of German Association of Crystal Growth (DGKK) German representative of the European Network of Crystal Growth (ENCG) Executive Committee of International Organization for Crystal Growth (IOCG) - until July 2025 Secretary of International Organization for Crystal Growth (IOCG) - since July 2025
C. Guguschev	Membership Commission on Crystal Growth and Characterization of Materials (IUCr)
R. Radhakrishnan Sumathi	Doctoral committee of radeep Chandra Paletti, LMU München
W. Miller	Deputy chairman BVMatwerk
C. Richter	DESY Photon Science Proposal Review Panel ESRF Beamtime Allocation Panel
T. Schröder	Deputy Chairman of the “Deutsche Gesellschaft für Kristallzüchtung“ DGKK Vice-chair (until September 2025) and Chair of the Leibniz-Section D (since September 2025) Member of the Leibniz Association Presidency Presidency Coordinator of the European Networks on Crystal Growth (ENCG)
J. Schwarzkopf	Opponent for the PhD defense of Eric Brand, DTU, Kopenhagen, 22.9.2025

Conferences

M. Bickermann	Program committee member of the 8th International Symposium on Growth of III-Nitrides (ISGN-8), Tainan, Taiwan, 9.-12.11.2025 Program committee DGKK Annual Meeting (DKT 2025), Frankfurt, 5.-7.03.2025
I. Buchovska	Materials for Advanced Detectors 2025 (MAD25), Berlin, 6.-7.10.2025: Head of Organizing Committee, Member of Scientific Committee
N. Dropka	Scientific committee on 21st International Conference on Crystal Growth and Epitaxy (ICCGE-21), Xi'an, China
C. Frank-Rotsch	International Conference on Crystal Growth and Epitaxy-ICCGE-21, Xián, China, 3.-8.08.2025; member of the International Advisory Board of the Conference
Z. Galazka	Galazka, Z.; International Workshop on Semiconductor Oxides; International Advisory Committee
C. Kränkel	Advanced Solid-State Lasers Conference 2025, Program Committee Chair Photonics Europe 2025, Program Committee Member European Optical Society Annual Meeting 2025, Program Committee Member 14th German-French Workshop on Oxides, Dielectrics, and Laser Crystals (WODIL 2025), Organization Committee
R. Menzel	Materials for Advanced Detectors 2025 (MAD25), Berlin, 6.-7.10.2025: Member of Organizing Committee and Scientific Committee
R. Radhakrishnan Sumathi	Session organizer, “Session-P: New methods and observation techniques for crystal growth”, 21st International Conf. on Crystal Growth and Epitaxy (ICCGE-21), China, 3.-8.08.2025 DGKK workgroup meeting "Bulk Semiconductors", 12.-13..11.2025, Freiberg; Session Chair
K. Stolze	Main-organizer, EMRS Fall Meeting 2025, Symposium V "Integration of advanced materials on silicon: from classical to neuromorphic and quantum applications", Warsaw, Poland, 15.-18.03.2025

Journals/editors

M. Bickermann	Editor Journal of Crystal Growth (Elsevier B.V.) Associate Editor Progress in Crystal Growth and Characterization of Materials (Elsevier B.V.)
N. Dropka	Associate editor Journal of Crystal Growth
W. Miller	Editorial Board Crystals

Teaching and education

M. Bickermann	Crystal Growth I – Fundamentals and Methods Crystal Growth II – Methods and Applications	Technische Universität Berlin, Institute of Chemistry
C. Kränkel, T. Schröder (HU Berlin)	Applied Photonics	Humboldt-Universität zu Berlin, Department of Physics
M. Schmidbauer	X-Ray Scattering: Basics and Applications in Materials Science	Humboldt-Universität zu Berlin, Department of Physics
T. Schröder, R. Radhakrishnan Sumathi, J. Martin	Grundlagen und Methoden der modernen Kristallzüchtung – Basics and Methods of Modern Crystal Growth	Humboldt-Universität zu Berlin, Department of Physics

Imprint

Leibniz-Institut für Kristallzüchtung (IKZ)
Director: Prof. Dr. Thomas Schröder
Max-Born-Straße 2
12489 Berlin
Germany

Phone +49 (0)30 246 499 115
Email cryst@ikz-berlin.de
Online ikz-berlin.de

Annual Report 2025

Photos
Page 4: Simon Eichmann
Page 12/13: Sebastian Rost
Page 7/8, 38/39, 56/57: HORNNISSEN
Page 30/31: Christo Guguschev
Page 48/49: Dan Zhou
Page 62/63: Moritz Thau

Editor
Dr. Maike Schröder

Layout & typesetting
HORNNISSEN, Berlin
hornnissen.de

Print
USE Union Sozialer Einrichtungen gemeinnützige GmbH

Cover photo
Sebastian Rost

Berlin, Oktober 2026

Leibniz-Institut für Kristallzüchtung (IKZ)

Max-Born-Straße 2
12489 Berlin
Germany

Phone +49 (0)30 246 499 115
Email cryst@ikz-berlin.de

ikz-berlin.de